On a Finite Element Approach to Modeling of Piezoelectric Element Driven Compliant Mechanisms

A Thesis

Submitted to the College of Graduate Studies and Research

in Partial Fulfillment of the Requirements

for the Degree of

Master of Science

in the

Department of Mechanical Engineering

University of Saskatchewan

Saskatoon, Saskatchewan

Canada

By

RANIER CLEMENT TJIPTOPRODJO

PERMISSION TO USE

In presenting this thesis in partial fulfilment of the requirements for a Master of Science degree from the University of Saskatchewan, the author agrees that the Libraries of this University may make it freely available for inspection. The author further agrees that permission for copying of this thesis in any manner, in whole or in part, for scholarly purposes may be granted by the professor or professors who supervised the thesis work or, in their absence, by the Head of the Department or the Dean of the College in which the thesis work was done. It is understood that any copying or publication or use of this thesis or parts thereof for financial gain shall not be allowed without the author's written permission. It is also understood that due recognition shall be given to the author and to the University of Saskatchewan in any scholarly use which may be made of any material in this thesis.

Requests for permission to copy or to make other use of material in this thesis in whole or part should be addressed to:

Head of the Department of Mechanical Engineering

University of Saskatchewan

Saskatoon, Saskatchewan S7N 5A9 CANADA

ABSTRACT

Micro-motion devices may share a common architecture such that they have a main body of compliant material and some direct actuation elements (e.g., piezoelectric element). The shape of such a compliant material is designed with notches and holes on it, and in this way one portion of the material deforms significantly with respect to other portions of the material – a motion in the conventional sense of the rigid body mechanism. The devices of this kind are called compliant mechanisms. Computer tools for the kinematical and dynamic motion analysis of the compliant mechanism are not well-developed.

In this thesis a study is presented towards a finite element approach to the motion analysis of compliant mechanisms. This approach makes it possible to compute the kinematical motion of the compliant mechanism within which the piezoelectric actuation element is embedded, as opposed to those existing approaches where the piezoelectric actuation element is either ignored or overly simplified. Further, the developed approach allows computing the global stiffness and the natural frequency of the compliant mechanism.

This thesis also presents a prototype compliant mechanism and a test bed for measuring various behaviors of the prototype mechanism. It is shown that the developed approach can improve the prediction of motions of the compliant mechanism with respect to the existing approaches based on a comparison of the measured result (on the prototype) and the simulated result. The approach to computation of the global stiffness and the natural frequency of the compliant mechanism is validated by comparing it with other known approaches for some simple mechanisms.

ACKNOWLEDGEMENTS

I need to acknowledge Dr. (Chris) W.J. Zhang that has been a superb and dedicated research supervisor. I like to acknowledge his moral and financial support. His vision and broad knowledge play an important role in this research work. I also like to thank him for pushing me to the stage that I thought I never could accomplish. I also like to thank my research co-supervisor, Dr. M. M. Gupta for his continuous moral support. Allow me to express my sincere gratitude to Dr. A. T. Dolovich, my academic and teaching mentor for his tremendous and sincere support during my study here. It is my honor to have had opportunity to work with these great minds and their great characters. Their supports, commitments and contributions have been an inspiration.

I need also to express my gratitude to the Department of Mechanical Engineering through student assistantship experience, in which I have an opportunity to gain some financial support. I like to thank these following people that have shared their teaching experience: Dr. I. Oguocha, Dr. C. M. Sargent, Dr. P. B. Hertz and Dr. G. J. Schoenau. Allow me to also acknowledge Dr. W. Szyszkowski and Dr. L. G. Watson for sharing their expertise in finite element method and using ANSYS. Also, I appreciate the moral support from Dr. R. T. Burton during my very first years of study. I also like to thank Dr. D.X.B. Chen for his support.

Many thanks also go out to my colleagues in the AEDL. P. Ouyang that has contributed significantly his expertise to help me completing the experiment results presented in this thesis. Also I like to express my gratitude to K. D. Backstorm, B. Zettl, and D. Handley for their supports that play important role in this thesis.

I also appreciate the supports from these people: A. Wettig, S. Haberman, D. Bitner, D. Braun, C. Tarasoff, D. Vessey, A. McIntosh and C. Jansen. I like also to acknowledge H. Sato from TOKIN Inc, J. Mueller from KAMAN, and H. Saadetian and P. Budgell from ANSYS for their patience in answering all of my questions.

I like to acknowledge Heli Eunike for her continuous support and understanding to deal with me during my tough times prior to completing this thesis. The last but definitely not the least, I like to thank my family for their love and support, in particular Herlina (mom), Lydiana (auntie), Kevin and Natalia (younger brother and sister).

DEDICATION

To my parents:

Rudy Prabowo Tjiptoprodjo (Liem Kie Boan)[†] *and Herlina Alimin (Lie Lian Hoa)*

TABLE OF CONTENTS

LIST OF FIGURES

Figure Page

LIST OF TABLES

LIST OF ABBREVIATIONS

AEDL	Advanced Engineering Design Laboratory
DC	Direct current
FEM/FEA	Finite element model/finite element analysis
PZT	Piezoelectric actuator that has material consists of ions Pb, Zr and Ti.
PRBM	Pseudo rigid body model
RRR	Revolute revolute revolute (a given name to the compliant mechanism based on its PRBM)

CHAPTER 1

INTRODUCTION

1.1 Research Background and Motivation

In applications such as chip assembly in the semiconductor industry, cell manipulation in biotechnology, and surgery automation in medicine, there is a need for a device to perform controlled small motion (less than 100 μm) with high positioning accuracy (in the submicron range) and complex trajectories. This range of motion is known as micro-motion [Hara and Sugimoto, 1989]. The need of such a kind of device is also found in many intelligent devices which have the capability of sensing and making decisions in response to external disturbances.

The devices of this kind share a common architecture as follows. The devices have a compliant main body, the shape of which is designed with notches and holes on it. One portion of the material deforms significantly with respect to other portions of the material and illustrates or results in a sort of motion in the conventional sense of the rigid body mechanism. It was reported that systems built based on the compliant structure concept make it possible to achieve 0.01 μm positioning accuracy [Hara and

Sugimoto, 1989; Her and Chang, 1994]. The devices of this kind are called compliant mechanisms. Driving components in the compliant mechanism are usually developed by means of the piezoelectric technology (PZT for short), because of its advantages of fast response, and smooth and high-resolution displacement characteristics [Lee and Arjunan, 1989]. The PZT actuator used in this thesis is capable in achieving a displacement of 15 μm, while its resolution is sub-nanometer.

The compliant structure incorporating the actuator is called the compliant mechanism. A compliant mechanism can be configured as a closed-loop layout. The closed-loop configuration can provide better stiffness and positioning accuracy. Figure 1.1 shows one example of a compliant mechanism.

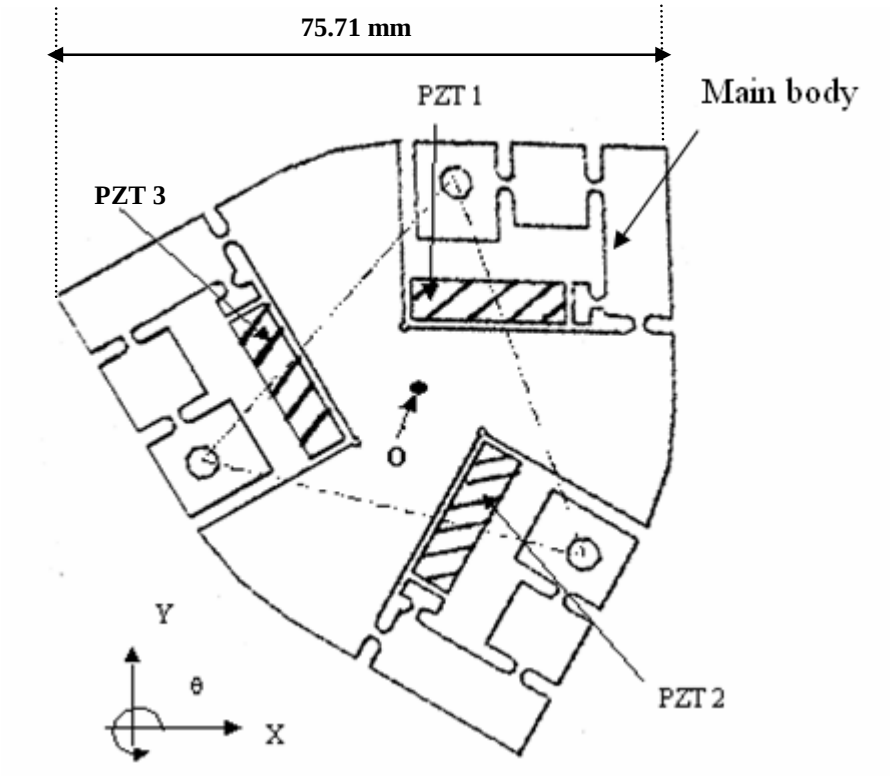

Figure 1.1 Schematic diagram of a RRR mechanism.

This mechanism consists of a compliant main body and a member of rigid material which is geometrically an equilateral triangle. The mechanism is driven by three PZT actuators (PZT 1, PZT 2 and PZT 3), while its end-effector motion is located at the center point O of the rigid member (Fig. 1.1). This mechanism is typically used to produce planar micro-motions with two translations (x and y) and one rotation (θ) and has been found in applications in the semiconductor industry [Ryu et al., 1997]. It is noted that in industrial applications, the terms *micro-positioning stage* and *single-axis stage* are used. They represent a kind of micro-motion system, and thus they are used interchangeably with the term *micro-motion system* in this thesis.

It is important to develop a model for the micro-motion device in order to simulate or predict behavior and performance of the device. The behaviors important to functions are the motion, stiffness, and natural frequency. For the micro-motion system, a large motion range is pursued; yet the large motion range may compromise the system stiffness. The information of the natural frequency is useful to determine the speed range of the PZT actuator such that the resonant situation can be avoided.

In this thesis, the compliant mechanism shown in Fig. 1.1 is studied comprehensively, and this compliant mechanism is thereafter called the RRR mechanism.

1.2 A Brief Review of the Related Studies

There have been several studies at the Advanced Engineering Design Laboratory at the Department of Mechanical Engineering at the University of Saskatchewan. Zou [2000] pioneered a study on the mechanism as shown in Figure 1.1. The work by Zou [2000] has not modeled the physical behaviour of piezoelectric actuators. In addition, the finite element model using the triangular type of element appears to contain some bad-shaped elements: refer to Figure 1.2. A popular approach, called pseudo rigid body (PRB) method, for compliant mechanisms, was also applied to kinematic and

dynamic analysis from Ref. [Zou, 2000]. It has been shown that the equation for the dynamic motion analysis is extremely complex, containing 600 lines of strings with the Maple V software [Maple, 1997].

Zettl [2003] developed a more effective 2D finite element model for the same compliant mechanism. The author led to a drastic reduction of the computational time for the motion analysis of the compliant mechanism yet without sacrificing prediction accuracy. In the study performed by Zettl [2003], consideration of the physical property of the PZT actuators is not systematic in the sense that the properties of the piezoelectric material were not fully explored. Only because conventional types of elements, e.g., spring, truss, or beam, was applied in his work.

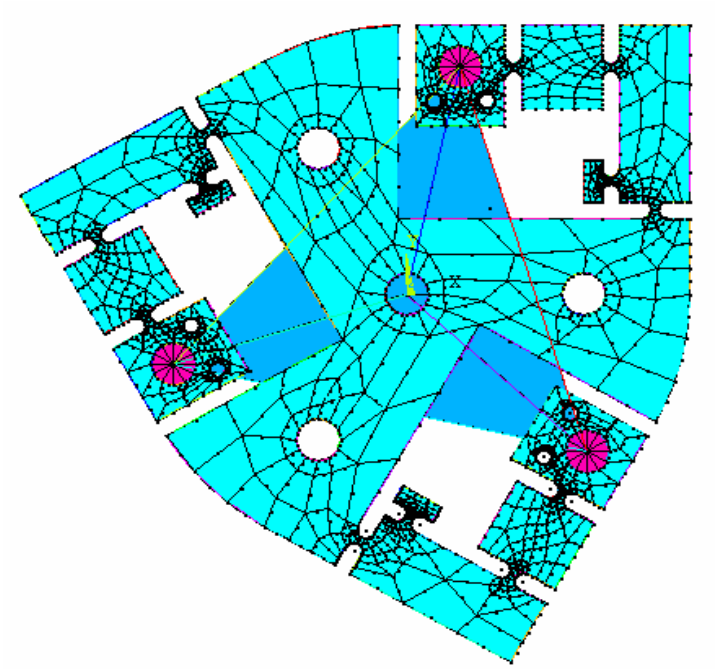

Figure 1.2 Finite element model of the compliant mechanism [Zou, 2000].

The modeling method developed by Zou [2000] for this compliant mechanism has been verified by experimental measurement. However, the previous experimental set up and the measurement technique for this compliant mechanism [Zou, 2000] were not very reliable. Furthermore, neither of these two studies has provided a tool for the

simulation of the system stiffness and the natural frequency. Those studies did not consider the prestress in the PZT actuator either.

1.3 Research Objectives

The primary goal of the study presented in this thesis was to improve the above methods and develop a method for the simulation of the system stiffness and the natural frequency. The secondary goal was to develop a more reliable test bed for the validation of the model for motion analysis. The following research objectives were defined.

Objective 1: *To develop a more accurate finite element model of the compliant mechanism (see Fig. 1.1) for motion analysis with special attention to capturing the physical behaviour of the piezoelectric actuators with the compliant mechanism.*

Objective 2: *To develop a more reliable test bed for the compliant mechanism (see Figure 1.1) with the objective to provide a test environment for the validation of the model for motion analysis.*

Objective 3: *To develop methods based on finite element analysis for predicting the system stiffness and natural frequency properties.*

1.4 General Research Method

The basic idea underlying this research is to apply a general-purpose finite element tool, ANSYS, in which several special types of elements are provided for the so-called multidisciplinary field or effect including the coupling of the mechanical displacement and electrical current (PZT actuator or sensor). The use of the finite element analysis for the compliant mechanism is a natural choice because the compliant material is by itself better to be viewed as an object with material

continuity. In other words, the compliant material is not lumped inherently. This means that the PRB method is inherently not suitable to the motion analysis of the compliant mechanism.

1.5 Organization of Thesis

This thesis consists of six chapters. Some general idea of discussions on each chapter will be concisely described as follows.

Chapter 2 discusses background for this research and provides a literature review. The literature review is focused on the PZT compliant mechanism and the methodology used for its analysis. The discussion in Chapter 2 further confirms the need of the research described in this thesis.

Chapter 3 presents a finite element model for the motion analysis of the PZT-RRR mechanism. The model is expected to overcome the shortcomings in the study by Zou [2000] and Zettl [2003]. An illustration is given to see how the simulation of motion can be generated with this model.

Chapter 4 presents finite element methods for the calculation of the system stiffness and the natural frequency.

Chapter 5 presents the development of a test bed for the verification of the finite element model for motion analysis developed in Chapter 3. A comparison is made between the three theoretical methods, namely the one developed in this thesis, the one developed by Zou [2000], and the one developed by Zettl [2003]. The experimental measurement will also be described.

Chapter 6 concludes this thesis with discussion of the results, contributions, and future work.

CHAPTER 2

BACKGROUND AND LITERATURE REVIEW

2.1 Introduction

This chapter provides both a literature review and the background necessary to facilitate the understanding this thesis, in particular its proposed research objectives and scope discussed in Chapter 1. *Section 2.2* introduces the piezoelectric material and its applications, as well as the use of the piezoelectric material as actuators. *Section 2.3* describes a compliant mechanism in more detail and explains the reasons behind using this specific type of compliant mechanism for micro-manipulation. *Section 2.4* introduces how a particular finite element analysis software package ANSYS addresses the problem which combines different disciplinary domains, in particular the modeling of PZT actuators embedded in a structure. *Section 2.5* discusses the concepts of system stiffness and natural frequency and the current method of calculating them.

2.2 Piezoelectric Material and its Applications

2.2.1 Piezoelectric Materials [Setter, 2002]

Piezoelectric materials have found applications in a wide range of fields, such as medical instrumentations, industrial process control, semiconductor manufacturing system, household electrical appliances, and environmental monitoring communications. Commercial equipment systems that use piezoelectric materials are found in pumps, sewing machines, pressure sensors, optical instruments, heads for dot and ink jet printers, and linear motors for camera auto focusing. The range of applications continues to grow.

Applications of piezoelectric materials generally fit into four categories: sensors, generators, actuators, and transducers. In the generator category, piezoelectric materials can generate voltages that are sufficient or larger to spark across an electrode gap, and thus can be used as ignitors in fuel lighters, gas stoves, and welding equipment. Alternatively, the electrical energy generated by a piezoelectric element can be stored. Such generators are excellent solid state batteries for electronic circuits. In the sensor category, piezoelectric materials convert a physical parameter, such as acceleration, pressure, and vibrations, into an electrical signal. In the actuator category, the piezoelectric materials convert an electrical signal into an accurately controlled physical displacement, to finely adjust precision machining tools, lenses, or mirrors. In the transducer category, piezoelectric transducer can both generate an ultrasound signal from electrical energy and convert an incoming sound into an electrical signal. Piezoelectric transducer devices are designed for measuring distances, flow rates, and fluid levels. The piezoelectric transducers are used to generate ultrasonic vibrations for cleaning, drilling, welding, milling ceramics, and also for medical diagnostics.

In the year of 1880, Jacques and Pierre Curie discovered an unusual characteristic of certain crystalline minerals: when subjected to the mechanical force, they became

electrically polarized. Subsequently, the inverse of this relationship was confirmed: if one of these voltage-generating crystals was exposed to an electric field, it lengthened or shortened according to the polarity of the field, and in proportion to the strength of the field. These behaviors were labeled the piezoelectric effect and the inverse piezoelectric effect, respectively. A piezoelectric material possesses a crystalline structure of lead zirconate titanate $PbZrO_3$-$PbTiO_3$ (abbreviated to PZT), which is the primary component of the piezoelectric material. The crystalline structure of the PZT controls the behavior of the piezoelectric material. The behaviors of the PZT actuator with respect to the crystalline structure can be classified into two conditions, unpolarized and polarized piezoelectric material (as illustrated in Fig. 2.1). In the unpolarized piezoelectric material condition (see Fig. 2.1a.), Ti and Zr ions are centered on the lattice (the arrangement of ions or molecules within the crystal). At this time, the piezoelectric material is electrically balanced and neither electrical polarization nor mechanical deformation arises in the material. Such a condition occurs when one does not apply electrical voltages on the piezoelectric material, or when one applies electrical voltages on the piezoelectric material in the temperature that exceeds the Curie temperature. The Curie temperature is a temperature that limits the piezoelectric material such that when the piezoelectric material is operated above this temperature, it will cease to work. In the polarized piezoelectric material condition, Ti and Zr ions are no longer centered on the lattice, due to the applied electrical field that causes the axis of the crystal to become longer in the direction parallel to the direction of the applied electric field. The specific behavior of the crystal also influences the neighboring crystals such that the entire domain behaves similarly (see Fig. 2.1b.). Such behavior occurs when one applies the electrical voltages to the piezoelectric material without exceeding the Curie temperature.

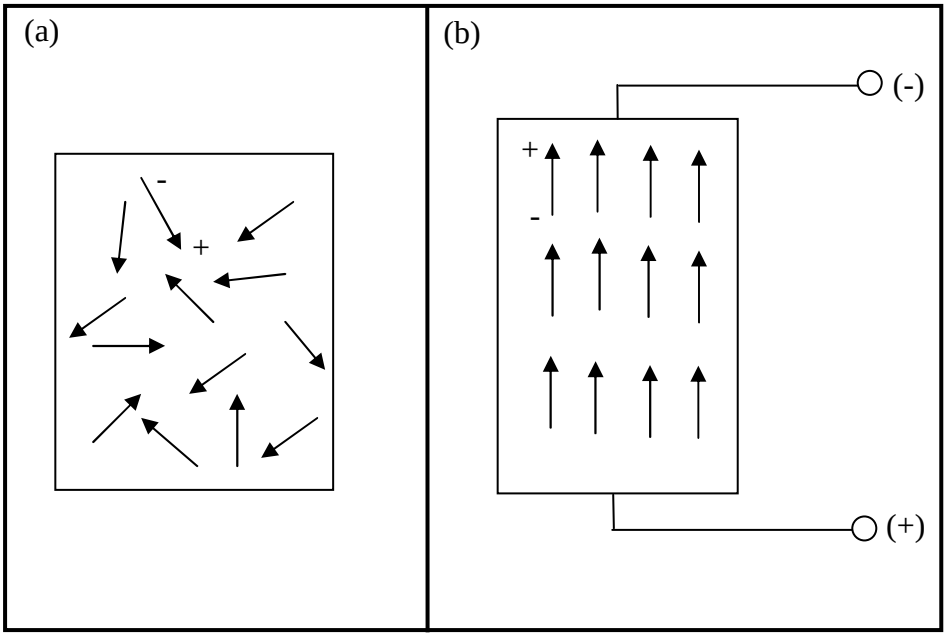

Figure 2.1 Unpolarized vs. polarized piezoelectric material.

Actuators made of the piezoelectric material are used in the RRR mechanism. The manufacturer of the actuator is Tokin America Inc. This actuator consists of multiple layers of piezoelectric sheets. The model name of the actuator is AE0505D16 (see Fig. 2.2). In the following, the properties of the PZT actuator, taking the AE0505D16 as an example, are discussed. The general knowledge is largely drawn from Ref. [Setter, 2002]; while the specific knowledge related to the actuator (AE0505D16) is based on its manufacturer [Tokin, 1996].

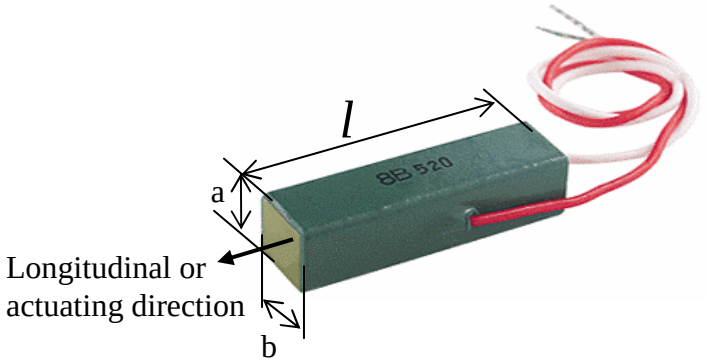

Figure 2.2 AE0505D16 [Tokin, 1996].

2.2.2 Properties of PZT actuator [Tokin, 1996]

By their nature, piezoelectric materials are anisotropic. Fig. 2.3 denotes the different direction and orientation axis of the piezoelectric material. In order to facilitate the understanding of the material properties of the piezoelectric actuators, those axes are explained. Axes 1, 2, and 3 are consecutively analogous to X, Y, Z of the classical right hand orthogonal axial set, while axes 4, 5, and 6 identify the rotations' axes. The direction of axis 3 is the direction of polarization. Polarization is the process that occurs when an electric field is applied between two electrodes. For actuator applications, the largest deformation is along the polarization axis (i.e., axis 3).

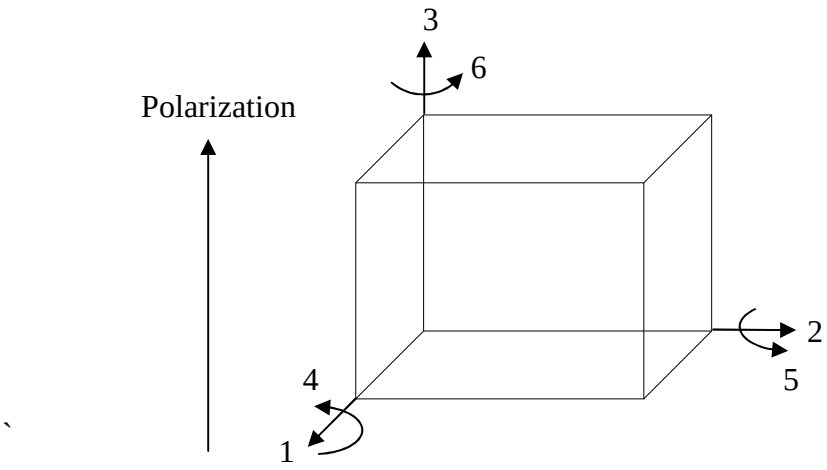

Figure 2.3 Direction and orientation axis of piezoelectric material.

The material properties of the piezoelectric actuator are listed below:

1. Relative dielectric constant,
2. Frequency constant,
3. Electromechanical coupling constant,
4. Elastic constant,
5. Piezoelectric constant,
6. Poisson's ratio,

7. Temperature coefficient,
8. Aging rate,
9. Mechanical quality factor,
10. Curie temperature, and
11. Density

(1) Relative dielectric constant

$$\left.\begin{aligned}\frac{\varepsilon^{T(S)}{}_{33}}{\varepsilon_0} &= 5440\\ \frac{\varepsilon^{T(S)}{}_{11}}{\varepsilon_0} &= 5000\end{aligned}\right\} \text{(AE0505D16)}$$

where ε_0 is the dielectric permittivity of a vacuum (= 8.85 x 10^{-12} Farads/meter).

Relative dielectric constant is the ratio of the dielectric permittivity of the material (in this case, ε^{T}_{33} and ε^{T}_{11}) to the dielectric permittivity of a vacuum (ε_0). The superscripts denote the boundary condition on material as the process of determination of the relative dielectric constant values; specifically the superscript T (in this case) describes the condition of constant stress (not clamped). Note that the superscript S refers to the condition where constant strains are measured.

As for the subscripts of the relative dielectric constant, the first subscript indicates the direction of dielectric displacement and the second subscript indicates the direction of electrical field. A formula to obtain the relative dielectric constant is given as follows [Tokin, 1996]:

$$\frac{\varepsilon^{T}{}_{ij}}{\varepsilon_0} = \frac{tC}{\varepsilon_0 S} \qquad (2.1)$$

where ε^{T}_{ij} : valid for either ε^{T}_{11} or ε^{T}_{33},

t : distance between electrodes (m),

S : electrode area (m^2),

and C : static capacitance (Farads).

(2) Frequency constant

N_3 = 1370 Hz-m (AE0505D16)

When an electrical voltage is applied to the piezoelectric actuator, the resulting frequency should be well below its resonance frequency. Otherwise, the actuator will vibrate in an uncontrollable manner. The directions of polarizations and vibrations are along the longitudinal axis in the core of the PZT actuator. A formula to obtain the frequency constant is given as follows [Tokin, 1996]:

$$N_3 = f_r \times l \tag{2.2}$$

where N_3 : frequency constant,

f_r : resonance frequency = 68500 Hz,

and l : the length of AE0505D16 = 20 mm.

(3) Electromechanical coupling constant

$K_{longitudinal}$ = 0.68 (AE0505D16)

A formula to obtain the electromechanical coupling constant for the longitudinal vibration is [Tokin, 1996]:

$$K_{longitudinal} = \sqrt{\left(\frac{\pi}{2}.\frac{f_r}{f_a}\right)\cot\left(\frac{\pi}{2}.\frac{f_r}{f_a}\right)} \qquad (2.3)$$

where f_r : resonant frequency (68500 Hz),

and f_a : anti-resonant frequency (79400 Hz).

The coefficient of electromechanical coupling is defined as the mechanical energy accumulated in a material, which is related to the total electrical input. This coefficient can be calculated by measuring the resonant and the anti-resonant frequencies. To measure those frequencies, an impedance analyzer is commonly used to depict the impedance-frequency characteristic of the piezoelectric actuator (see Fig. 2.4).

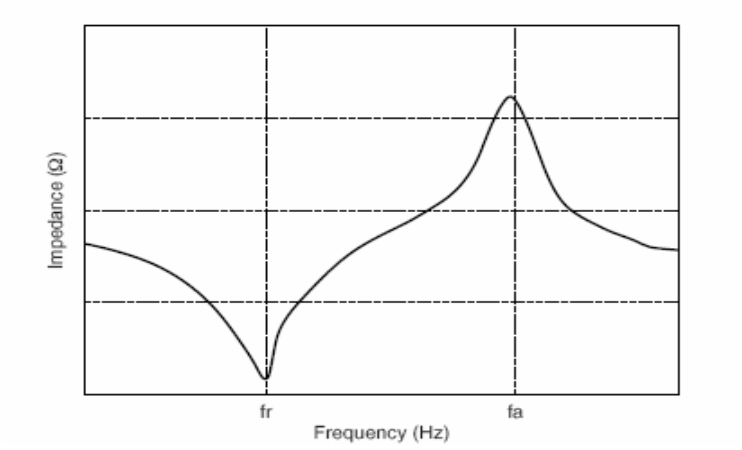

Figure 2.4 Impedance-frequency characteristic of the piezoelectric actuator [Tokin, 1996].

By its nature, the resonance frequency occurs when the system has very small resistance, while the anti-resonance frequency occurs when the system has very large resistance. In Fig. 2.4, the frequency that minimizes the impedance is chosen as resonant frequency (f_r) and the frequency that maximizes the impedance is chosen as anti-resonance frequency (f_a).

(4) Elastic constant

$S^{E(D)}_{11}=14.8 \times 10^{-12}\ m^2/N$
$S^{E(D)}_{33}=18.1 \times 10^{-12}\ m^2/N$ } (AE0505D16)

Elastic constant (S) defines the strain due to an applied stress (compliance). The superscripts denote the imposed conditions on material. The superscript E describes the boundary condition of the constant electrical field (the electrodes connected together or short circuit), while the superscript D indicates the boundary condition of the constant dielectric displacement (no current flows or open circuit). As for two digits in subscripts, they represent the directions of stress and strain. The first subscript indicates the direction of strain, and the second subscript indicates the direction of stress.

(5) Piezoelectric constant

$d_{31}= -287 \times 10^{-12}$ m/V
$d_{33} = 635 \times 10^{-12}$ m/V
$d_{15} = 930 \times 10^{-12}$ m/V
$g_{31} = -6 \times 10^{-3}$ Vm/N
$g_{33} = 13.2 \times 10^{-3}$ Vm/N
$g_{15} = 21 \times 10^{-3}$ Vm/N } (AE0505D16)

There are two types of piezoelectric constants: the piezoelectric strain constants (d) and the coefficient of voltage output (g).

(5a) Piezoelectric strain constant

This is a measure of the strain that occurs when a specified electric field is applied to a PZT material. A formula to obtain the piezoelectric strain constant is as follows:

$$d = k\sqrt{\frac{\varepsilon^T}{Y^E}} \text{ (m/V)} \qquad (2.4)$$

where k : coefficient of electromechanical coupling,

ε^T : dielectric constant,

and Y^E : Young's modulus (Newton/m^2).

(5b) Voltage output constant

It is defined as the intensity of the electrical field caused when a specified amount of stress is applied to a material (under the condition of zero displacement). A formula to obtain the voltage output constant is given below [Tokin, 1996]:

$$g = \frac{d}{\varepsilon^T} \text{ (mV/N)} \qquad (2.5)$$

where d : piezoelectric strain constants (m/V), and

ε^T : dielectric constant.

(6) Poisson's ratio

Poisson's ratio for AE0505D16 is 0.34

(7) Temperature coefficient

Tk(fr) for -20 to 20^o C = 200 (parts/million/^{o}C)
Tk(fr) for 20 to 60^o C = 900 (parts/million/^{o}C)
Tk(^{o}C) for -20 to 20^o C = 3800 (parts/million/^{o}C)
Tk(^{o}C) for 20 to 60^o C = 3500 (parts/million/^{o}C)
} (AE0505D16)

The temperature coefficient is a measure of the variation of the resonant frequency and the static capacitance with change in temperature. The formulas to obtain the voltage output constant are given below [Tokin, 1996]:

$$\text{Tk(f)}= \frac{1}{\Delta t}\frac{f(t_1)-f(t_2)}{f_{20}} x10^6 (PPm/°C) \quad (2.6)$$

$$\text{Tk(C)}= \frac{1}{\Delta t}\frac{C(t_1)-C(t_2)}{C_{20}} x10^6 (PPm/°C) \quad (2.7)$$

where Tk(f) : Temperature coefficient of resonant frequency (PPm/^{o}C),

$f(t_1)$: Resonant frequency at temperature t_1 ^{o}C (Hz),

$f(t_2)$: Resonant frequency at temperature t_2 ^{o}C (Hz),

f_{20} : Resonant frequency at temperature 20^{o}C (Hz),

Tk(C) : Temperature coefficient of static capacitance (PPm/^{o}C),

C (t_1) : Static capacitance (F) at temperature t_1 ^{o}C,

C (t_2) : Static capacitance (F) at temperature t_2 ^{o}C,

C20 : Static capacitance at 20^{o}C (F),

and Δt : Temperature difference (t_2-t_1) (^{o}C).

(8) Aging rate

For the PZT actuator (AE0505D16), the aging rate (AR) for the resonant frequency and the static capacitance, (%/10 years) are 0.5 and -5, respectively.

The aging rate is an index of the change in resonant frequency and static capacitance with age. To calculate this rate, after polarization the electrodes of transducer are connected together, and are heated for specific period of time. Measurements are taken of the resonant frequency and static capacitance every 2^n (at 1, 2, 4 and 8) days. The aging rate is calculated with:

$$(AR)=\frac{1}{\log t_2 - \log t_1}\frac{Xt_2 - Xt_1}{Xt_1} \qquad (2.8)$$

where (AR) : aging rate for resonant frequency or static capacitance,
t1, t2 : number of days aged after polarization,
and X_{t1}, X_{t2} : resonant frequency or static capacitance at t_1 and t_2 days after polarization.

(9) Mechanical quality factor (Q_m)

For the AE0505D16, the mechanical quality factor (Q_m) is 70. The formula to obtain mechanical quality factor (Q_m) is given below [Tokin, 1996]:

$$Q_m=\frac{fa^2}{2\pi f_r Z_r C(f_a^2 - f_r^2)} \qquad (2.9)$$

where f_r : resonant frequency (Hz),
f_a : antiresonant frequency (Hz),
Z_r : resonant resistance (Ω),
and C : static capacitance (C).

Applications based on the piezoelectric resonance, e.g., resonators, require high mechanical quality (Q_m).

(10) Curie temperature

For the AE0505D16, the Curie temperature is 145°C. This is the temperature at which polarization disappears (the piezoelectric qualities are lost); see also the previous discussion.

(11) Density

For the AE0505D16, the density is 8000 kg/m^3. A formula to calculate the density is given below [Tokin, 1996]:

$$D = \frac{W}{V} (kg/m^3) \qquad (2.10)$$

where W : mass (kg) of ceramic material,
and V : volume (m^3) of material.

2.2.3 PZT Actuator Manufacturing and Operation [Setter, 2002]

The piezoelectric material's properties can be tailored to the system's requirements by controlling the actuator's chemical composition and the fabrication process of piezoelectric actuators. In the beginning of the development process of piezoelectric actuator, sheets of the piezoelectric material are chosen from the standardized material types and there is a dialog between the manufacturer and the user. Then, the chosen sheets of piezoelectric material are inspected in order to suit the specific requirements. During this process, the manufacturer might add a number of certain substances in order to increase the specific features of piezoelectric material properties such as an increase dielectric constant, control conductivity, and an increase the piezoelectric coefficients. Next, the holes pattern shown in Fig. 2.5 is punched into the sheets.

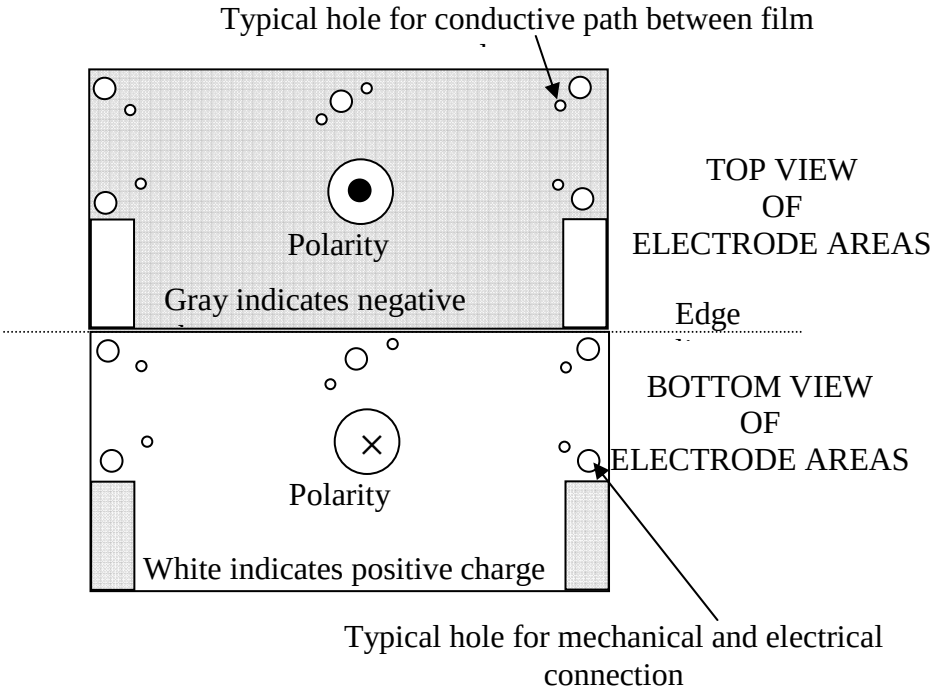

Figure 2.5 The holes pattern for manufacturing sheets.

The holes and electrode areas on a piezoelectric layer provide mechanical and electrical connections among stacked identical layers. Next, the inspected and punched sheets are pressed and burned (so-called the sintering process) at a certain temperature and a certain pressure, to form a coherent mass (see Fig. 2.6). The sintering temperature and pressure vary, as they depend on the chosen standardized material. With such a sintering technique, the thickness of one ceramic layer (mainly containing Ag-Pd alloy) can be reduced to less than 110 μm, thereby resulting in a compact multilayer piezoelectric actuator. Later, the stacked and burned ceramic layers are then patterned on and coated by the green sheet. The piezoelectric actuator is retested to verify the adequacy of the mechanical output as a function of an applied DC voltage. Fig. 2.6 presents the final product of the multilayer piezoelectric actuator.

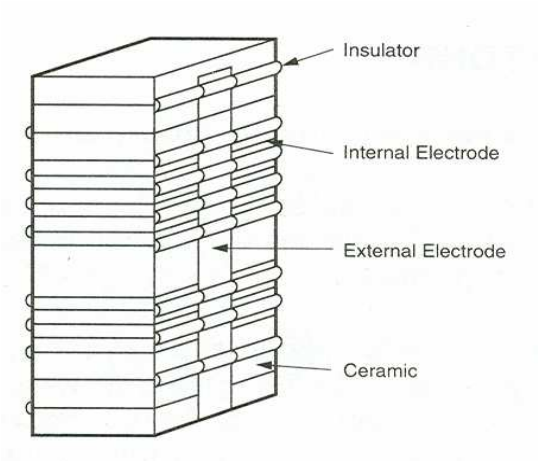

Figure 2.6 Stacked layers of piezoelectric actuator AE0505D16 [Tokin, 1996].

The piezoelectric actuators also have several advantages including large generated force (AE0505D16 = 850 N), fast response speed (AE0505D16 = 22.8 KHz), nanometers accurate positioning, compact (AE0505D16 = 1/10 the volume of a conventional multilayer actuator), and low cost. However, the piezoelectric actuator also entails several disadvantages, such as its poor ability in receiving tension, flexing and twisting type of loads. To prevent the load conditions from occurring, the prestress technique is the most commonly recommended by manufacturers. The piezoelectric actuator also has limited operating voltages and stroke that also influences the overall mechanism's work range. The maximum drive DC voltage for AE0505D16 is 150 volts, but the recommended drive is 100 volts. The displacement of AE0505D16 resulting from the maximum drive voltage is 17.4 $\pm$ 2 microns, while that resulting from applying the recommended drive voltage is 11.6 $\pm$ 2 microns.

2.2.4 Modeling and analysis of PZT devices

PZT devices (actuators and sensors) contain multi-domains of sciences and engineering. This has resulted in diverse standardized terminology, which has

hindered an efficient development of design knowledge for these devices. Several efforts have been made to unify the terminology of PZT devices: see Standards committee and Piezoelectric Crystals committee [1949] for material properties, Committee on Piezoelectric and Ferroelectric Crystals [1958] for measurement of the properties, and IEEE [1978] for the properties, concepts, and measurements. Mason and Jaffe [1954] compared several methods of measuring the piezoelectric material properties; in particular, the piezoelectric, dielectric and elastic coefficients of crystals. Such studies are believed to have a positive impact to the standard development.

The modeling of PZT devices usually goes along with numerical methods such as finite element method (FEM). Alik and Hughes [1970] discussed a finite element formulation for a single PZT device based on the variation principle. These authors appear to have laid down a foundation for ANSYS.

Lerch [1990] used a finite element method to perform a vibration analysis of the piezoelectric parallelepiped piezoceramic. Specifically, the author used a dedicated FEM package which was developed to model the piezoelectric effect. The author compared the simulation result with measurements and obtained errors from 5 % to 30 %. Peelamedu et al. [2001] studied several different scenarios of PZT devices in order to verify that their finite element code is versatile. In the finite element model, the base of specimen of the piezoelectric PZT-4 is constrained to be in contact with the XY plane to eliminate the rigid body motion in the X and Y direction. Such an approach to constrain the PZT could suffer from several problems: (1) impeding the understanding of the actual response of the PZT, which becomes very sensitive to the precise control of the PZT device behavior when the motion range of a PZT actuation is very small (in micron), and (2) introducing a constraint that might be difficult to realize in the real application situation, where the PZT device drives another mechanism. One approach is to use glue, which might, however, create some unwanted tension in the PZT device. The pre-stress approach is usually

recommended for this purpose. It is noted that the results produced by Peelamedu et al. [2001] remain to be verified.

There have been many other studies on the finite element modeling of PZT devices for various applications: for example [Kim et al., 1999] for noise rejection, [Preissig and Kim, 2000] for a piezoelectric bending actuator, [Piefort and Preumont, 2000] for a bimorph PZT actuator using an element type called bimorph beam, and [Cattafesta et al., 2000] for piezoelectric actuators in active flow control systems.

In [Kim et al., 1999], there was no mention of the rationales behind choosing those particular elements or whether this work had investigated several different mesh densities prior to determining this particular type of mesh density. The results remain to be experimentally verified. In [Preissig and Kim, 2000], there was no mention about the use of the manufacturer data of the piezoelectric bending actuator, and the necessity to transfer the published data into ANSYS format (which is found necessary; see later discussion in this thesis). In [Piefort and Preumont, 2000], there was no mention about the rationales of using those certain mesh densities as well as the element properties of the bimorph beam. The verification of the theoretical data with the real motion of bimorph beam might also need to be presented in order to more adequately understand the real behavior of the bimorph beam.

Last, in [Cattafesta et al., 2000], the chosen finite elements to model the system were not illustrated. The comparison between the experiment and the FEM shows some disagreement. The authors argued that a likely cause for the observed discrepancies between the theory and the experiment is an over-simplification of the bonding layer. Thus, the FEM may need to be modified to model the shear deformation in the bonding layer.

2.3 Compliant Mechanisms

Compliant mechanisms are devices used to transfer or transform motion, force and energy by use of the deflection of its members [Howell, 2001]. Unlike rigid link mechanisms, compliant mechanisms gain their mobility from the deflection of flexible members rather than from movable joints. Because compliant mechanisms gain their mobility from the deflection of flexible members rather than from movable joints, the required total number of components in the compliant mechanism is significantly reduced. This enables compliant mechanisms to be manufactured as a single piece. An example of the compliant mechanism discussed in this thesis work, is illustrated in Fig. 2.7. The motion of a single piece prevents assembly errors and also some inherent problems with the rigid joint (backlash and frictions) from occurring. These advantages motivate certain applications to employ compliant mechanisms, particularly applications that require an accurate and stable operation such as the cell manipulation system discussed in this thesis work.

The concept of compliant mechanisms has existed for millennia. Archaeological evidence suggests that bows (one of the earliest examples of compliant mechanisms) have been in use since 8000 B.C [McEwen et al., 1991]. Catapults are an example of the use of compliant mechanisms as early as the fourth century B.C. [De Camp, 1974]. At present, compliant mechanisms have found numerous applications from daily use objects (such as skateboards, computer joysticks, and door hinges) to more sophisticated systems (such as surgery automation in medical devices, chip assembly in the semiconductor industry, and cell manipulation in biotechnology).

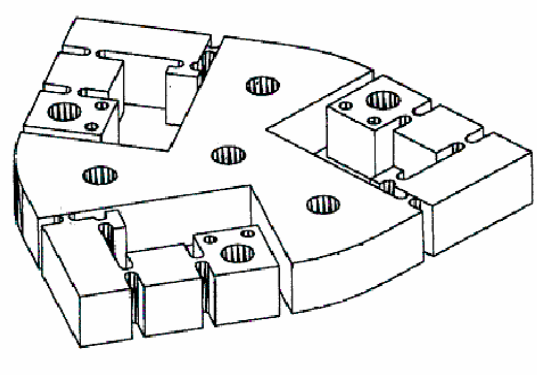

Figure 2.7 Manufactured compliant main body [Zou, 2000].

Despite many of these advantages, compliant mechanisms have several disadvantages, specifically; the flexure hinges of compliant mechanisms have certain limitations. First, the flexure hinges have a limited range of motion in the desired axis of rotation, whereas the conventional revolute joints have an infinite range of motion in the desired axis of rotation as illustrated in Fig. 2.8. Consequently, the mechanisms that employ revolute joints may have a larger work range compared to those that employ flexure hinges.

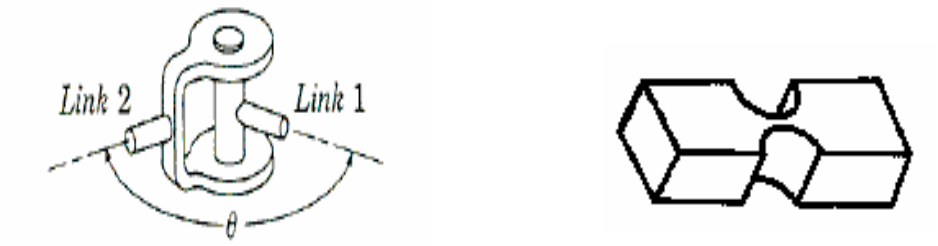

Revolute joint type in rigid body **Revolute joint type in compliant body (Flexure hinges)**

Figure 2.8 Revolute joint of rigid body versus compliant body [Zou, 2000].

Second, unlike the revolute joints, the flexure hinges are not fully fixed in all directions of loading except at the desired axis of rotation. Thus, flexure hinges will twist when subjected to torsional loads and exhibit shear deformation when subjected to shear loads. Last, a compliant mechanism could easily induce the fatigue problem

because its operation relies on the deformation of the material especially repeated deformations.

In [Lorenz et al., 1990], a compliant fingertip sensor is presented (Fig. 2.9). Such a sensor was intended for use in grippers where force feedback information was needed. The compliant mechanism was made up of room temperature vulcanizing (RTV) silicone rubber (see Fig. 2.9). The PZT sensor was made up of polyvinylidene fluoride (PVDF) film. There were four strips of such PZT sensors (or films) pasted on the compliant mechanism. This sensor could detect normal force, two tangential force components, and torque about the normal axis. The deformation in the RTV body occurs when a force is applied to the finger tip sensor. Next, this deformation is transferred to the piezoelectric film materials. The shift in electrical charge in the strained piezoelectric film is the signal used to measure the forces applied to the sensor. Each different component of the force applied to the sensor (whether it is normal, tangential, or torque) will produce a unique signal in each of the four pieces of the piezoelectric film. After the signals have been amplified, they are sent to a computer for decoupling (which translates the applied force into its independent components)**.** In their work, finite element analysis was used to determine the optimal shape of the fingertip and the location/size of the PVDF film piezoelectric sensing element. However, there was no mention in this paper regarding the particular finite element commercial software that was used, the procedure to perform the finite element model of the RTV body, the piezoelectric film, and the modeling interaction between the piezoelectric film and the RTV body does not follow. The procedure in attaching the piezo elements (PVDF) onto the compliant mechanism (RTV) was organized into three steps. *First*, it was required to form the rubber into the correct fingertip shape. Such process was accomplished by pouring the liquid rubber into a mold. *Second*, the piezo elements (PVDF) were cut with a good-quality scissors. Yet, because the fact that the PVDF is anisotropic by nature; care must be taken to cut the film in the proper direction (not explained further). To complete the process, the wire leads were added by use of a conductive epoxy. *Third*, a primer was used to bond the piezoelectric film to the rubber. A primer is a chemical additive that simultaneously

bonds to the film and vulcanizes the rubber. Finally, the authors compared the simulation and experimental results for the sensitivity ratio (the sensitivity ratio was defined as the ratio of length of the major axis of the ellipse to its minor axis corresponding to the largest amplitude of the signal for a given force). The experimental results were greater than the simulation results by 25%.

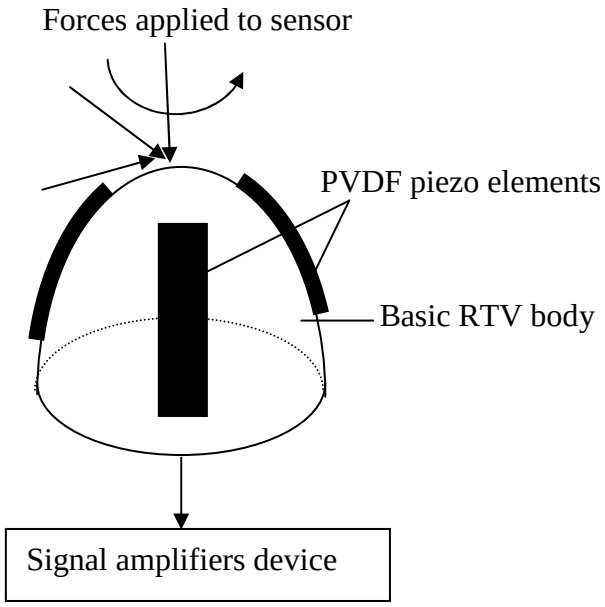

Figure 2.9 Finger tip sensor.

Several other studies on finite element modeling for the PZT compliant mechanism may be noticed, e.g., [Angelino and Washington, 2002; Abdalla et al. 2003; Chen and Lin, 2003; Bharti and Frecker, 2004]. Among these works, only Bharti and Frecker [2004] provided a reasonably detailed discussion of the finite element modeling. The authors used three PZT actuators and a compliant mechanism to develop a stabilized rifle mechanism. Such a mechanism stabilizes the rifle position by removing error sources (the undesired movement of the barrel resulting from extreme psychological stress experienced by a soldier during combat). The actuators compensate for the small undesired motions of the barrel, thereby stabilizing the barrel assembly. The objective of this work was to predict an optimal compliant mechanism design surrounding the PZT actuator with maximum stroke amplification. The authors used

commercial software called ProMechanica. A main body was made of Aluminum 7075, while the employed piezoelectric actuator was PZ26. In their experiment, the stack actuators were preloaded by press fitting them into the compliant mechanism. Equal preload on each actuator was assured by previously measuring the voltage change due to the compressive preload. In the finite element model however, the connection between the piezoelectric element and the compliant mechanism was not discussed. In addition, an equivalent temperature change was applied to the piezoelectric. It seems that the model was not completely inclusive in the finite element model. In particular, a customized code which computes the voltage from the temperature was needed and integrated with the rest of the finite element model.

2.4 Finite Element Analysis by Use of ANSYS

ANSYS is a finite element software package that was first commercially available in 1970 (Swanson Analysis Systems, Inc.). Since then, ANSYS has been used by design engineers throughout the world for such engineering applications as structural, thermal, fluid, and electrical analyses. In this thesis work, ANSYS was used as a computational tool for modeling the RRR mechanism. It is noted that the RRR mechanism basically consists of a compliant main body and three PZT actuators (see Fig. 2.10).

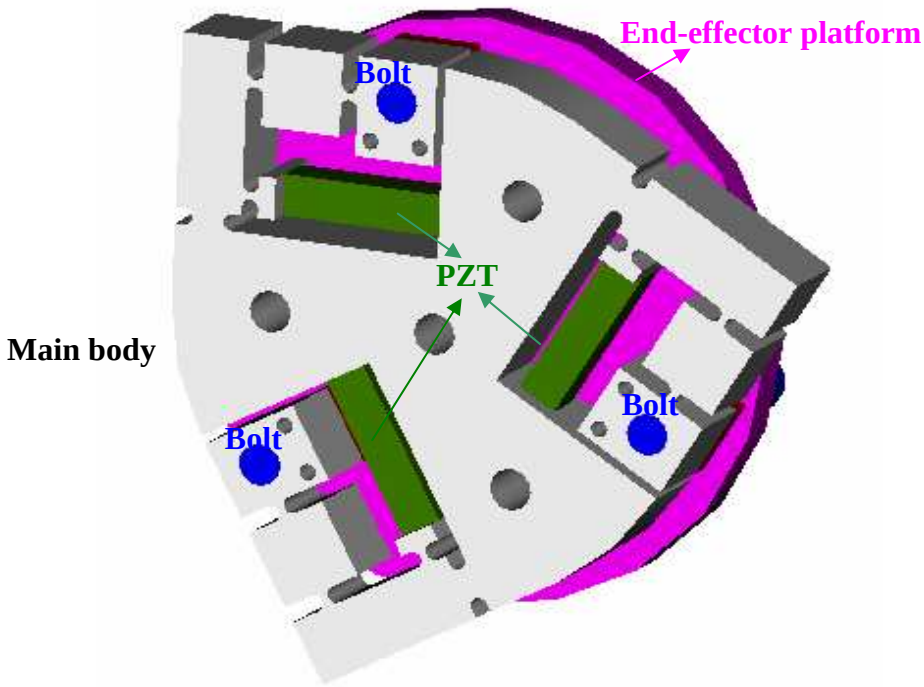

Figure 2.10 RRR mechanism.

In ANSYS, there are five typical steps for performing a finite element analysis as illustrated in Fig. 2.11. The first step is to gather the data of the problem. Such data may be available in forms of engineering drawings on paper, data specifications from manufacturer, or conceptual design. The second step is to build a finite element model for the application problem. This step consists of such activities as defining units, selecting types of elements, defining material properties, and creating the finite element model. As for defining a system of units, it should be noted that the ANSYS program does not assume a system of units. Thus, the users are responsible to maintain the consistency of system of units for all the input data in the ANSYS program. As for selecting element types, the decision is based on the characteristics of element type to best model that application problem geometrically and physically. The material properties are required for most element types. Depending on the element types, material properties may be linear or non-linear; isotropic, orthotropic, or anisotropic; and constant temperature-independent or temperature-dependent.

There are two methods to create a finite element model in ANSYS: automatic meshing (also called the solid modeling in ANSYS terminology) and manual meshing (also called the direct generation in ANSYS terminology). In automatic meshing, users are required to have a solid model available prior to the creation of a finite element model. When such a solid model becomes available, the users then can instruct ANSYS to automatically develop a finite element model (nodes and elements). The purpose of using automatic meshing is to relieve the user of the time-consuming task of building a complicated finite element model. However, this method requires significant amounts of CPU time and sometimes fails to maintain the connectivity of nodes and elements. In manual meshing, the users are to define the nodes and the elements directly (development of a solid model is not required). The manual meshing method offers a complete control over the geometry and connectivity of every node and every element, as well as, the ease of keeping track of the identities of nodes and elements. However, this method may not be as convenient as the automatic meshing when dealing with a complicated finite element model. It is possible to combine both methods.

The third step is to build a solution. This step includes such activities as applying loads, selecting boundary conditions, and selecting types of analysis. The loads are defined in several disciplines such as structural (displacements and forces), thermal (temperatures and heat flow rates), electrical (electric potentials and electric current) and fluid (velocity and pressure). In terms of region of where the loads are applied, loads can be classified as a nodal load (a concentrated load applied at a node in the model such as forces and moments in structure), a surface load (a distributed load applied over a surface such as pressures in fluid), and a body load (a volumetric load such as heat generation rates in thermal analysis). The fourth and fifth steps could be achieved with some sufficient understanding of the finite element software and the real system respectively.

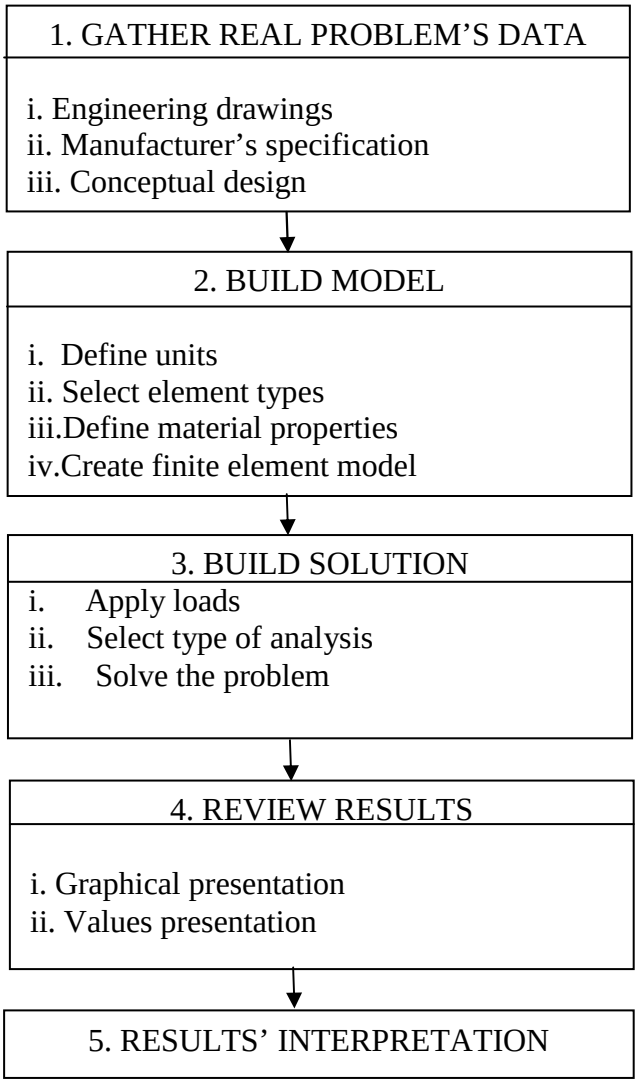

Figure 2.11 General procedures to perform FEA by use of ANSYS**.**

2.5 The Natural Frequency of the Compliant Mechanism

By definition [Braun et al., 2001], the natural frequency of a system describes the individual ways in which the system will choose to vibrate without any external applied excitation other than natural disturbances (such as gravitational force,

centrifugal force, and elastic restoring force). The natural frequency is positively correlated to the stiffness of a system. The higher natural frequency means the higher stiffness. Therefore, the natural frequency is a measure of the stiffness. For the mechanism, there are sets of configurations. At each configuration, the mechanism is like a structure with its degree of freedom (DOF) being zero. The natural frequency for a mechanism is then calculated at each configuration.

Kitis and Lindenberg [1989] used the transfer matrix method, as an alternative of the finite element method, to compute the natural frequencies of the four-bar mechanism. By use of the transfer matrix, the mechanism was modeled as a combination of massless beam sections, while the lump masses can be calculated through successive multiplication of point and field matrices along the link. To calculate the overall link transfer matrices, it is required to develop a transfer matrix to relate the state vectors of the adjoining links (pin joint transfer matrix). In the transfer matrix approach, the size of the system matrix is reduced. The results from the transfer matrix method were compared to those from the finite element approach from a different work study [Turcic, 1982]. The comparison results indicated considerably agreement.

Jen and Johnson [1991] calculated the natural frequencies of a planar robot, in particular three-link manipulator. The authors also studied the effect of variations of the physical parameters on the natural frequencies, by use of the component mode synthesis (CMS) approach. The CMS approach basically disassembles a complete structure into substructures and then computes the mode for each component. The corresponding mass matrix and stiffness matrix are then derived for each component and subsequently “assembled” by use of the displacement compatibility conditions at the component interfaces. The system was modeled by three beam elements connected by two stiff revolute joints. All the computations were performed by use of a general purpose language package (MATLAB in particular) without using special purpose finite element packages. The obtained results have not been verified with experimental results.

Li and Sankar [1992] focused on the development of a procedure to derive dynamic equations of motion for flexible robot manipulators. The derived dynamic equations of motion would facilitate the computation of the manipulator's behaviors (particularly the position and velocity of first mode and second mode, the joint angle position and velocity, and the joint actuator torque) with regard to the elapsing time. The procedure consisted of the development of kinematics of flexible links, lagrangian equations of motion for flexible manipulators (kinetic energy and potential energy of flexible links, development of flexible manipulator equations of motion). That method has been verified by use of computer simulation from other papers. The authors claimed that the method proposed in their paper was simple, more systematic, and efficient. It should be noted, however, this method is relatively simpler as it deals with a single-link robot manipulator.

Iwatsuki et al. [1996] proposed a new approach to study the vibration behavior of spatial serial manipulators composed of multiple elastic links. This method was used to calculate the internal forces and moments interactively acting between the two adjacent links connected with joint. The calculated results have been validated with the experimental results for various motions. Such an approach may be applied more effectively to the system with few joints. However, for the parallel manipulators that might have large numbers of joints, this approach becomes difficult to use due to the complex nature of the approach.

Lyon et al. [1999] proposed the pseudo-rigid-body model (PRBM) approach to predict the first modal frequency of compliant mechanisms. Their approach was verified by the experimental set-up approach (by use of digital oscilloscope). The results of the two theoretical approaches showed good agreement (within 9 % deviation) with the experimental results.

2.6 The Stiffness of the Compliant Mechanism

Several earlier studies have shown that accurate control and large work range are related to the stiffness and the natural frequency of the micromanipulation system. Han et al. [1989] proposed a procedure to optimize a 6 degree-of-freedom (6-DOF) fully-parallel micromanipulator for enhanced accuracy. They observed a need of trade-off between large work range and control accuracy through the stiffness property of a micromanipulator. Tomita et al. [1992] proposed a method of determining the design of a ultra precision stage (for the semiconductor manufacturing application) using a parallel linkage mechanism. As well, the authors discussed the necessity of high displacement resolution and high frequency response to compensate for the vibrating disturbances of the environment. Sanger et al. [2000] explained that the accuracy of a manipulator particularly under different loads is directly related to its stiffness, and that knowledge of the stiffness can be used to develop a means of simultaneously controlling the force and displacement for a partially constrained end-effector. Portman et al. [2000] proposed a new structural concept for a type of closed kinematic chain mechanism, (e.g., a 6 x 6 parallel platform mechanism). This new concept involved the application of welded joints. The objective of this structural concept is to obtain high stiffness and high accuracy. The stiffness of a mechanism is also related to the so-called singularity posture of the mechanism [Gosselin, 1990].

There are generally two kinds of methods available to model the system stiffness. The first method is the structural analysis method in which the system stiffness is directly associated with the number of nodes of elements that model a structure (a mechanism at a particular configuration). The second method considers the relationship between the force (including the moment) and the displacement (including the angular displacement) at the end-effector. In literature, such a stiffness may be called global stiffness. Gosselin [1990] presented a method for calculating the global system stiffness, which results in Eqn. (2.13).

$$[K] = k\, J^T J \tag{2.13}$$

where: [K] : the global stiffness matrix,

k : the stiffness along the actuator axis,

J^T : the transpose of Jacobian matrix of the mechanism,

and J : the Jacobian matrix of the mechanism.

Zhang and Gosseline [1999] went on to develop a similar formula as Eqn. (2.13), with inclusion of the stiffness of each link component. El-Khasawneh and Ferreira [1999] further studied the maximum and minimum stiffness, as well as, their orientation. In their study, they defined the so-called general stiffness.

$$S = \sqrt{\frac{\tau^T \tau}{\Delta p^T \Delta p}} \tag{2.14}$$

where: S : the general stiffness matrix,

Δp : the position and orientation of the end-effector,

and τ : the required input to cause the platform to experience Δp.

Also,

$$\tau = kJ^T J \Delta p \tag{2.15}$$

The eigenvalue of $J^T J$ can be found, assuming $\lambda_{min} = \lambda_1 \leq \lambda_2 \leq \ldots \leq \lambda_6 = \lambda_{max}$. Then they found

$$K\,\lambda_{min} \leq S \leq K\,\lambda_{max} \tag{2.16}$$

The direction of λ_{min} (λ_{max}) corresponds to the normalized eigenvectors corresponding to λ_{min} (λ_{max}). It is noted that their method has not considered the stiffness of the link and has assumed that all the actuators have the same axial stiffness.

2.7 Concluding Remark

The compliant mechanism is a very promising concept to build the micro-motion device. The conventional approach to modeling a compliant mechanism is the pseudo rigid body method. There are two problems with this method. First, the method can not capture the whole material distribution in the compliant mechanism domain. Second, the dynamic model with this method is extremely complex and lengthy (despite its analytic form) as shown by Zou [2000], which can subsequently prohibit any exploration of the dynamic model for the real-time control of a compliant mechanism. The finite element method is definitely a useful tool for the analysis of compliant mechanisms. However, the use of general-purpose finite element methods for (1) motion analysis with consideration of couplings of the PZT actuator and the compliant material and (2) natural frequency and stiffness analysis warrants further study.

CHAPTER 3

FINITE ELEMENT ANALYSIS OF DISPLACEMENT OF RRR MECHANISM

3.1 Introduction

This chapter presents a study of finite element analysis of the RRR mechanism by making use of the finite element commercial software called ANSYS. Zou [2000] previously conducted finite element analysis (FEA) for the RRR mechanism with some limitations. This thesis work is expected to overcome these limitations; specifically by including the PZT actuator in the FEM model. The organization of this chapter is as follows: Section 3.2 will present some fundamental information that is necessary to facilitate discussions in this chapter. Section 3.3 will present a model for the kinematic analysis of the RRR mechanism. Section 3.4 will present finite element modeling of the PZT actuator. Section 3.5 will discuss a procedure to incorporate PZT into the RRR mechanism. Section 3.6 illustrates how the model works by using an example. Section 3.7 presents a summary with some discussion.

3.2 Basic Information of ANSYS

ANSYS provides several new types of elements to model the piezoelectric effects, or in general to model those effects that are related to domains of disciplines, e.g., electrical-pressure, electrical-thermal, etc. In this section, a type of element for modeling the piezoelectric effect will be presented.

3.2.1 Multidisciplinary Element Type [ANSYS, 2004]

Multidisciplinary element types are used to capture the effects that are related to two different domains of disciplines, e.g., electrical-pressure, electrical-thermal, etc. In this section, the type of element for modeling the piezoelectric effect will be presented. The PZT actuator system has electrical behavior (the electrical current as input to the PZT actuator) and mechanical behavior (the existence of PZT actuator's deformation as the output for the PZT actuator). Finite elements must capture this mechanical-electrical joint behavior. In ANSYS, there are two types of elements for modeling the piezoelectric effect, namely SOLID 5 and PLANE 13.

- SOLID 5

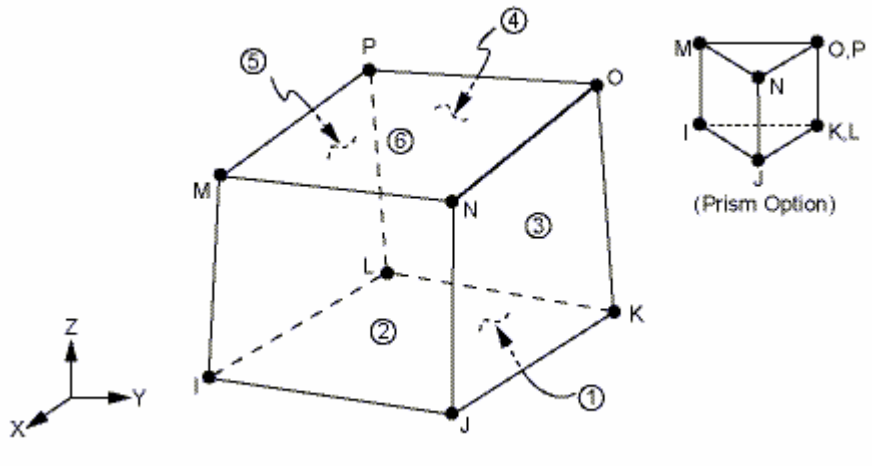

Figure 3.1 Geometry of SOLID 5 [ANSYS, 2004].

DISCIPLINE	DEGREES OF FREEDOM	ACTIVATION
Coupling of structural, thermal, electrical and magnetic	UX, UY, UZ, TEMP, VOLT, MAG	KEYOPT (1) =0
Coupling of thermal, electrical and magnetic	TEMP, VOLT, MAG	KEYOPT (1) =1
Structural	UX, UY, UZ	KEYOPT (1) =2
Coupling of structural and electrical, also called as piezoelectric	UX, UY, UZ, VOLT	KEYOPT (1) =3
Thermal	TEMP	KEYOPT (1) =8
Electrical	VOLT	KEYOPT (1) =9
Magnetic	MAG	KEYOPT (1) =10

Figure 3.2 Disciplines in SOLID 5 [ANSYS, 2004].

SOLID 5 is a type of element that occupies three-dimensional space. It has eight nodes. Each node has three displacements along the x, y, and z axis, respectively. A prism-shaped element is formed by defining duplicate node numbers as described in

Fig. 3.1. In particular, one can define a prism-shaped element by defining nodes K, L and nodes O, P in same locations, respectively. The prism-shaped element may be useful in modeling a system that has a geometric curvature (e.g., cylinder). In this thesis work, the brick-shaped element is chosen due to the fact that the geometrical shape of the piezoelectric actuator does not have any curvature.

The SOLID 5 element is capable of modeling seven different types of disciplines (see Fig. 3.2). The meaning of these terms in the second column in Fig. 3.2 is presented in Fig. 3.3. The third column in Fig. 3.2 is used in the ANSYS code to select one particular discipline. For the discipline corresponding to the problem discussed in this thesis, KEYOPT (1) =3 is chosen. When this particular type of discipline is chosen, ANSYS will only consider (compute) the behaviors of SOLID 5 in UX, UY, UZ and VOLT degrees of freedom. It should be noted that UX, UY and UZ are to indicate the displacements in the X, Y and Z directions (X, Y and Z axes are based on the global coordinate system), while VOLT is to indicate the difference in potential energy of the electrical particles between two locations.

- PLANE 13

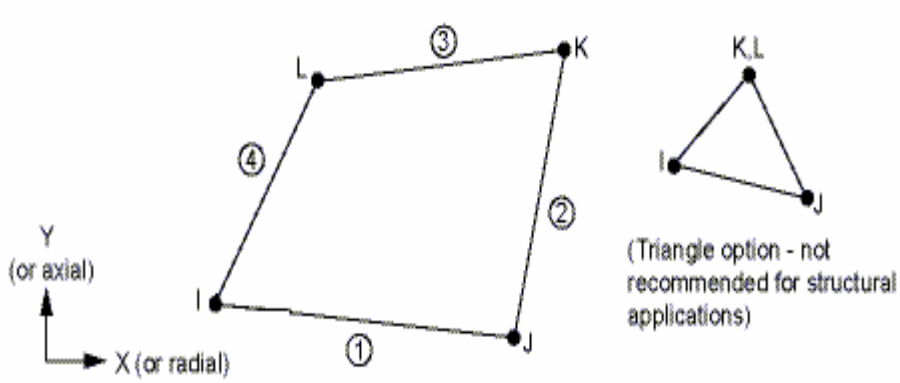

Figure 3.3 Geometry of PLANE 13 [ANSYS, 2004].

PLANE 13 is a type of element that occupies the two-dimensional space. It has four nodes. Each node has two displacements along the X and Y axes respectively. A triangle-shape element can be formed by defining node K and node L in a same

location. Triangle-shape element is more adaptable to complex shapes of the object. Due to the regularity in shape with a real PZT actuator, the quadrilateral-shape element was chosen to model the piezoelectric actuator in the two-dimensional space. For the problem under study in this thesis, KEYOPT (1) = 7 (see Fig. 3.4) was chosen.

DISCIPLINE	**DEGREES OF FREEDOM**	**ACTIVATION**
Magnetic	AZ	KEYOPT (1) =0
Thermal	TEMP	KEYOPT (1) =2
Structural	UX, UY	KEYOPT (1) =3
Coupling of structural, thermal and magnetic	UX, UY, TEMP, AZ	KEYOPT (1) =4
Thermal and Magnetic	VOLT, AZ	KEYOPT (1) =6
Coupling of structural and electrical	UX, UY, VOLT	KEYOPT (1) =7

Figure 3.4 Disciplines in PLANE 13.

DEGREES OF FREEDOM	MEANING
UX	Translation in the X direction
UY	Translation in the Y direction
UZ	Translation in the Z direction
TEMP	Temperature
VOLT	Electric potential (source current)
MAG	Scalar magnetic potential
AZ	Z-component of vector magnetic potential

Figure 3.5 Degrees of freedoms.

3.2.2 Piezoelectric material data

- *Manufacturer data versus ANSYS data*

Section 2.2.2 presented and discussed the entire data specification of the PZT actuator (in particular, those material properties for the AE0505D16 model from TOKIN). However, not every single data presented in Section 2.2.2 is required in modeling the PZT actuator with ANSYS. There are two reasons for this situation.

First, the real piezoelectric materials entail the mechanical and electrical dissipations, strong non-linear behavior, hysterisis effects, and aging effects [IEEE, 1978]. However, these characteristics are not considered in a linear theory of piezoelectricity

by Allik and Hughes [1970]. The linear theory of piezoelectricity is a theory in which the elastic, piezoelectric, and dielectric coefficients are treated as constants. In the real situation, the elastic, piezoelectric and dielectric coefficients are in the form of functions of the magnitude and frequency of applied mechanical stresses and electric fields. Allik and Hughes [1970] laid a foundation of the mathematical procedure of ANSYS in solving a piezoelectric material problem. Therefore, ANSYS only considers those properties, including elastic constant matrix, permittivity constant matrix and piezoelectric constant matrix. *Second*, the entire data specification of the PZT actuator is to provide the complete measured performance of the PZT actuators under certain testing conditions. Particular applications may only need a subset of these conditions. Therefore, they may only need a subset of the material property data.

Furthermore, the data specification from manufacturers cannot be directly entered into the ANSYS program. This is because the matrix format supplied by most of the PZT manufacturers (including TOKIN) do not have the same definition as the matrix formats provided by ANSYS. Such a gap in the material property data between the manufacturer and ANSYS can be further illustrated.

ANSYS requires three types of data for modeling the PZT actuator, which are the stiffness matrix (mechanical discipline), permittivity at constant strain (electrical discipline) and piezoelectric stress matrix (coupling-discipline between mechanical and electrical disciplines). However, most PZT manufacturers only provide compliance matrix (mechanical discipline), permittivity at constant stress (electrical discipline) and piezoelectric strain matrix (coupling-discipline between mechanical and electrical disciplines). Thus, a conversion to create the same definition is necessary. Such a conversion is realized by a program called PIEZMAT macro provided by ANSYS.

- *The PIEZMAT macro*

The work of Allik and Hughes [1970] that underlies the mathematical procedure of ANSYS in solving a piezoelectric problem resulted in the constitutive equations for piezoelectricity, and such equations are represented in ANSYS as follows:

$$\{T\} = [c^E]\ \{S\} - [e]\ \{E\} \tag{3.1}$$

$$\{D\} = [e]^T\{S\} + [\varepsilon^S]\ \{E\} \tag{3.2}$$

where $\{T\}$: stress vector (six components x, y, z, xy, yz, xz),
$\{S\}$: strain vector (six components x, y, z, xy, yz, xz),
$\{D\}$: electric displacement vector (three components x, y, z),
$\{E\}$: electric field vector (three components x, y, z),
$[c^E]$: stiffness matrix evaluated at constant electric field,
$[e]$: piezoelectric matrix relating stress and electric field,
$[e]^T$: transpose of [e],
and $[\varepsilon^S]$: dielectric matrix evaluated at constant strain.

However, most of the manufacturers of piezoelectric materials publish the data specification based upon the following equations:

$$\{S\} = [s^E]\ \{T\} + [d]\ \{E\} \tag{3.3}$$

$$\{D\} = [d]^T\{T\} + [\varepsilon^T]\ \{E\} \tag{3.4}$$

where $\{T\}$: stress vector (six components x, y, z, yz, xz, xy),
$\{S\}$: strain vector (six components x, y, z, yz, xz, xy),
$\{D\}$: electric displacement vector (three components x, y, z),
$\{E\}$: electric field vector (three components x, y, z),
$[s^E]$: compliance matrix evaluated at constant electric field,
$[d]$: piezoelectric matrix relating strain and electric field,

$[d]^T$: transpose of [d],

and $[\varepsilon^T]$: dielectric matrix evaluated at constant stress.

ANSYS requires the data specifications (in particular piezoelectric matrix, compliance matrix and permittivity matrix) that provide their data specifications based on Eqns. (3.1) and (3.2). However, the PZT manufacturers are based on Eqns. (3.3) and (3.4). In order to realize the conversion, Eqns. (3.3) and (3.4) can be rewritten into the following forms:

$$\{S\} = [s^E]\{T\} + [d]\{E\} \qquad \textit{from Eqn. (3.3)}$$

$$[s^E]\{T\} = \{S\} - [d]\{E\}$$

$$\{T\} = [s^E]^{-1}[S] - [s^E]^{-1}[d]\{E\} \qquad (3.5)$$

$$\{D\} = [d]^T\{T\} + [\varepsilon^T]\{E\} \qquad \textit{from Eqn. (3.4)}$$

$$\{D\} = [d]^T\{[s^E]^{-1}[S] - [s^E]^{-1}[d]\{E\}\} + [\varepsilon^T]\{E\}$$

$$\{D\} = [d]^T[s^E]^{-1}[S] + ([\varepsilon^T] - [d]^T\{s^E\}^{-1}[d])\{E\} \qquad (3.6)$$

Comparing Eqns. 3.5 and 3.6 with Eqns. 3.1 and 3.2, respectively, results in the following relations.

$$[c^E] = [s^E]^{-1} \qquad (3.7)$$

$$[\varepsilon^S] = [\varepsilon^T] - [d]^T\{s^E\}^{-1}[d] \qquad (3.8)$$

$$[e] = \{s^E\}^{-1}[d] = [d]^T[s^E]^{-1} \qquad (3.9)$$

3.3 Kinematic Analysis of the RRR Mechanism

Zou [2000] presented a preliminary study on the kinematic analysis of the RRR mechanism using ANSYS. The model is parametric in the sense that a set of kinematic parameters govern the model. The model used the quadrilateral element type. This model suffers from the following defects: *First*, there are some poor shaped elements (see Fig. 3.6). This point was also observed by Zettl [2003]. *Second*,

the PZT actuator is not considered in the model. Specifically time-dependent prescribed motions at three actuators are implemented by giving the time-dependent nodal displacement. This has introduced a considerable approximation with respect to the real situation. The next several sub-sections will discuss how these limitations are overcome to result in a better model.

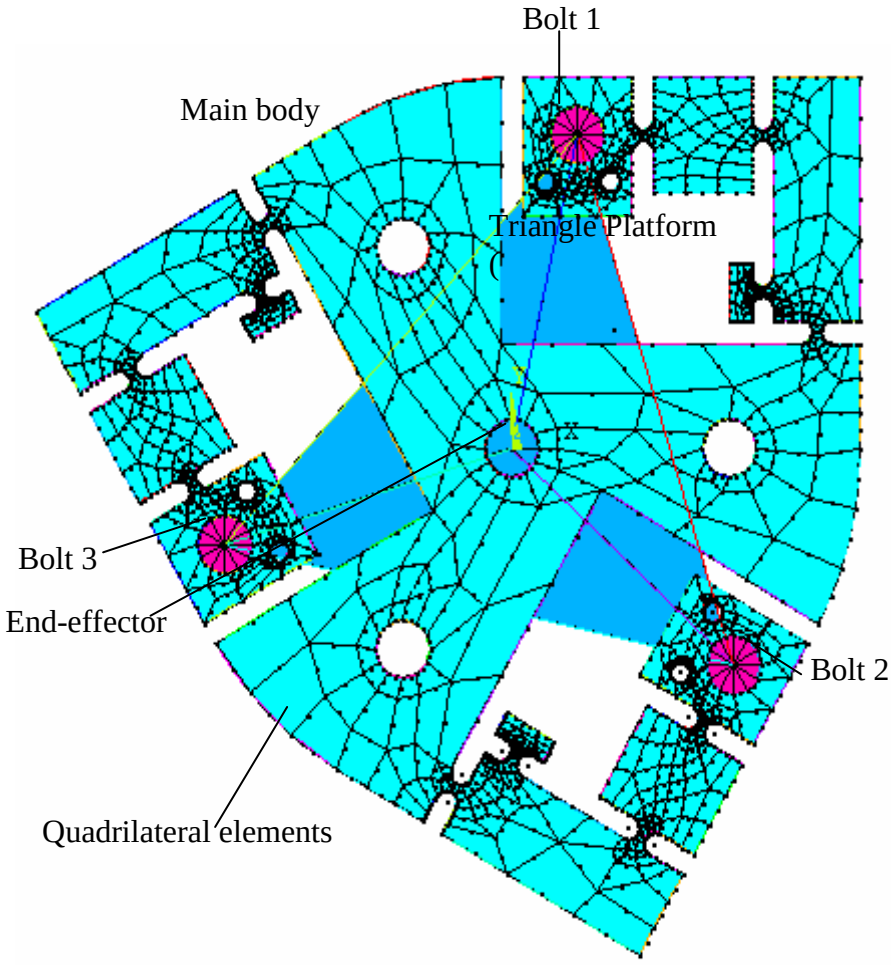

Figure 3.6 Zou's Finite Element Model of the RRR mechanism.

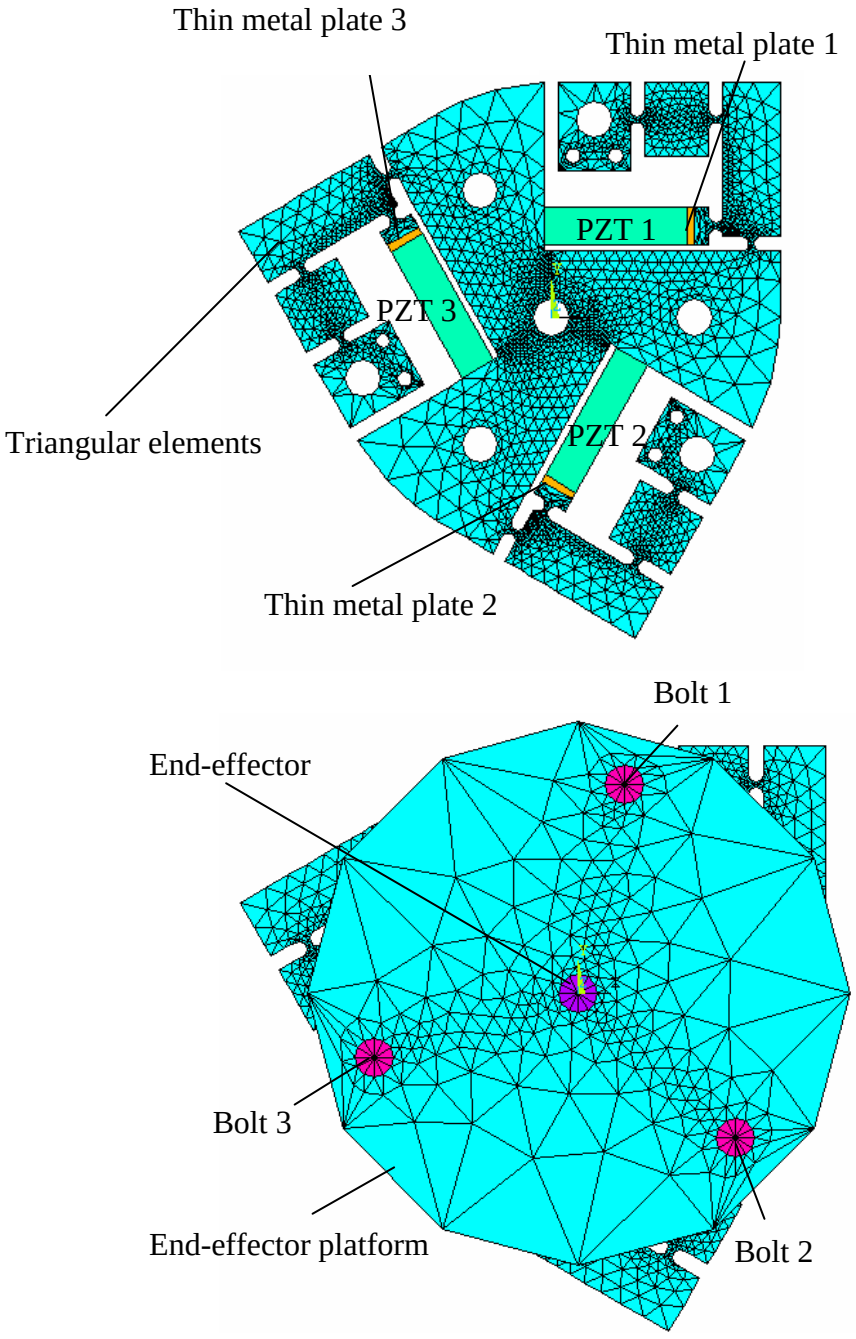

Figure 3.7 Finite Element Model of the RRR mechanism in this thesis.

Note that the physical prototype of the RRR mechanism can be found in Appendix A. Fig. 3.7 illustrates the current finite element model of the RRR mechanism. The

model takes the piezoelectric actuators behavior into consideration. The triangular elements with 6 nodes (Fig. 3.7) replace the previous quadrilateral elements with 8 nodes (Fig. 3.6). By considering the fact that the shape of the actual end-effector platform in the experiment is circular, hence, the shape of the end-effector platform in the current finite element model is also modeled to be circular.

To avoid the three-dimensional analysis that requires tedious and large numerical effort, the RRR mechanism was modeled by two-dimensional finite elements. For the two-dimensional finite element, one needs to determine whether to apply the plane stress or the plain strain model. Zou [2000] used the plane stress model for the RRR mechanism by arguing the depth of the RRR mechanism was considerably thin. Zettl [2003] observed that in the region of the flexural hinge, the plane stress model was not a proper choice based on a three-dimensional finite element analysis conducted by him. This observation does imply a finite element model which takes the plane stress for most of the regions of the compliant mechanism and the plane strain for the region of the flexure hinge. However, the physical setting upon which Zettl [2003] made his observation, is an “isolated” flexural hinge in the sense he considered the material other than the flexure hinge to be rigid. In the real mechanism, the flexural hinge is somewhat “merged” in a relatively large main body that deforms substantially, and that material is very thin. Therefore, the plane strain behavior in a small region may be constrained by the plane stress behavior in a relatively large region, which is a speculation. In this thesis work, the plane stress model was applied for the whole region of the material except for the PZT actuator which was modeled with the plane strain model. The plane strain model was chosen to model the two-dimensional PZT actuator because its deformation results were closer to the deformation results of the three-dimensional PZT actuator in the finite element model. Such a treatment may help examine the speculation, as raised before.

Fig. 3.8 is to facilitate explanation of the motion nature of the RRR mechanism. In the current finite element model, one may input directly the electrical voltages on the PZT actuators in the so-called parametric PZT loading constants. The parametric

loading constants are the constants that are placed in the beginning of the developed ANSYS codes such that the user may vary or change the loading conditions of the PZT actuators without any difficulty. The location of the nodes, in which the electrical voltages are applied, is given in the following example. If one wants to apply (100, 80, 0) volts onto (PZT 1, PZT 2 and PZT 3), the locations of the nodes, in which the electrical voltages are applied, are given in Fig. 3.9. It should be noted that the indicated nodes in Fig. 3.9 belong to the piezoelectric element.

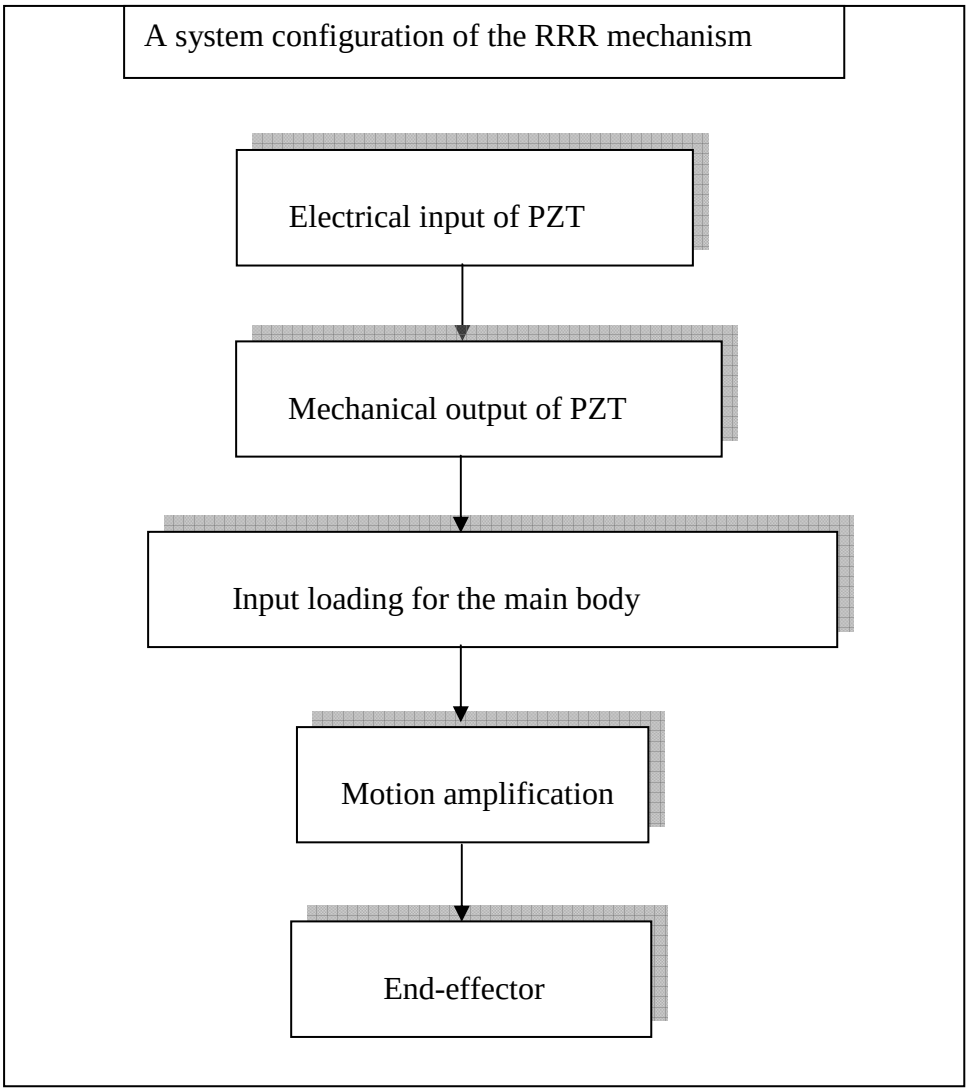

Figure 3.8 The motion nature of the RRR mechanism.

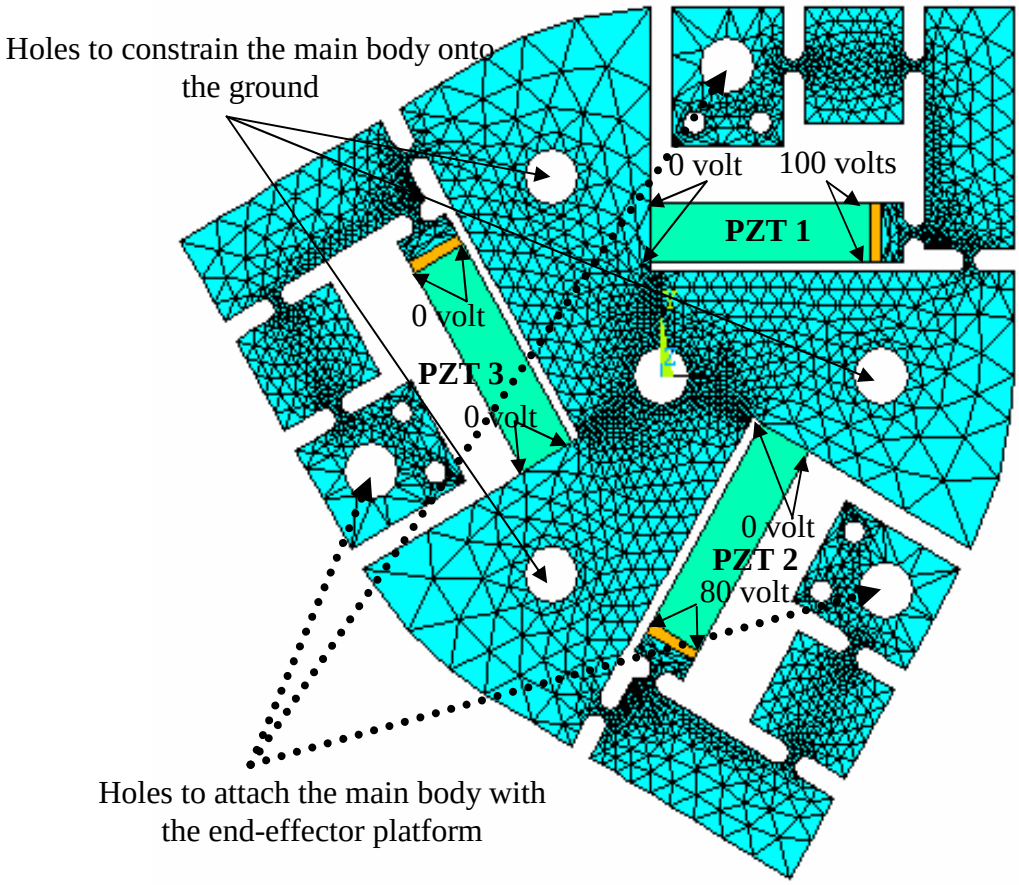

Figure 3.9 The application of electrical input on the PZT actuators.

Due to its coupling-field nature, the PZT converts the applied electrical current into mechanical deformation (the mechanical output of PZT; see Fig. 3.8). The mechanical deformations of the PZT actuators then push the material in the direction of the PZT actuators' deformations. The specially designed notches and holes on the material amplify these deformations during the process of transferring the actuator's deformations onto the displacement of the end-effector platform (the circular plate as illustrated in Fig. 3.7). It should be noted that the end-effector platform is connected to the material by use of bolts. After the deformations from the PZT actuators have been completely transferred, the whole system will be at a rest position. An achieved position and orientation of the end-effector at rest due to the electrical inputs of the PZT actuators (PZT 1, PZT 2 and PZT 3) are defined as one system configuration. Therefore, to achieve a different system configuration, one uses different values of

the PZT actuators (PZT 1, PZT 2, and PZT 3). Because there are numerous possible different values of the PZT actuators, consequently the RRR mechanism also has numerous system configurations. In this way, one sees a series of changes of configurations, which is translated to the kinematic motions from a view point of rigid body mechanisms.

3.4 Modeling of the PZT Actuator for the RRR Mechanism

For the RRR mechanism driven by the PZT actuator, the modeling of the PZT actuator is described as follows:

Step 1. Choose a suitable type of finite element

The RRR mechanism, i.e., the compliant material, is considered as a planar finite element problem. Furthermore, the plane stress model was considered over the whole material region. There could be some errors produced due to such a treatment (i.e., the planar finite element problem). However, the error produced at the end-effector is relatively small in comparison with the measured result (see Chapter 5 for the deformation results at the end-effector). To incorporate the finite element model of the PZT actuator into that of the RRR mechanism (without the PZT element), two finite element models must be consistent. In this connection, element type (PLANE 13) is chosen for modeling the PZT actuator.

Fig. 3.10 shows the geometric boundaries of the actual piezoelectric actuator. The piezoelectric actuator has dimensions of 5 x 5 x 20 mm. In ANSYS, the geometry of the PZT actuator was created by use of its solid modeling.

Step 2. Build the PZT actuator in ANSYS

a. Create a geometric model of the PZT actuator

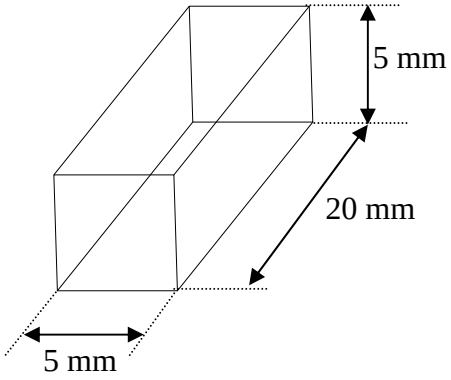

Figure 3.10 Geometric boundaries of the PZT actuator.

b. Inputting the manufacturer data into ANSYS format

The modeled material properties of the PZT actuator in ANSYS consist of mechanical matrix (compliance constant matrix), electrical matrix (permittivity constant matrix), and mechanical-electrical matrix (piezoelectric constant matrix). Each type of matrix is discussed as follows (note that the polarization of the PZT actuator is in the direction of the Z-axis before working on these three-dimensional matrices).

- Mechanical matrix (compliance constant matrix)

$$[s^E] = \begin{bmatrix} s_{11}^E & s_{12}^E & s_{13}^E & 0 & 0 & 0 \\ & s_{11}^E & s_{13}^E & 0 & 0 & 0 \\ & & s_{33}^E & 0 & 0 & 0 \\ & & & \dfrac{1}{2(s_{11}^E - s_{12}^E)} & 0 & 0 \\ & & & & s_{44}^E & 0 \\ & & & & & s_{44}^E \end{bmatrix} \qquad (3.10)$$

Eqn. (3.10) shows the arrangement of the manufacturer data within the ANSYS format. Such an arrangement occurs because the manufacturer's data has mechanical vector in the form {x, y, z, yz, xz, xy}, whereas ANSYS's mechanical vector is in the

form {x, y, z, xy, yz, xz}. [s^E] is the compliance constant matrix obtained at constant electrical field. The first subscript indicates the direction of strain, while the second subscript indicates the direction of stress. To completely model the three-dimensional manufacturer's material data in ANSYS, the properties of the compliance matrix ($s_{11}^E, s_{12}^E, s_{13}^E, s_{33}^E,$ and s_{44}^E) are required. Note however that the manufacturer of the PZT actuator in this thesis (TOKIN) only supplies two kinds of material properties (s_{11}^E and s_{33}^E). To completely model the three-dimensional manufacturer's material data in ANSYS, hence, the other material properties ($s_{12}^E, s_{13}^E,$ and s_{44}^E) are to be computed. To facilitate computation, [s^E] can also be presented in the format shown in Eqn. (3.11).

$$[s^E] = \begin{bmatrix} \frac{1}{E_X} & \frac{-\nu_{XY}}{E_X} & \frac{-\nu_{XZ}}{E_X} & 0 & 0 & 0 \\ & \frac{1}{E_Y} & \frac{-\nu_{YZ}}{E_Y} & 0 & 0 & 0 \\ & & \frac{1}{E_Z} & 0 & 0 & 0 \\ & & & \frac{1}{G_{XY}} & 0 & 0 \\ & & & & \frac{1}{G_{YZ}} & 0 \\ & & & & & \frac{1}{G_{XZ}} \end{bmatrix} \quad (3.11)$$

By comparing Eqn. (3.10) and Eqn. (3.11), Eqn. (3.12a-f) can be presented as follows.

$$E_X = \frac{1}{s_{11}^E} = E_Y \quad (3.12a)$$

$$E_Z = \frac{1}{s_{33}^E} \quad (3.12b)$$

$$G_{XY} = \frac{1}{2(s_{11}^E - s_{12}^E)} = \frac{E_X}{2(1+\upsilon_{xy})} \quad (3.12c)$$

$$G_{YZ} = \frac{1}{s_{44}^E} = G_{XZ} \quad (3.12d)$$

$$\nu_{XY} = -\frac{s_{12}^E}{s_{11}^E} \tag{3.12e}$$

$$\nu_{YZ} = -\frac{s_{13}^E}{s_{33}^E} = \nu_{XZ} \tag{3.12f}$$

where E_x : Young's modulus in the x direction,

ν_{XY} : Poisson's ratio in the X and Y directions,

G_{XY} : shear modulus in the XY plane,

G_{YZ} : shear modulus in the YZ plane,

and G_{XZ} : shear modulus in the XZ plane.

Besides s_{11}^E and s_{33}^E, the poisson ratio of AE0505D16 (ν_{XZ}) is given by the manufacturer. s_{13}^E can be found through Eqn. (3.12f). s_{12}^E is assumed to be zero, while s_{44}^E can be found through Eqn. (3.12c) and Eqn. (3.12d) by assuming $G_{XY} = G_{YZ} = G_{XZ}$. Thus, s_{44}^E can be expressed by $2(s_{11}^E - s_{12}^E)$.

- Electrical matrix (permittivity constant matrix)

Most manufacturers (including TOKIN), presents permittivity matrix of the material evaluated under the condition of constant stress $[\varepsilon^T]$, while ANSYS requires the permittivity matrix of the material evaluated under the condition of constant strain $[\varepsilon^T]$. The first subscript in the matrix $[\varepsilon^T]$ indicates the direction of the dielectric displacement and the second subscript indicates the direction of the electrical field. PIEZMAT macro, which is also based on Eqn. (3.8) in particular, is to perform conversion. The permittivity constant material in Eqn. (3.13) is input into ANSYS.

$$[\varepsilon^S] = \begin{bmatrix} \varepsilon_{11}^S & 0 & 0 \\ 0 & \varepsilon_{11}^S & 0 \\ 0 & 0 & \varepsilon_{33}^S \end{bmatrix} \tag{3.13}$$

- Mechanical-electrical matrix (piezoelectric constant matrix)

$$[d] = \begin{bmatrix} 0 & 0 & 0 & 0 & d_{15} & 0 \\ 0 & 0 & 0 & d_{15} & 0 & 0 \\ d_{31} & d_{31} & d_{33} & 0 & 0 & 0 \end{bmatrix} \quad (3.14)$$

Eqn. (3.14) shows the arrangement of the piezoelectric constant matrix from the manufacturer's data within the ANSYS format. The matrix $[d]$ presents the piezoelectric constant matrix that describes the relationship between strain (mechanical properties) and a specified electrical field (electrical properties). The first subscript indicates the direction of the electrical field, while the second subscript indicates the direction of strain.

There are several notes that one needs to pay attention regarding modeling the PZT actuator by using ANSYS. *First*, the author employed several ANSYS versions (from ANSYS educational version 5.5 until ANSYS educational version 8.1) in modeling the PZT actuator by using ANSYS. The author has found that ANSYS has been updating its features in a gradual manner. In ANSYS educational version 8.1, ANSYS has added new features and new types of elements that eliminate the need of using the PIEZMAT macro. In particular, there are some new kinds of multidisciplinary elements that are capable of modeling the piezoelectric actuator directly based on the manufacturer data, i.e. PLANE 223, SOLID 226, and SOLID 227. *Second*, it is necessary to ensure that the test method and terminology related to the PZT actuator have been standardized. Some manufacturers might use their own test method. Thus, it is very important to consult with the manufacturer prior to performing any kind of modeling regarding the defined material properties in the data specification.

The general model of the PZT finite element model is three-dimensional with the Z-axis as the polarization direction. For the two-dimensional PZT element (PLANE

13), the Y-axis is the polarization direction. Therefore, there is a need of transformation from the 3-D material property matrix to the 2-D material property matrix. The transformation is implemented by Eqn. (3.15), Eqn. (3.16) and Eqn. (3.17).

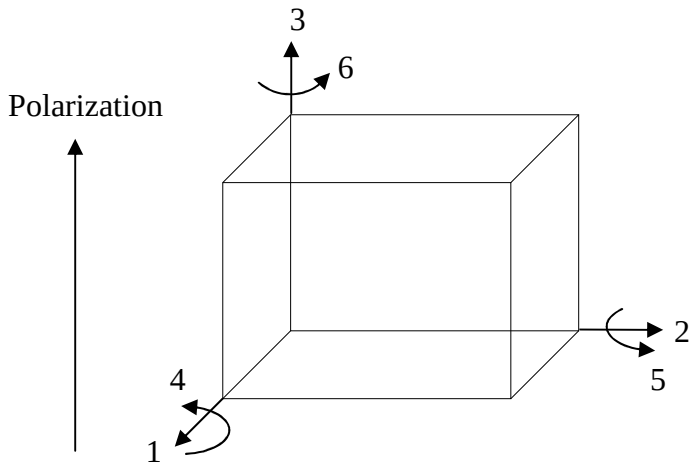

Figure 3.11 Axis of piezoelectric material.

$$\left[\varepsilon^{S}\right]=\begin{array}{c}\begin{matrix}\text{X} & \text{Y} & \text{Z}\end{matrix}\\ \begin{bmatrix}\varepsilon_{11}^{S} & 0 & 0\\ 0 & \varepsilon_{11}^{S} & 0\\ 0 & 0 & \varepsilon_{33}^{S}\end{bmatrix}\end{array}\begin{matrix}\text{X}\\ \text{Y}\\ \text{Z}\end{matrix}\longrightarrow\begin{array}{c}\begin{matrix}\text{X} & \text{Y}\end{matrix}\\ \begin{bmatrix}\varepsilon_{11}^{S} & 0\\ 0 & \varepsilon_{33}^{S}\end{bmatrix}\end{array}\begin{matrix}\text{X}\\ \text{Y}\end{matrix}\qquad(3.15)$$

$$[e]=\begin{array}{c}\begin{matrix}\text{X} & \text{Y} & \text{Z}\end{matrix}\\ \begin{bmatrix}0 & 0 & e_{31}\\ 0 & 0 & e_{31}\\ 0 & 0 & e_{33}\\ 0 & 0 & 0\\ 0 & e_{15} & 0\\ e_{15} & 0 & 0\end{bmatrix}\end{array}\begin{matrix}\text{X}\\ \text{Y}\\ \text{Z}\\ \text{XY}\\ \text{YZ}\\ \text{XZ}\end{matrix}\longrightarrow\begin{array}{c}\begin{matrix}\text{X} & \text{Y}\end{matrix}\\ \begin{bmatrix}0 & e_{31}\\ 0 & e_{33}\\ 0 & e_{31}\\ e_{15} & 0\end{bmatrix}\end{array}\begin{matrix}\text{X}\\ \text{Y}\\ \text{XY}\\ \text{XZ}\end{matrix}\qquad(3.16)$$

$$[s^E] = \begin{array}{c} \begin{matrix} X & Y & Z & XY & YZ & XZ \end{matrix} \\ \begin{bmatrix} s_{11}^E & s_{12}^E & s_{13}^E & 0 & 0 & 0 \\ & s_{11}^E & s_{13}^E & 0 & 0 & 0 \\ & & s_{33}^E & 0 & 0 & 0 \\ & & & 2(s_{11}^E - s_{12}^E) & 0 & 0 \\ & & & & s_{44}^E & 0 \\ & & & & & s_{44}^E \end{bmatrix} \end{array} \begin{matrix} X \\ Y \\ Z \\ XY \\ YZ \\ XZ \end{matrix} \longrightarrow \begin{array}{c} \begin{matrix} X & Y & XY & XZ \end{matrix} \\ \begin{bmatrix} s_{11}^E & s_{12}^E & s_{13}^E & 0 \\ & s_{33}^E & s_{12}^E & 0 \\ & & s_{11}^E & 0 \\ & & & s_{44}^E \end{bmatrix} \end{array} \begin{matrix} X \\ Y \\ XY \\ XZ \end{matrix} \quad (3.17)$$

Step 3. Mesh the PZT element

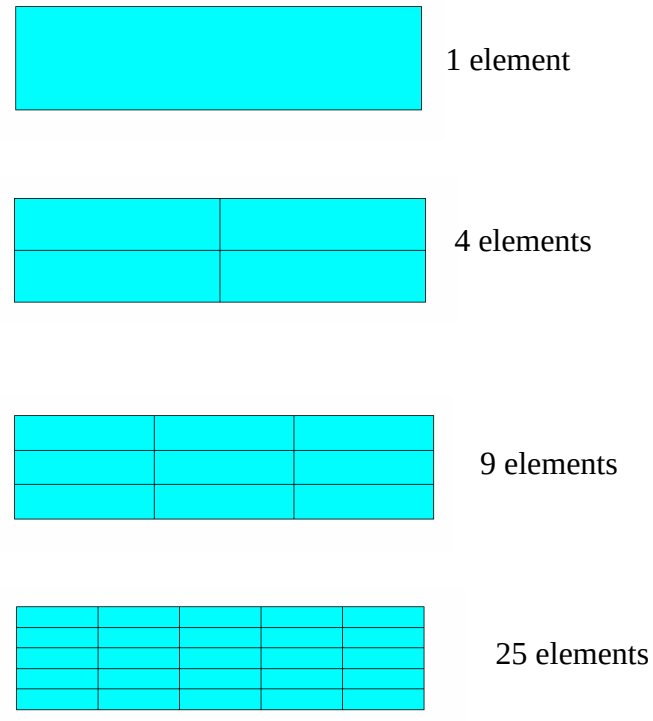

Figure 3.12 Different types of meshing density on PZT

Fig. 3.12 shows several meshing schemes for the PZT element. The objective here was to find the least number of elements without loss of accuracy. This work investigated twelve possible mesh configurations for various different loadings. The ANSYS results indicated that there was no significant difference in the PZT motions

for the twelve mesh configurations. Therefore the one element mesh configuration was chosen to model the PZT actuator.

3.5 Finite Element Modeling of the PZT RRR Mechanism

The PZT actuator and the RRR material are assembled into the RRR mechanism, which is called the PZT RRR mechanism. There are several issues to be addressed for modeling the PZT RRR mechanism, and they are discussed as follows.

- *Model the prestress of the PZT Actuator*

The effect of the prestress in finite element modeling is such that the nodes at the interface are the subject to the extra workload. This load is calculated with the following equation:

$$F = E \times A \times \frac{\Delta l}{l} \tag{3.18}$$

where F : the prestress force or load (N),

E : the Young modulus of the PZT material (N/m^2),

A : the cross sectional area of the PZT actuator (m^2),

l : the length of the PZT slot (m),

and Δl : the displaced length of the PZT slot due to the prestress (m).

By measuring Δl (the pre-deformation), one can find F from Eqn. (3.18). For the RRR mechanism concerned, The pre-deformed forces of PZT 1, PZT 2, and PZT 3 are 3.981×10^4N, 2.56667×10^4N, and 5.395×10^4N, respectively. The detailed procedure for measuring Δl can be found in Appendix B.

- *Model the Thin Metal Plate*

The prestress is currently implemented through inserting a metal piece between the PZT actuator and the RRR material; details about the prestress can be found in Appendix B. The metal piece is modeled using the element type COMBIN 14 (see Fig. 3.13). This element is also known as a spring-damper element

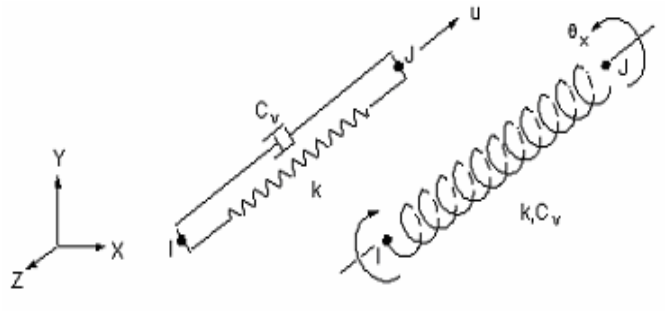

Figure 3.13 COMBIN 14 [ANSYS, 2004]

The stiffness of the COMBIN 14 element can be calculated with the following equation.

$$k = \frac{EA}{L} \tag{3.19}$$

where k : the spring constant (N/m),

E : the Young modulus of the plate (N / m^2),

A : the cross-sectional area of the plate (m^2),

and L : the length of the thin metal plate (m).

- *Model PZT within the RRR mechanism*

The relationship among the PZT actuator, the metal piece, and the RRR mechanism is illustrated in Fig. 3.14, where the extra workloads due to the prestress are also shown, respectively.

- *Specify of the boundary conditions*

All the nodes along the perimeter of A, B and C are constrained such that these nodes do not translate (see Fig. 3.15). This is to represent the fact that the RRR mechanism is fixed onto the ground.

- *Model the bolts*

The bolts E, F and G (see Fig. 3.15) in the PZT RRR mechanism fasten the main body with the end-effector platform. The modeling should ensure that all the corresponding elements share the same nodes on the interfaces. To ensure that the main body and the bolts share the same nodes, the mesh for the bolts was developed manually. First, a node in the center was created. Next, the element of the bolt was created by connecting the node in the center with the nodes of the main body which interface with the bolts.

- *Model the end-effector platform*

The finite element model of the end-effector platform should be able to accurately receive the transferred deformations from the bolts and the main body. First, the circular platform was modeled through the solid modeling facility. Next, the elements of circular platform were developed by use of the automatic meshing facility. At this step, the nodes of the circular platform will in particular follow the location of the nodes of the elements for the bolts which were previously defined.
Consequently, there were two sets of nodes developed. One set of nodes belonged to the end-effector platform, while another set of nodes belonged to the elements of the bolts (see Fig. 3.16). Finally, CP command was used to couple the end-effector platform and the bolts-main body components in ANSYS.

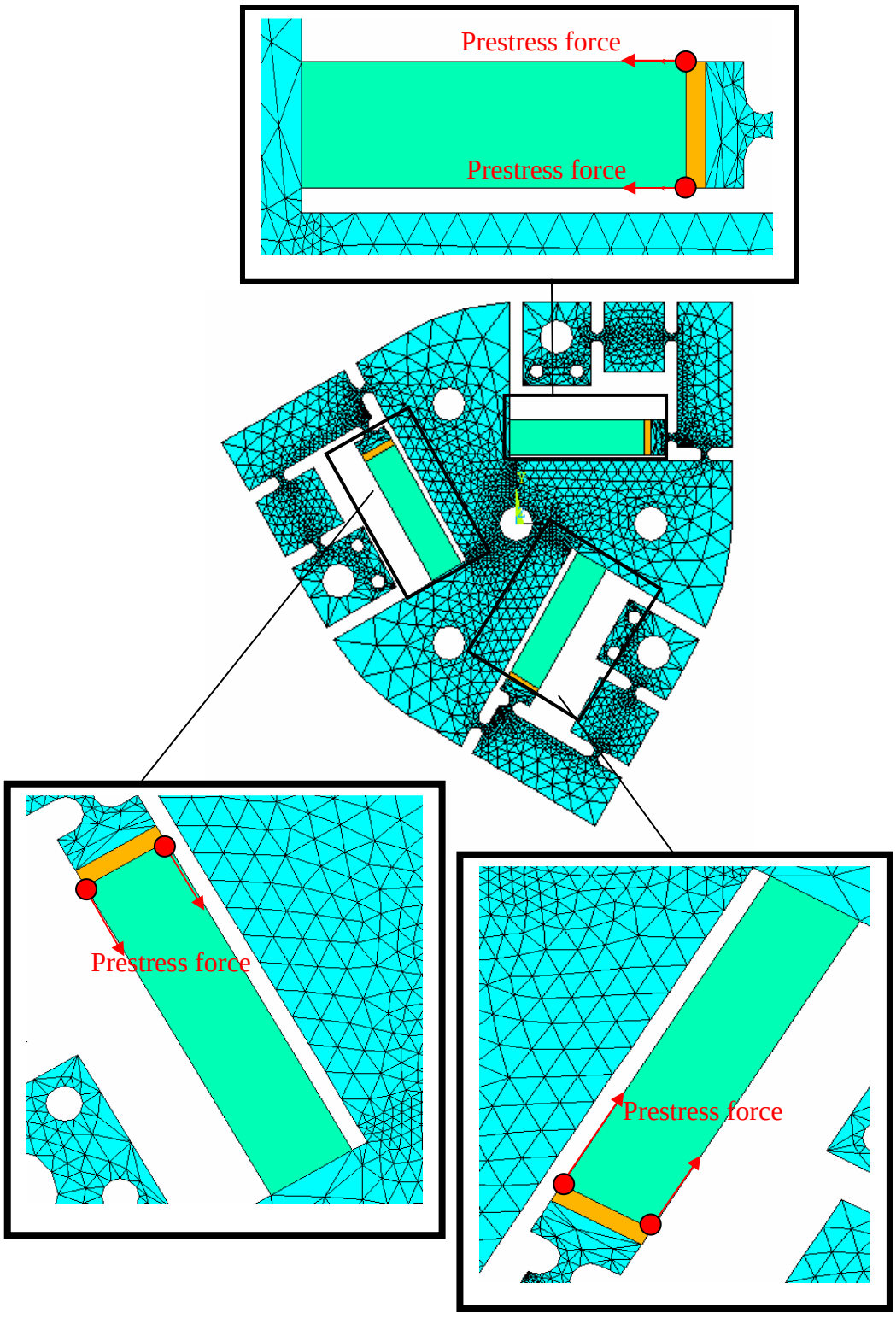
Prestress force
Prestress force
Prestress force
Prestress force

Figure 3.14 The modeled PZT, plate, and compliant piece.

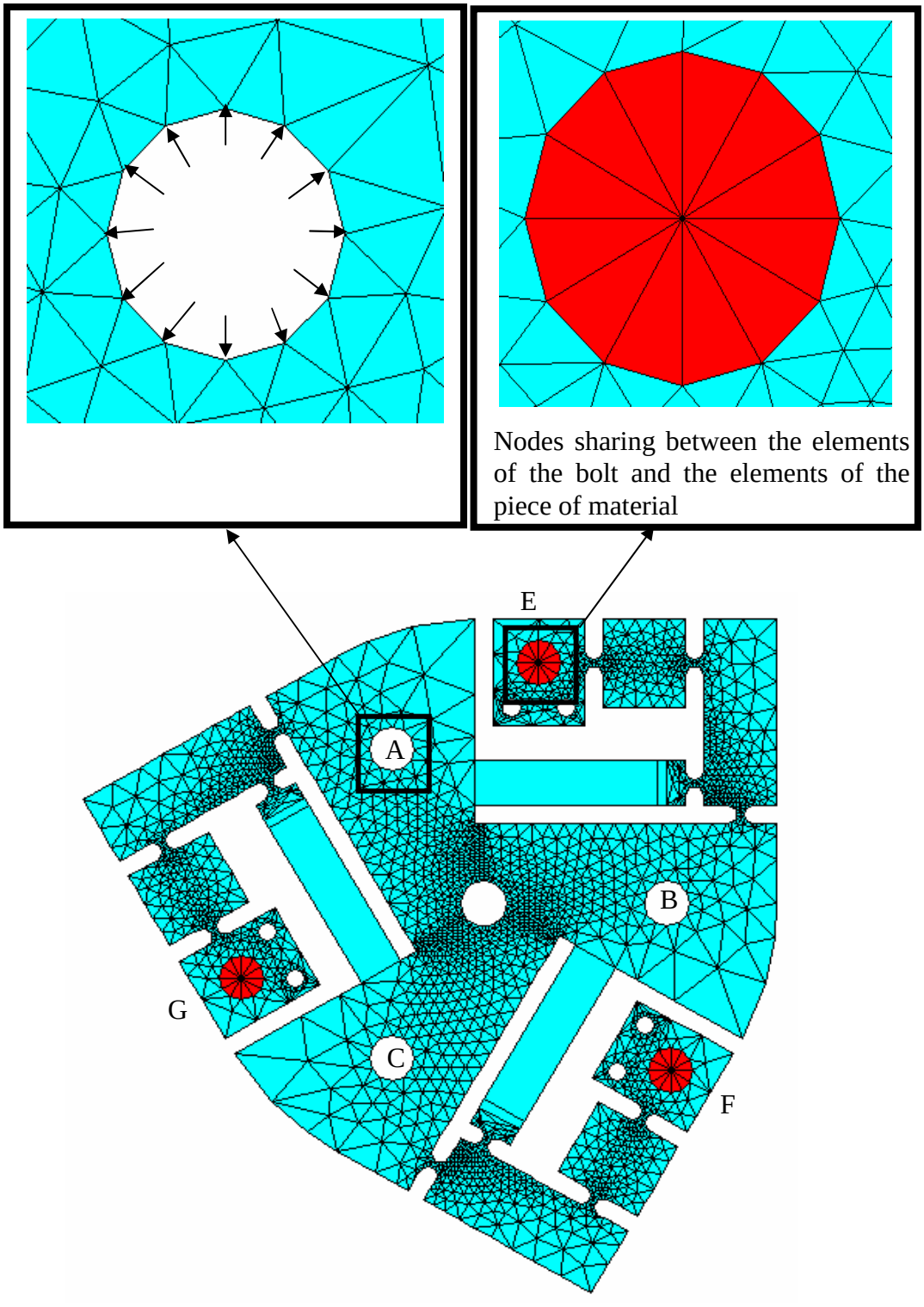

Figure 3.15 Modeling the boundary conditions and the bolts.

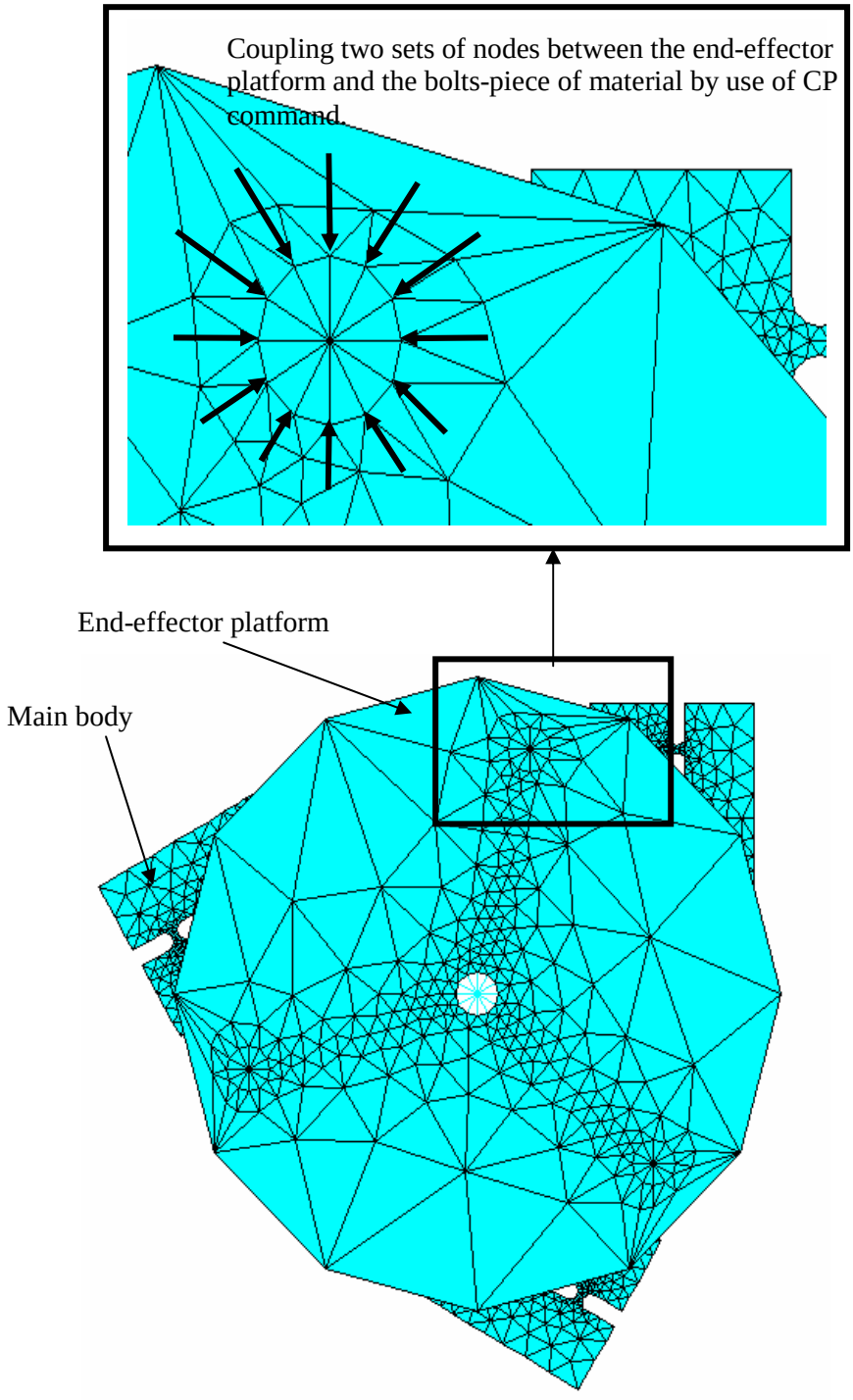

Figure 3.16 Modeling the end-effector platform.

3.6 Illustrations

The purpose of this section is to illustrate the deformations of the RRR mechanism in ANSYS for several critical positions. Generally, to achieve such positions, one needs to apply the electrical voltages into one, or two, or three PZT actuators. Specifically, such positions are divided into three categories: (1) the RRR mechanism positions when only single PZT actuator is activated, as illustrated in Fig. 3.17a, Fig.3.17b and Fig.3.17c, respectively; (2) the positions of the RRR mechanism when two PZT actuators are activated. Fig. 3.18a, Fig 3.18b and Fig. 3.18c respectively illustrate the RRR mechanism positions when PZT 1 and PZT 3, PZT 1 and PZT 2, and PZT 2 and PZT 3 are activated ; (3) the RRR mechanism positions when all the PZT actuators are activated, as illustrated in Fig. 3.19. The shape of the RRR mechanism prior to the loading (so-called the original shape) is indicated by the discrete lines. In other words, the parts of the RRR mechanism that do not situate within the discrete lines have some deformation. In addition, the deformation shapes of the RRR mechanism (see Figs. 3.17, 3.18 and 3.19) are presented by showing the RRR mechanism both with and without the end-effector platform, for the purpose of clarity. The code for this illustration is documented in Appendix C.

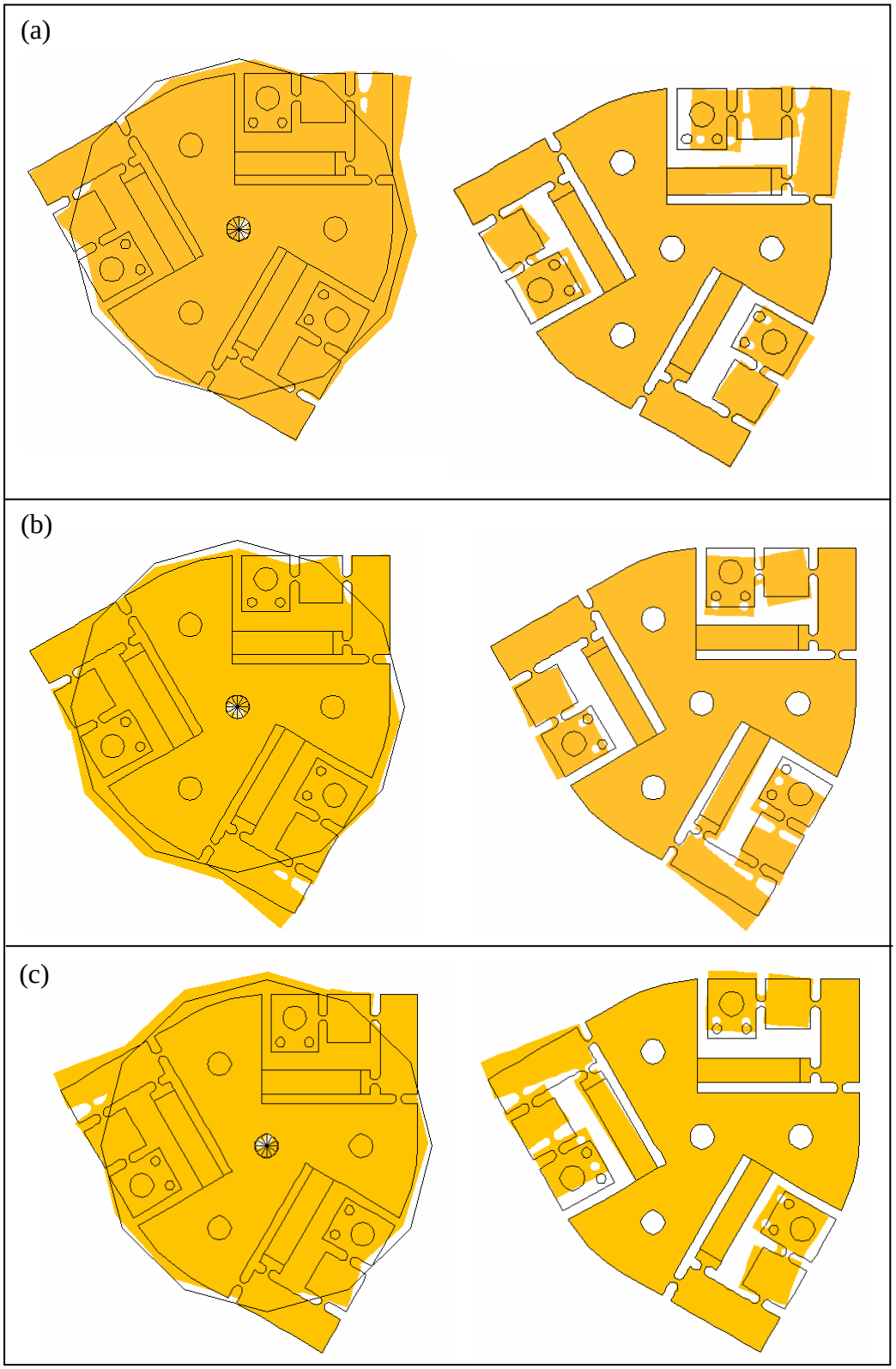

Figure 3.17 The deformation of the RRR mechanism by activating the single PZT actuator (a: PZT 1; b: PZT 2; c: PZT 3).

Figure 3.18 The deformation of the RRR mechanism by activating two PZT actuators (a: PZT 1 and 3; b: PZT 1 and 2; c: PZT 2 and 3).

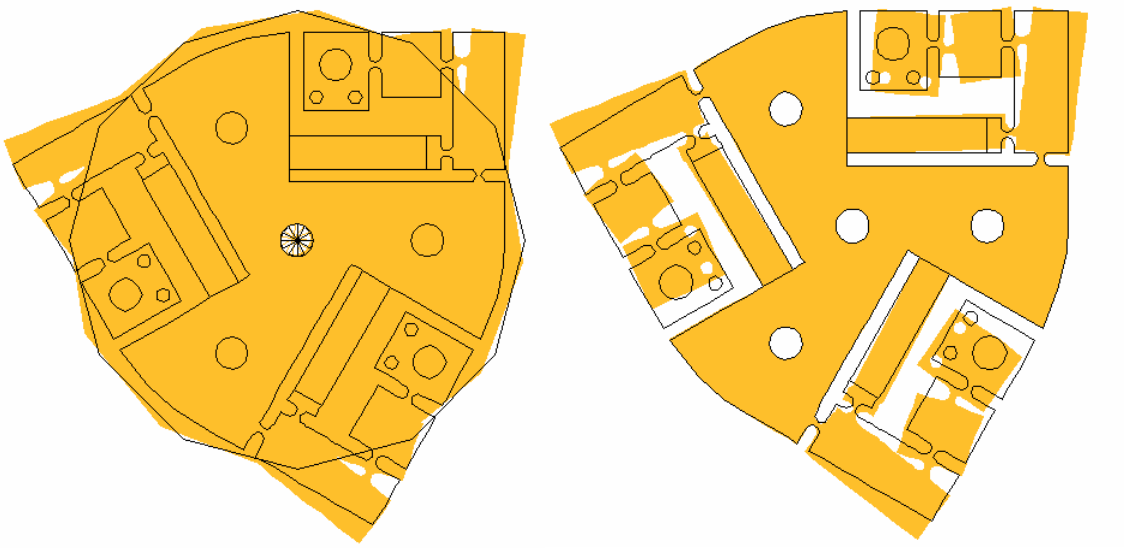

Figure 3.19 The deformation of the RRR mechanism by activating all PZT actuators.

3.7 Summary and Discussion

The ANSYS finite element model of a compliant mechanism driven by three PZT actuators (PZT RRR mechanism for short) was described in this chapter. This model can be used for motion analysis without consideration of inertia. When the voltages of the PZT actuators are prescribed, one can obtain the displacement at the end-effector. From the literature review, it is believed that the model is unique for the problem under study.

Traditionally, the motion analysis of the compliant mechanism is based on a concept called the pseudo rigid body (PRB). In the PRB concept, a compliant mechanism is first modeled by a PRB mechanism, and then motion analysis for the rigid body mechanism is applied to the PRB mechanism (which is now a rigid body mechanism). This procedure is not very accurate, as opposed to finite element approach in general. In the finite element approach, the method developed by Zettl [2003] can be considered as improvement of the PRB method, but it requires the availability of more accurate 3D motion information which is usually obtained

through 3D finite element analysis. 3D finite element modeling and simulation is costly, which may not be available in practical design exercises.

The major disadvantage of a full finite element model, as the one presented in this chapter, is of high computation resource as opposed to the PRB method. This has restricted its application in real time control problem. Another limitation with the model presented here is that it does not consider the inertia in the model.

CHAPTER 4

NATURAL FREQUENCY AND STIFFNESS

4.1 Introduction

As reviewed in Chapter 2, the natural frequency and global stiffness of a compliant mechanism are two very important design indices concerning dynamic behaviors of the mechanism. These two indices are, indeed, traditional elements in structural analysis, but they are not well-studied in the application of mechanisms (especially compliant mechanisms). In this chapter, two approaches based on ANSYS are presented. In particular Section 4.2 addresses the natural frequency, and Section 4.3 addressed the stiffness. Section 4.4 gives a summary.

4.2 Natural Frequency of Compliant Mechanisms

4.2.1 Basic concepts

ANSYS uses modal analysis to compute the natural frequencies of the RRR mechanism**.** Modal analysis aims to find a set of parameters that represents the vibration behavior of a structure. The set of parameters includes the natural frequencies and mode shapes (patterns of vibration). In ANSYS, the modal analysis

uses several numerical methods, which are Reduced Method, Subspace Method, Block Lanczos Method, Damped Method, and QR Damped Method [ANSYS, 2004]. These methods are briefly discussed below.

Reduced Method

Guyan [1965] provides the theoretical basis of the Reduced Method in ANSYS. The reduced method is basically a way to reduce the size of the matrices of a model for the purpose of performing fewer computations. One distinctive feature of this method is the implementation of so-called master degrees of freedom. The master degrees of freedom are the key degree-of-freedoms that characterize the dynamic portion of the model. Thus, instead of considering the entire finite element model, this method requires a user to select the dynamic portion of the model. The key assumption in this method is that the inertia forces on the so-called slave degrees of freedom (those DOF being reduced out, thus the opposite of master degrees of freedom) are negligible compared to elastic forces transmitted by the master DOF. Therefore, the total mass of the structure is divided among only the master DOF. The net result is that the reduced stiffness matrix is exact and the reduced mass matrix is approximate. Consequently, the determination of the master degrees of freedom contributes significantly in the accuracy that can be achieved with this method.

Subspace Method

Bath [1982] and Wilson et al. [1983] provide the theoretical basis of the Subspace Method in ANSYS. The Subspace Method uses the subspace iteration technique, which internally uses the generalized Jacobian iteration algorithm. The algorithm seeks to solve the eigenvalue problem by use of full [K] and [M] matrices. The Subspace Method is much slower than the Reduced Method. This method is typically used in cases where high accuracy is required or where selecting master DOF is not practical. However, this method is not applicable to the system that contains piezoelectricity degrees of freedom.

Block Lanczos Method

Rajakumar et al. [1991] and Grimes et al. [1994] provide the theoretical basis of Block Lanczos method in ANSYS. To solve the eigenvalue problem, the Block uses a combination of the automated shift strategy and the sturm sequence check strategy. The two strategies aim to reduce the number of iterations in solving the eigenvalue problem yet maintaining good accuracy.

Unsymmetric Method

This method uses a combination of the works of Rajakumar [1991] and Wilkinson [1988]. The Unsymmetric Method, which also uses the full [K] and [M] matrices, is meant for problems where the stiffness and mass matrices are unsymmetrical (for example, acoustic fluid-structure interaction problems involving element FLUID 30 and MATRIX 27).

Damped Method

The works of Rajakumar and Ali [1992] and Wilkinson [1988] provide the basis for the damped method. This method is applicable to problems where the damping is considered. The method considers full matrices [K], [M], and [C].

QR Damped Method

The QR damped method combines the advantages of the Block Lanczos Method and the Hessenberg Method. The Hessenberg Method can be found in [Kardestuncer et al. 1987]. The main idea of the QR damped method is to approximately represent the first few complex damped eigenvalues by a linear combination of a small number of eigenvectors of the corresponding undamped system.

Power Dynamics Method

The power dynamics method uses a combination of the subspace method and the preconditioned conjugate gradient (PCG). The PCG is basically an iterative solver in which the equations are not solved directly but instead, an initial estimate of the solution is made, and a computational procedure is defined whereby the estimate is improved until it satisfies the equations within some specified tolerance. The power dynamic method is considerably faster than the subspace method and the block lanczos in computation speed, because this method does not perform a Sturm sequence check and uses a reduced mass matrix (instead of a full mass matrix). Accuracy achieved with this method may be compromised because of the reduced mass matrix.

The Block Lanczos method was chosen in this work to compute the natural frequency. It is noted that for a compliant mechanism, each set of prescribed actuations corresponds to a "frozen" configuration. The natural frequency is then associated with this configuration. In other words, the modal analysis as described before will be applied on this structure. Fig. 4.1 is a flow chart is to compute the natural frequency of the "frozen" structure. Each step in the flow chart is explained below.

4.2.2 Procedure

(1) Finite element modeling

A finite element model of the compliant mechanism must be available prior to computing the natural frequency of the compliant mechanism. For the PZT RRR mechanism, the finite element model presented in Chapter 3 was used.

(2) Selection of a calculation method

As discussed previously, there are seven calculation methods in ANSYS. The Block Lanczos method was selected to compute the natural frequency of the RRR mechanism. This was based on the following reasons. The Reduced Method and the Power Dynamic Method were not chosen because of the accuracy concern. Due to the complex nature of the RRR mechanism, the process of locating master degrees of freedom on the RRR mechanism was difficult. The Power Dynamic Method was not chosen because it also uses a reduced mass approximation, instead of a full mass matrix. The damped method and the QR damped method were not chosen because they are not designed for obtaining the natural frequency information. The unsymmetric method was not chosen because none of the components of RRR mechanism that has the unsymmetric stiffness. Finally, the Subspace Method was not chosen because the RRR mechanism entails the piezoelectricity degree-of-freedom.

(3) Activation of the prestress option is activated

The prestress option is an option in ANSYS to calculate the natural frequencies of this system. The prestress option in ANSYS considers the possibility that a system is prestressed prior to computing the natural frequencies of the system. The prestress option needs to be activated in ANSYS due to the fact that in the modal analysis the system is assumed to be stress-free (by default). However, the PZT RRR mechanism is pre-stressed to become a “frozen” structure. Therefore for the RRR mechanism (or in general compliant mechanism), the prestress option should be considered.

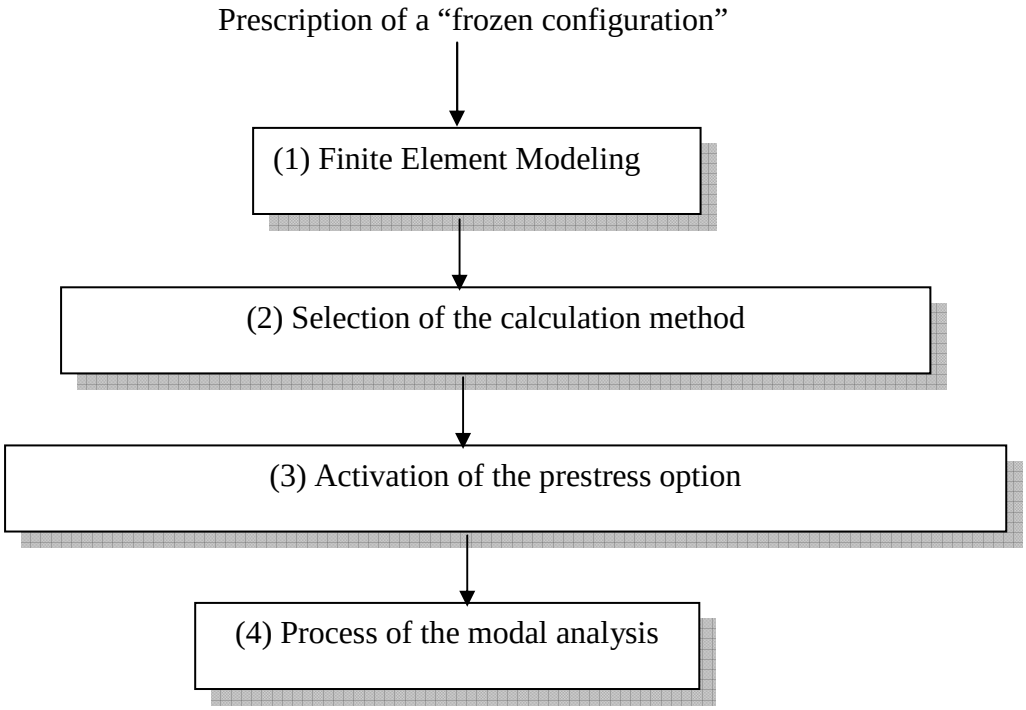

Figure 4.1 The procedure to compute the system frequency.

4.2.3 Validation

The work performed by Kitis and Lindenberg [1989] was used to validate the proposed approach described in Section 4.2.2. They used the transfer matrix method to compute the natural frequencies of a four-bar mechanism (see Fig. 4.2) for several configurations. Different configurations are determined by giving different values of the crank angle (θ_2). A finite element model of this mechanism can be found from Appendix E.6. In their work, they used two modeling strategies for a component. The first, two segments were chosen to model each component (also called model 2); the second, three segments were chosen to model each component (also called model 3). Our finite element model corresponded to their model 2 (two finite elements used for one component) and model 3 (three finite elements used for one component). Fig. 4.3, Fig. 4.4, and Fig. 4.5 present the results of comparison between their approach and our approach, in particular the first mode, the second mode, and the third mode, respectively. Fig 4.3 shows a strong correlation between their approach and our

approach when the crank angle is from 0 to 250 degrees. However, two of the largest deviations occur when the crank angles are 300 degrees (8 rad/sec or 1.273 Hz) and 350 degrees (30 rad/sec or 4.77 Hz), respectively. Fig 4.4 indicates also some good agreement. For model 2 in Fig. 4.4a, the results of natural frequency for the second mode show that the largest deviation occur when the crank angle is 100 degrees (9 rad/sec or 1.432 Hz), while for model 3 in Fig. 4.4.b, the results of the natural frequency for the second mode show that the largest deviation occur when the crank angle is also 100 degrees (6.74 rad/sec or 1.073 Hz).

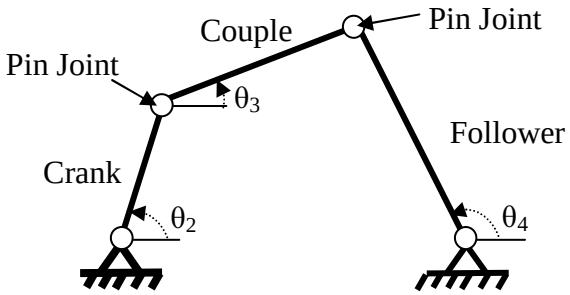

Figure 4.2 A four-bar mechanism.

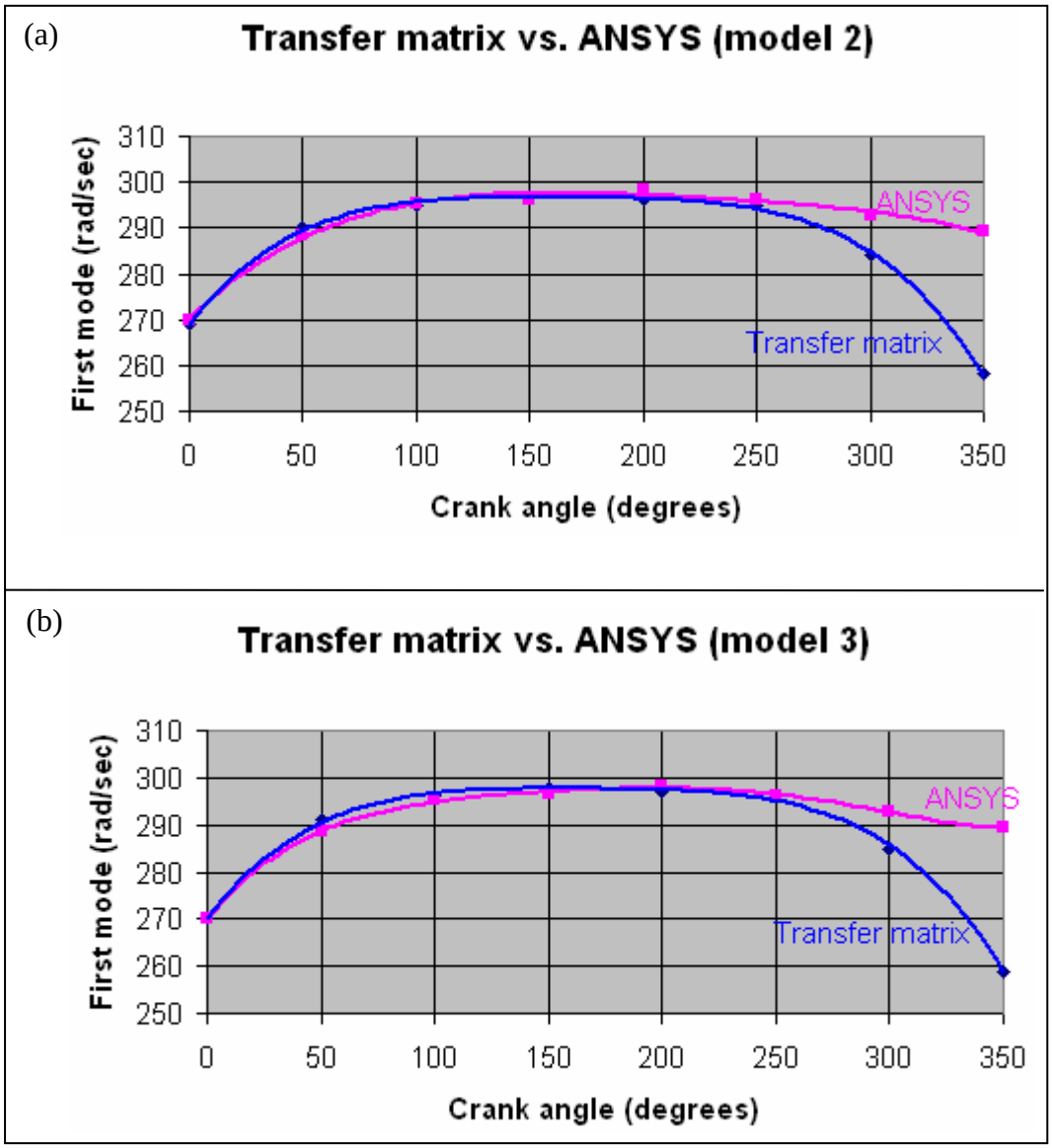

Figure 4.3 The result of comparison for the first mode.

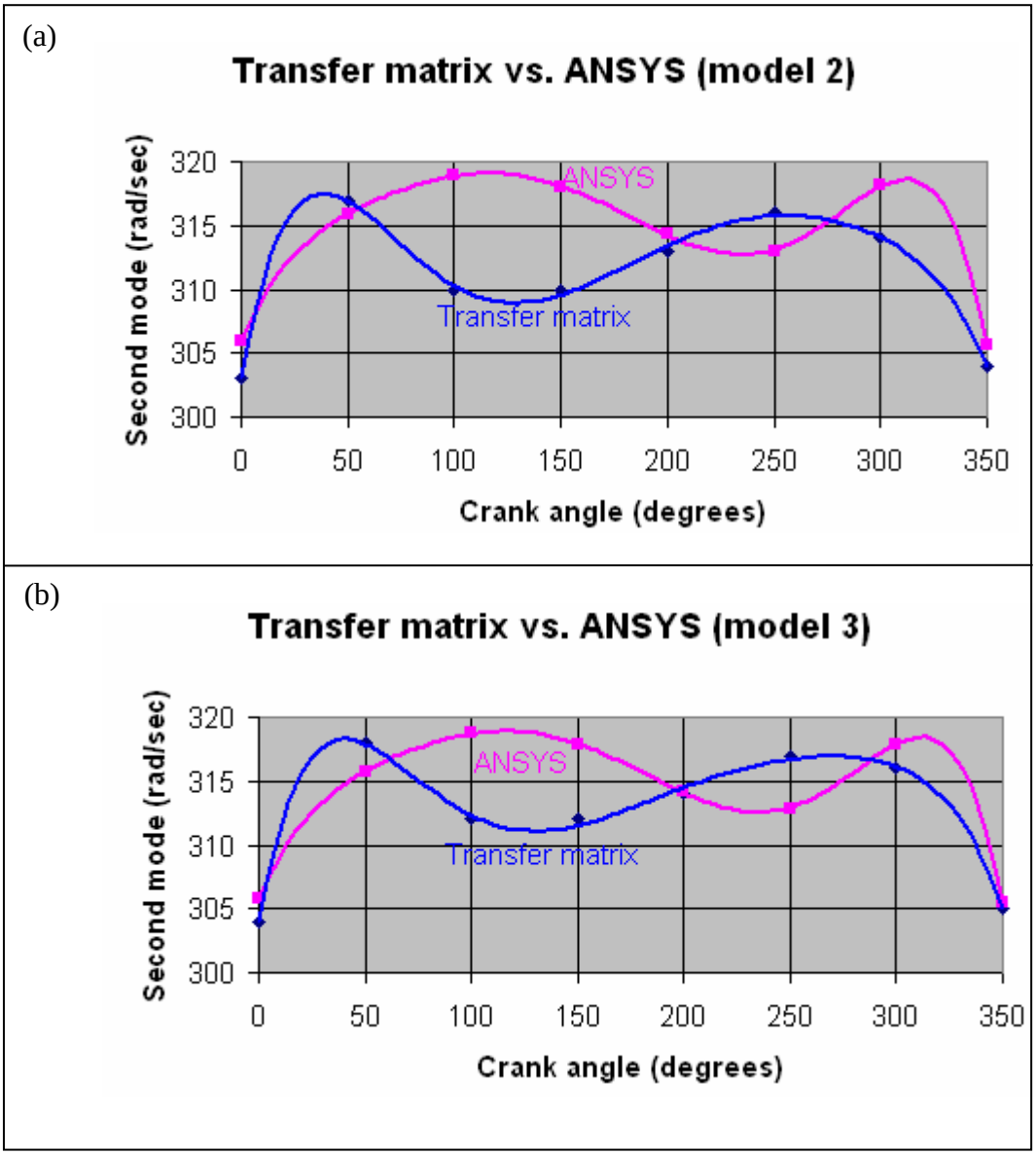

Figure 4.4 The result of comparison for the second mode.

Fig 4.5 indicates the least agreement compared to the results presented in Fig. 4.3 and Fig. 4.4. For model 2 in Fig. 4.5a, the results of the natural frequency for the third mode show that the largest deviation occur when the crank angle is 250 degrees (235.14 rad/sec or 37.43 Hz), while for model 3 in Fig. 4.5.b, the results of natural frequency for the third mode show that the largest deviation occur when the crank angle is also 250 degrees (238.18 rad/sec or 37.91 Hz).

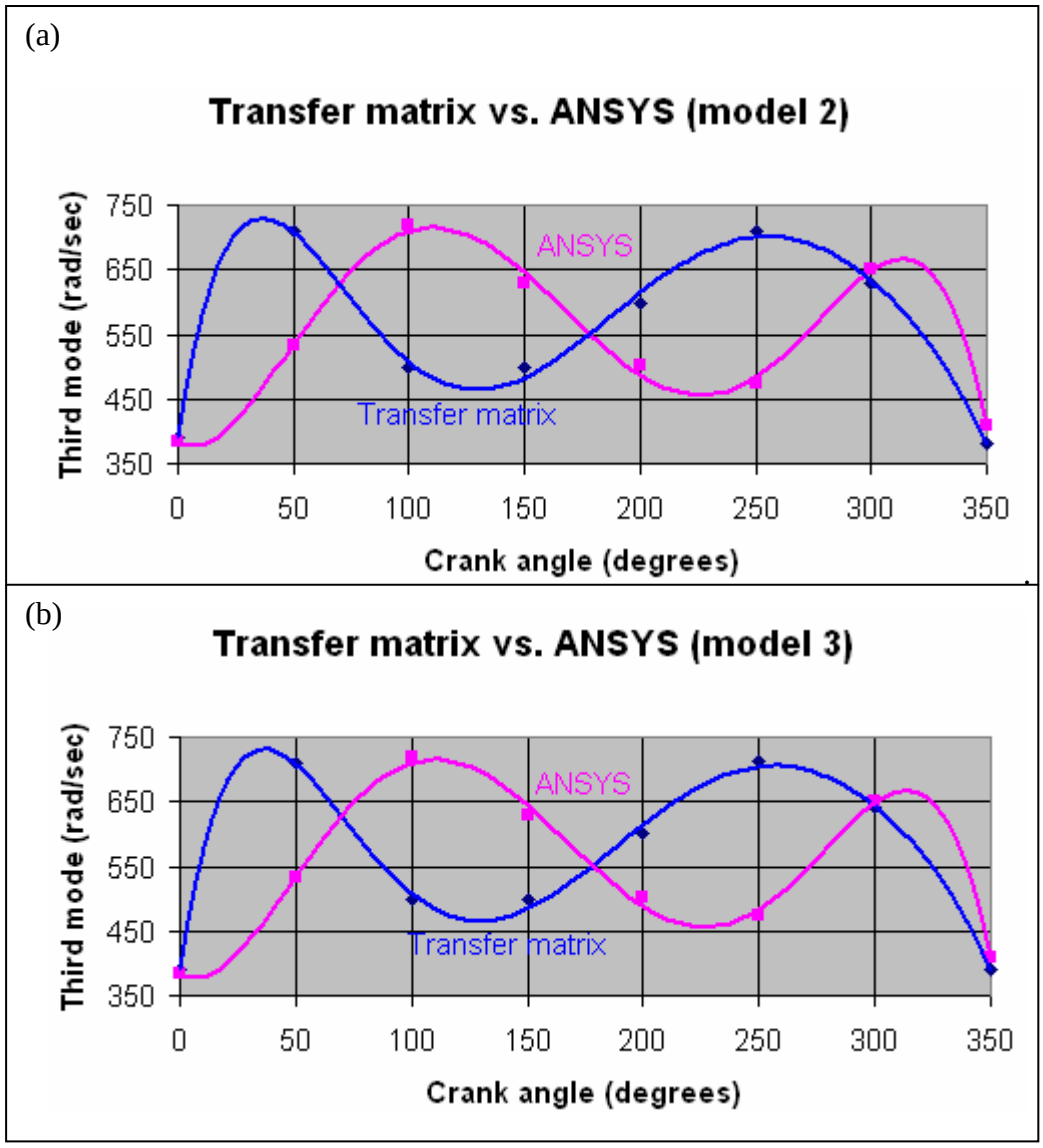

Figure 4.5 The **r**esult of comparison for the third mode.

In summary, the two approaches have obtained some good agreement for the first two modes. For the third mode, the results have shown less agreement. The disagreement of the two approaches increases when the mode of shape increases, which is evidenced by the results shown in Fig. 4.5. However, the two approaches obtained the similar minimum and maximum values, for the third mode (approximately at 380 rad/sec to 710 rad/sec). Also, there is a trend that is when the number of elements (or segments) increases, the two approaches agree more. The

finite element model is generally more accurate than the transfer matrix model because the latter introduces more assumptions with regard to ideal status of a structure system. Our approach is thus reliable for predicting the natural frequency of a compliant mechanism.

4.2.4 Results

The computation of the RRR mechanism has been performed for several critical conditions. Fig. 4.6, Fig. 4.7, and Fig. 4.8 present the natural frequencies of the RRR mechanism as only single PZT is activated: PZT 1, PZT 2, and PZT 3, respectively. Fig. 4.9, Fig. 4.10, Fig. 4.11 show the natural frequencies of the RRR mechanism as two PZT actuators are activated: PZT 1 and PZT 2, PZT 1 and PZT 3 , and PZT 2 and PZT 3, respectively. Fig. 4.12 presents the natural frequencies of the RRR mechanism as three PZT actuators are activated: PZT 1, PZT 2 and PZT 3.

In summary, in the current design of the RRR mechanism, the natural frequencies of the first and second modes are relatively independent of the configurations of the system, and they are also very close (~268 Hz). While the natural frequency of the third mode is relatively dependent on the configuration of the system; specifically ranging from 402 Hz to 405 Hz depending on different configurations.

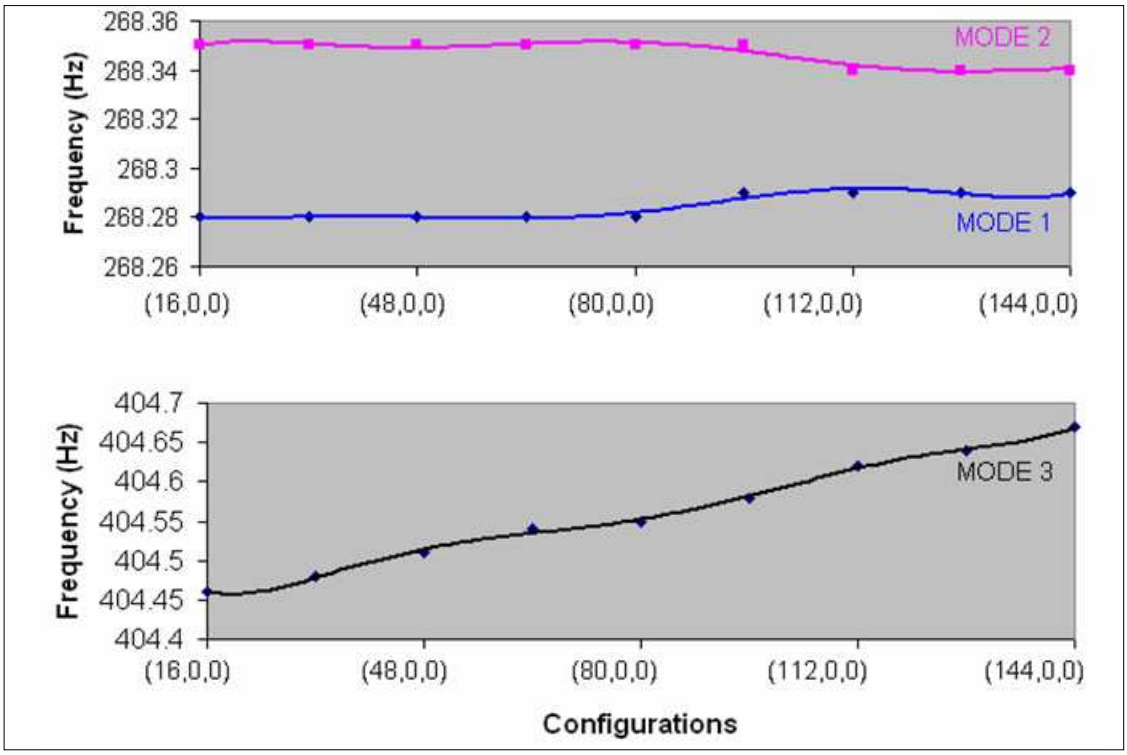

Figure 4.6 The natural frequencies of the PZT 1 actuation.

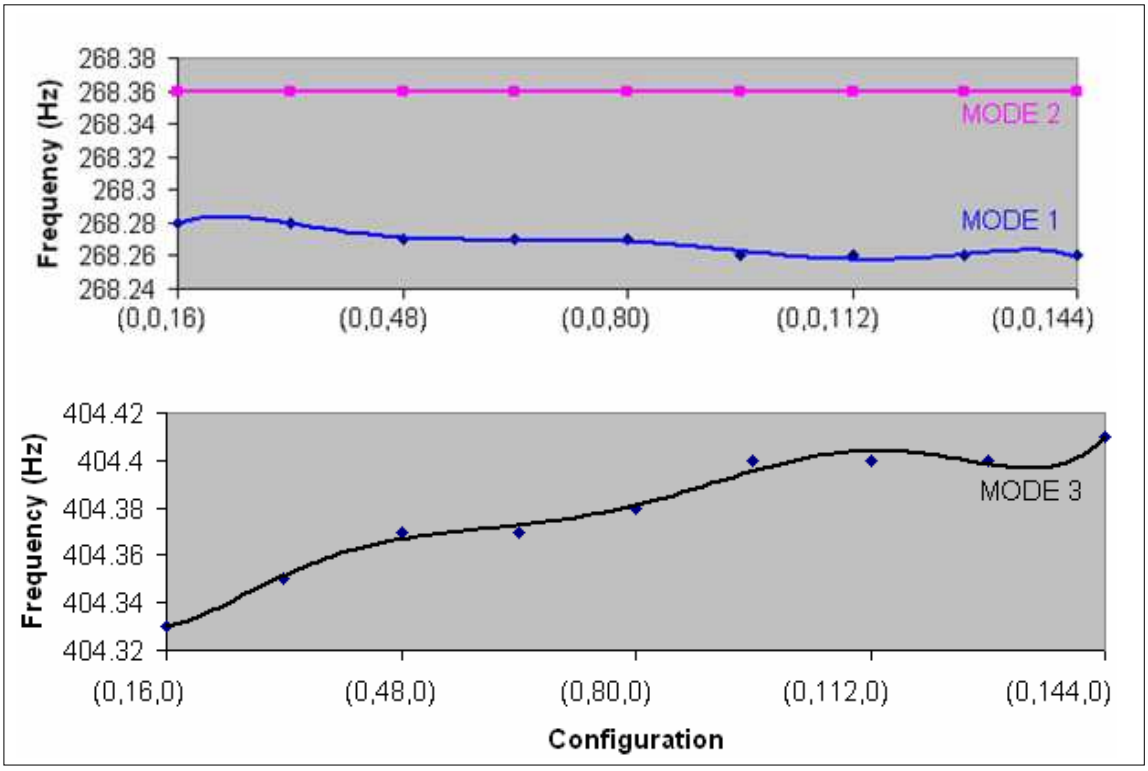

Figure 4.7 The natural frequencies of the PZT 2 actuation.

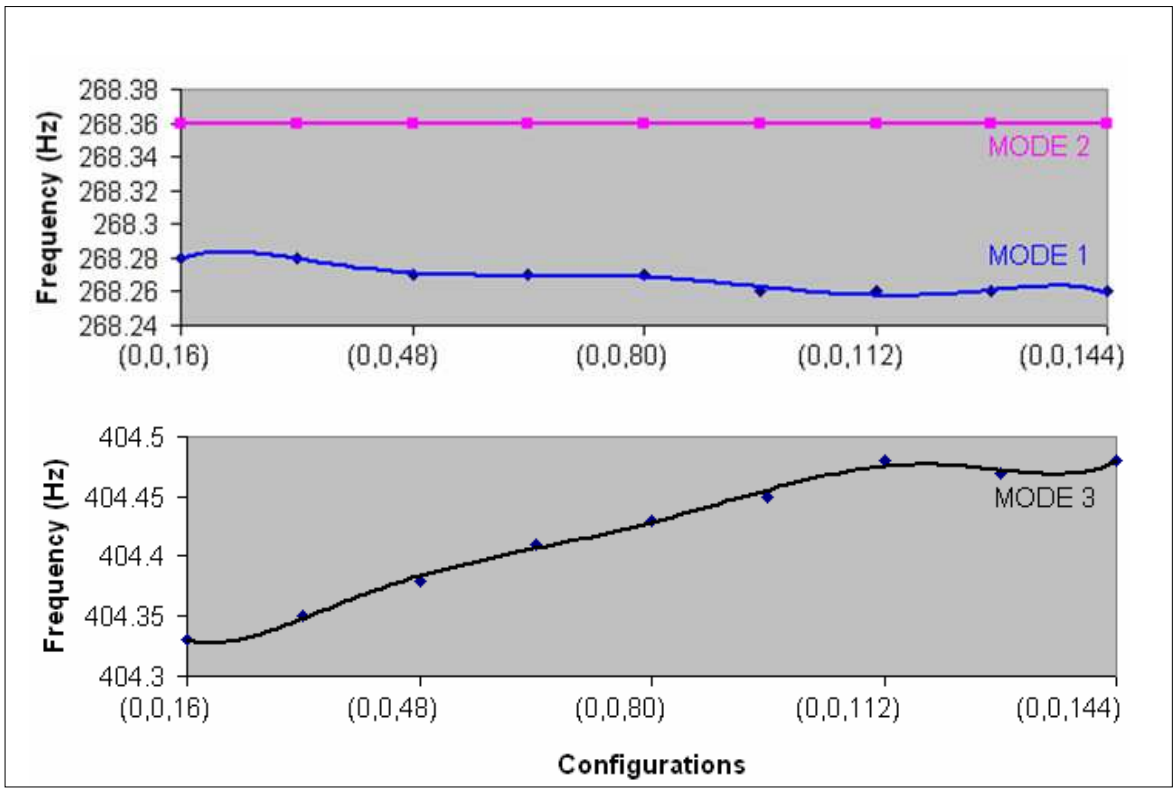

Figure 4.8 The natural frequencies of the PZT 3 actuation.

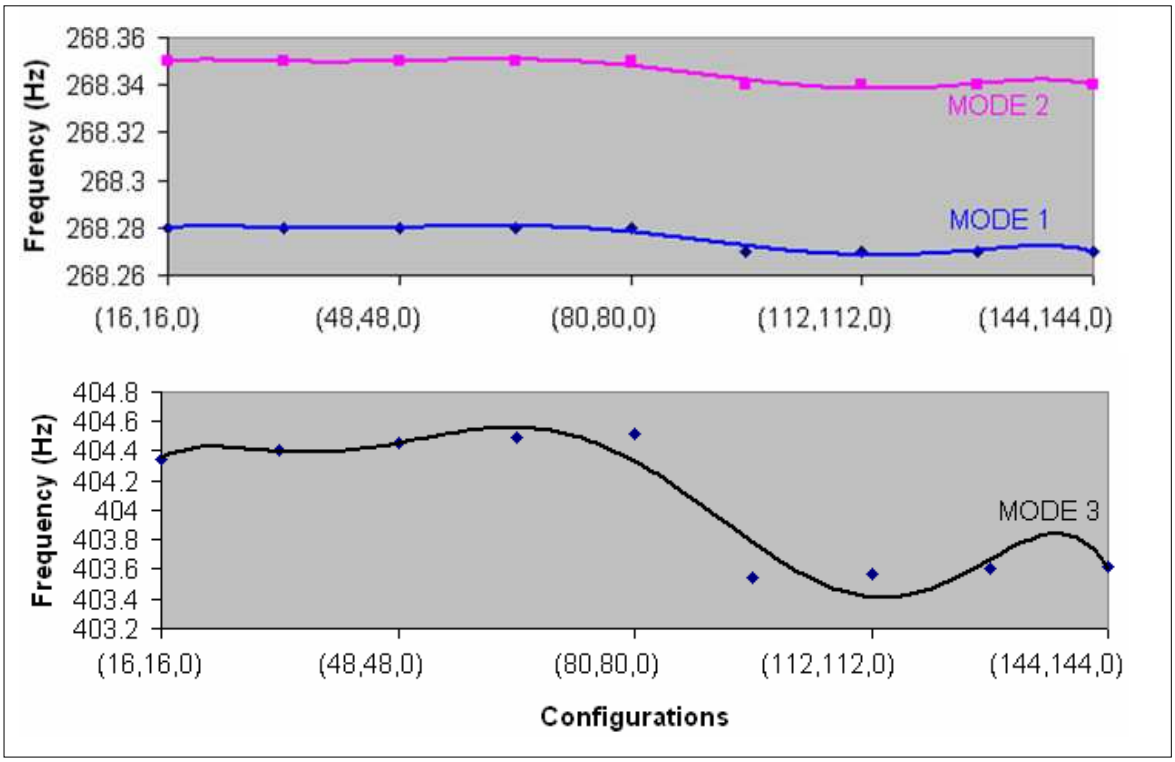

Figure 4.9 The natural frequencies of the PZT 1 and 2 actuation.

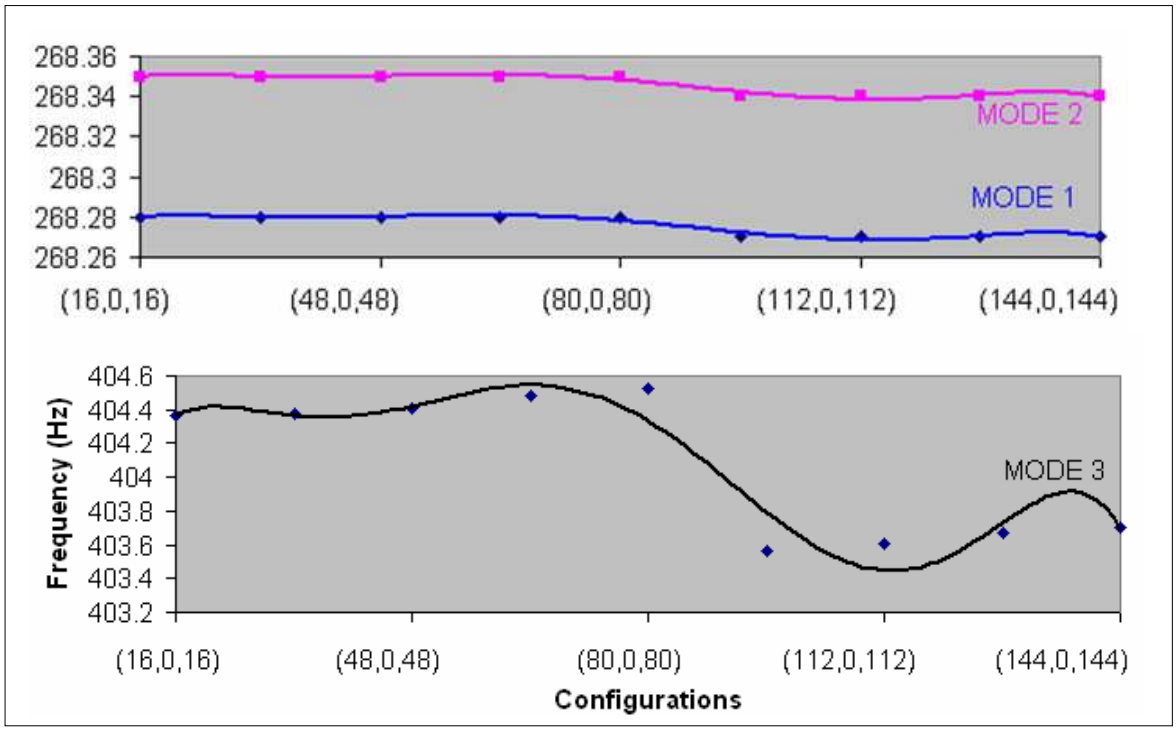

Figure 4.10 The natural frequencies of the PZT 1 and 3 actuation.

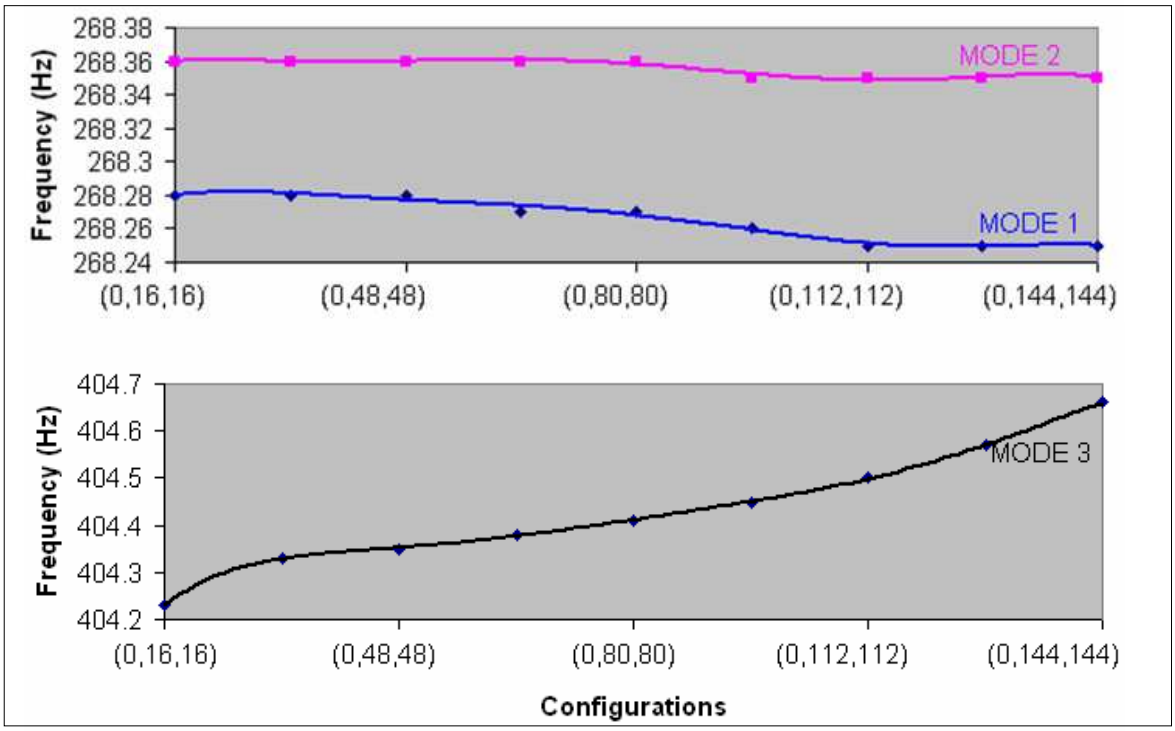

Figure 4.11 The natural frequencies of the PZT 2 and 3 actuation.

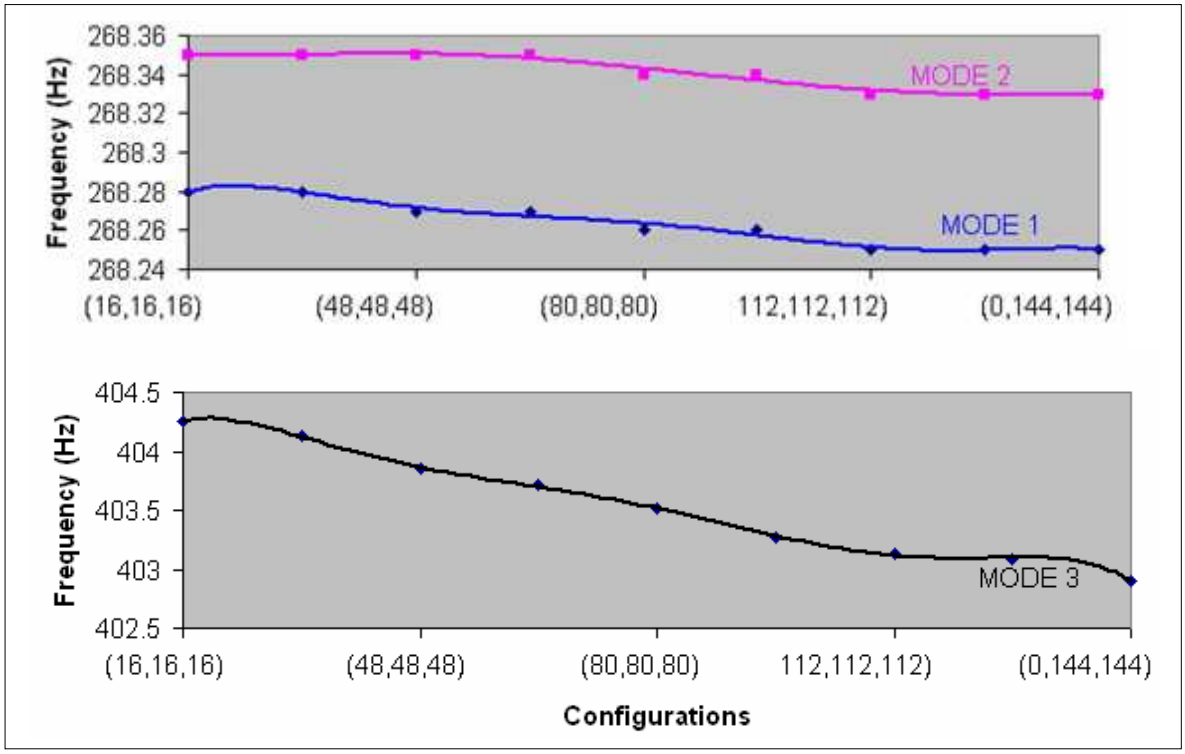

Figure 4.12 The natural frequencies of the PZT 1, 2, and 3 actuation.

4.3 System Stiffness

4.3.1 Basic concepts

Elsewhere in Chapter 2 (Section 2.6) the concept of system stiffness has been elaborated. It is understood that the interest of stiffness in mechanisms or robots lies in the so-called global stiffness at the end-effector. In the following, a procedure based on a general-purpose finite element program (i.e., ANSYS) is proposed.

4.3.2 Procedure

A planar mechanism is considered without loss of generality.

Step 1:

Add F_X (F_1) = 1, F_Y (F_2) = 1, and M (F_3) =1, respectively, on the end-effector.

Step 2:

Execute the finite element model with F_1, F_2, and F_3, and get the end-effector displacement (position and orientation): X (x_1), Y (x_2), θ (x_3), respectively, i.e.,

$$\vec{X}_1 = \begin{bmatrix} x_{11} \\ x_{12} \\ x_{13} \end{bmatrix};\ \vec{X}_2 = \begin{bmatrix} x_{21} \\ x_{22} \\ x_{23} \end{bmatrix};\ \vec{X}_3 = \begin{bmatrix} x_{31} \\ x_{32} \\ x_{33} \end{bmatrix}$$

In the above x_{ij} denotes the displacement i produced due to the force j. There should be the following equation:

$$\Delta\vec{X} = (\vec{X} - \vec{X}_0) = [C]\begin{bmatrix} F_1 \\ F_2 \\ F_3 \end{bmatrix} \tag{4.1}$$

$$[C] = \begin{bmatrix} x_{11} & x_{21} & x_{31} \\ x_{12} & x_{22} & x_{32} \\ x_{13} & x_{23} & x_{33} \end{bmatrix} \tag{4.2}$$

$$[K] = [C]^{-1} \tag{4.3}$$

In the above, [K] is the global stiffness matrix, and $\vec{X}_0$ is the displacement of the end-effector at a particular configuration.

Step 3:

Find the Jacobian matrix for the mechanism system;. The PRBM of the RRR mechanism was developed by Zou [2000]; see the schematic diagram of this

mechanism in Fig. 4.13. In the case of the PZT RRR mechanism, Jacobian matrix, J_l^0 can be found as follows [Zou, 2000]:

$$J_l^0 = -\frac{L_{AB}}{R_0}\sin(\psi_3)\begin{bmatrix} \frac{-\sqrt{3}}{3}\sin(\psi)-\frac{1}{3}\cos(\psi) & \frac{2}{3}\cos(\psi) & \frac{\sqrt{3}}{3}\sin(\psi)-\frac{1}{3}\cos(\psi) \\ \frac{\sqrt{3}}{3}\cos(\psi)-\frac{1}{3}\sin(\psi) & \frac{2}{3}\sin(\psi) & \frac{-\sqrt{3}}{3}\cos(\psi)-\frac{1}{3}\sin(\psi) \\ \frac{1}{3R\sin(\psi)} & \frac{1}{3R\sin(\psi)} & \frac{1}{3R\sin(\psi)} \end{bmatrix} \quad (4.4)$$

where L_{AB} : the length of the link A_iB_i , i=1,2,3,

L_{BC} : the length of the link B_iC_i , i=1,2,3,

R : the length of OC_i , i=1,2,3,

ψ : $\psi_1 + \psi_2$, in which ψ_1 and ψ_2 are illustrated in Fig. 4.10,

and ψ_3 : $\psi_2 + \arcsin(\frac{L_{BC} \times \sin\psi_2}{L_{AB}})$.

Step 4:

Find the system global stiffness limits; that is, first get the eigenvalues from the matrix [K][J_l^{0T}][J_l^0]; second, get $\gamma_{\min}$ (the minimum eigenvalue) and $\gamma_{\max}$ (the maximum eigenvalue).

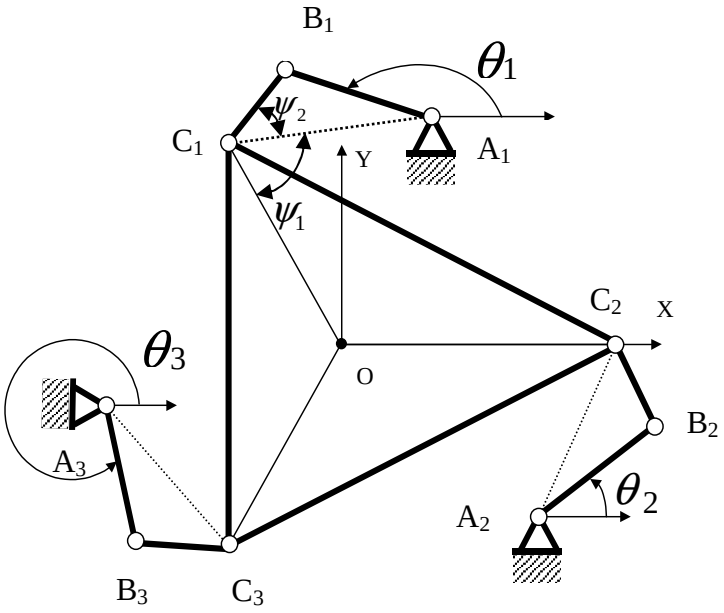

Figure 4.13 The PRBM of the RRR mechanism [Zou, 2000].

4.3.3 Validation

The work of Sanger et al. [2000] was chosen to validate our approach. The mechanism has two degrees-of-freedom: q_1 and q_2; while P denotes the position of the end-effector in the global coordinate system (X-O-Y). The length of links OQ, QP and PO are 10 cm, 10 cm, and 14.14 cm, respectively; while the stiffness of the actuators (q_1 and q_2) are 10 N/cm.

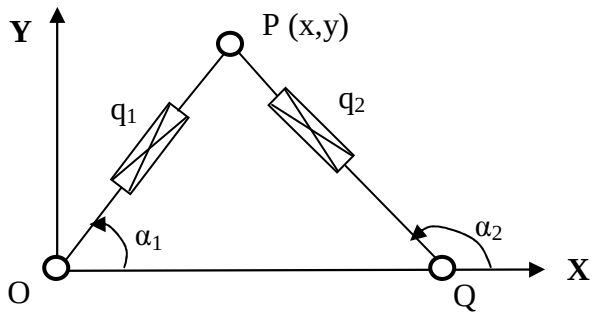

Figure 4.14 A two-legged planar manipulator.

Four methods were employed to find the global stiffness for this mechanism.

(1) The procedure proposed in [Sanger et al., 2000]

Sanger et al. [2000] derived a formula to compute the stiffness matrix at the end-effector as follows:

$$K = JkJ^T - \eta\lambda^T \tag{4.5}$$

where K : the stiffness matrix at the end-effector,
J : the Jacobian matrix relating to the actuated joints,
J^T : the transpose of the Jacobian matrix relating to the actuated joints,
η : the matrix describing the incremental change in J due to changes in the unactuated joint displacements,
and λ^T : the transpose of the the Jacobian matrix relating to the unactuated joints.

At the position of P (10,10) cm, the stiffness matrix is equal to $\begin{bmatrix} 20 & 0 \\ 0 & 20 \end{bmatrix}$ N/cm.

When P = (18,25) cm , the stiffness matrix is $\begin{bmatrix} 18.8813 & 0.5290 \\ 0.5290 & 19.7076 \end{bmatrix}$ N/cm.

(2) Our approach

When P = (10, 10) cm, K = $\begin{bmatrix} 5 & 5 \\ 5 & 15 \end{bmatrix}$ N/cm. When P = (10, 10) cm, K = $\begin{bmatrix} 4.348 & 7.648 \\ 7.648 & 15.652 \end{bmatrix}$ N/cm.

(3) The procedure proposed in [Dawe, 1984]

The matrix displacement approach was proposed in [Dawe, 1984]. The following steps were taken in this procedure. *First*, each link of the two-legged planar manipulator (see Fig. 4.14) is put into the following table.

Table 4.1 Table of structural elements as P (10, 10) cm

Element	**The stiffness Of actuator (k)**	**The angle of link**	**The element stiffness k_0**
OP	10 N/cm	45 degrees	$10\begin{bmatrix}0.5 & 0.5\\ 0.5 & 0.5\end{bmatrix}$ N/cm
PQ	10 N/cm	90 degrees	$10\begin{bmatrix}0 & 0\\ 0 & 1\end{bmatrix}$ N/cm

The presented element stiffness in Table 4.1 is based on:

$$k_0 = k \times \begin{bmatrix} \cos^2\alpha & \cos\alpha\sin\alpha \\ \cos\alpha\sin\alpha & \sin^2\alpha \end{bmatrix} \qquad (4.6)$$

Next, the global stiffness matrix is assembled as follows.

$$\begin{array}{c} \begin{matrix} \quad O \quad & \quad P \quad & \quad Q \quad \end{matrix} \\ \left[\begin{array}{c|c|c} k_0^{QO} + k_0^{OP} & k_0^{OP} & k_0^{PQ} \\ \hline k_0^{PO} & k_0^{QP} + k_0^{PQ} & k_0^{PQ} \\ \hline k_0^{QO} & k_0^{QP} & k_0^{PQ} + k_0^{QO} \end{array}\right] \begin{matrix} O \\ P \\ Q \end{matrix} \end{array}$$

Because the two-legged planar manipulator is constrained in O and Q (see Fig. 4.10), the rows and columns corresponding to O and Q can be eliminated. Therefore, the global stiffness matrix of the two-legged planar manipulator is [$k_0^{QP} + k_0^{PQ}$], or equal to

$$K = \begin{bmatrix} 5 & 5 \\ 5 & 15 \end{bmatrix} \text{ N/cm.}$$

A similar procedure can be applied for P (18, 25) cm, which results in

$$K = \begin{bmatrix} 4.348 & 7.648 \\ 7.648 & 15.652 \end{bmatrix} \text{ N/cm.}$$

(4) The procedure proposed in [Gosselin, 1990]

Gosselin [1990] derived an equation for the planar manipulators, as presented below.

$$K = k\, J^T J \tag{4.7}$$

Note that Eqn. (4.7) is part of Eqn (4.5). Eqn (4.7) was also presented in [Sanger et al., 2000] for the application of the two-legged planar manipulator application.

$$JkJ^T = \begin{bmatrix} \cos^2\alpha_1 k_1 + \cos^2\alpha_2 k_2 & \sin\alpha_1\cos\alpha_1 k_1 + \sin\alpha_2\cos\alpha_2 k_2 \\ \sin\alpha_1\cos\alpha_1 k_1 + \sin\alpha_2\cos\alpha_2 k_2 & \sin^2\alpha_1 k_1 + \sin^2\alpha_2 k_2 \end{bmatrix} \tag{4.8}$$

The use of Eqn. (4.11) results also in the similar stiffness matrices that were obtained with the second and the third approaches.

From the above comparison, the first approach does not produce the same result as the other three. Our approach to compute the global stiffness matrix for the compliant mechanism agrees with the third and fourth approaches and is thus reliable. Further, our approach may be better than the third and fourth approaches because they have introduced some assumptions of a mechanism under investigation. For example, Gosselin [1990]'s approach assumed that all actuators should have the same axial stiffness along with their actuating axes and the stiffness of the link and other passive joints are not considered. The approach proposed by Gosselin and Zhang [1999] extended the one by Gosselin [1990] by considering the stiffness of the link component. It should be noted that both the third and the fourth approaches are strongly associated with the structures that contain truss members or beam members. So, these approaches are inherently not suitable for the compliant mechanism which

is often not characterized by beam members or truss members. Gosselin and Zhang [1999] mentioned in their work that the problem with the first approach lies in the consideration of the unactuated joint.

4.3.4 Results

The minimum and maximum stiffness of the PZT RRR mechanism for different configurations was calculated using our approach, and their results are shown in Fig. 4.15, Fig. 4.16, Fig. 4.17, Fig. 4.18, Fig. 4.19, Fig. 4.20, and Fig. 4.21.

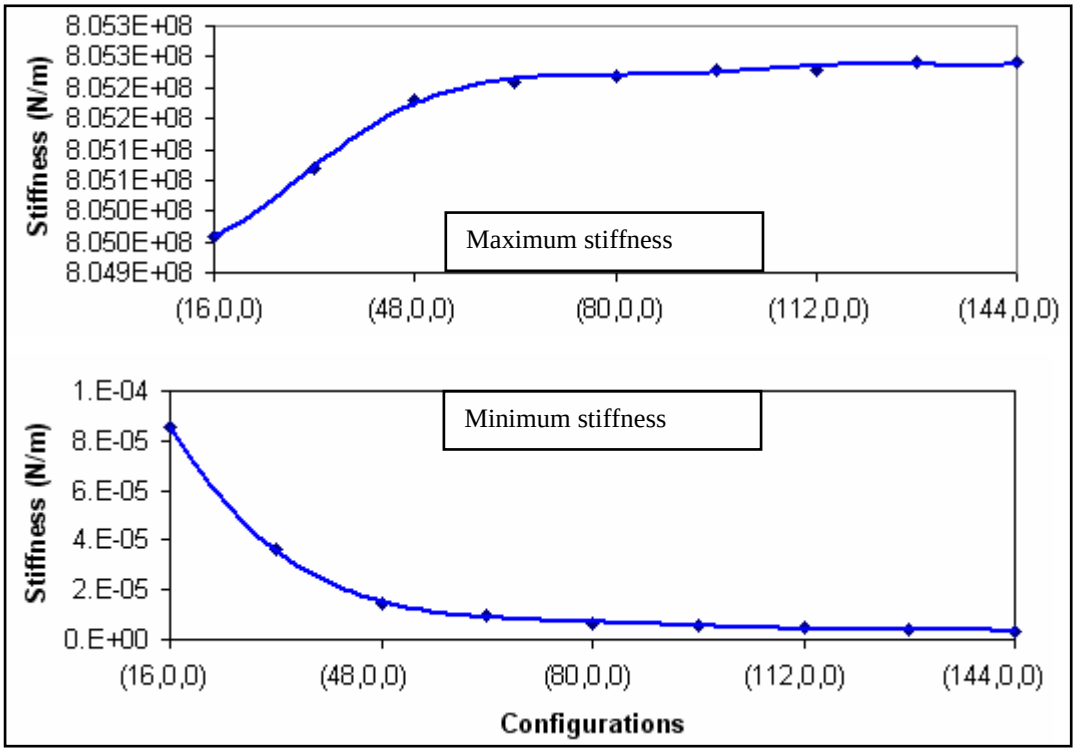

Figure 4.15 The stiffness of the PZT 1 actuation.

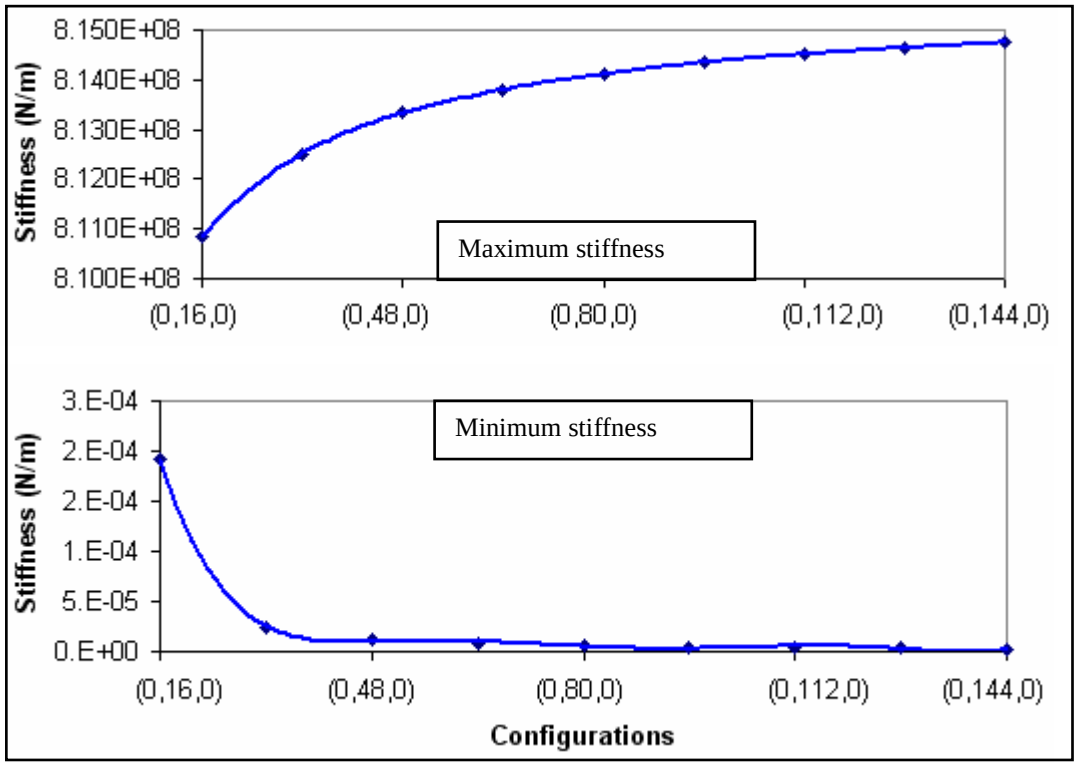

Figure 4.16 The stiffness of the PZT 2 actuation.

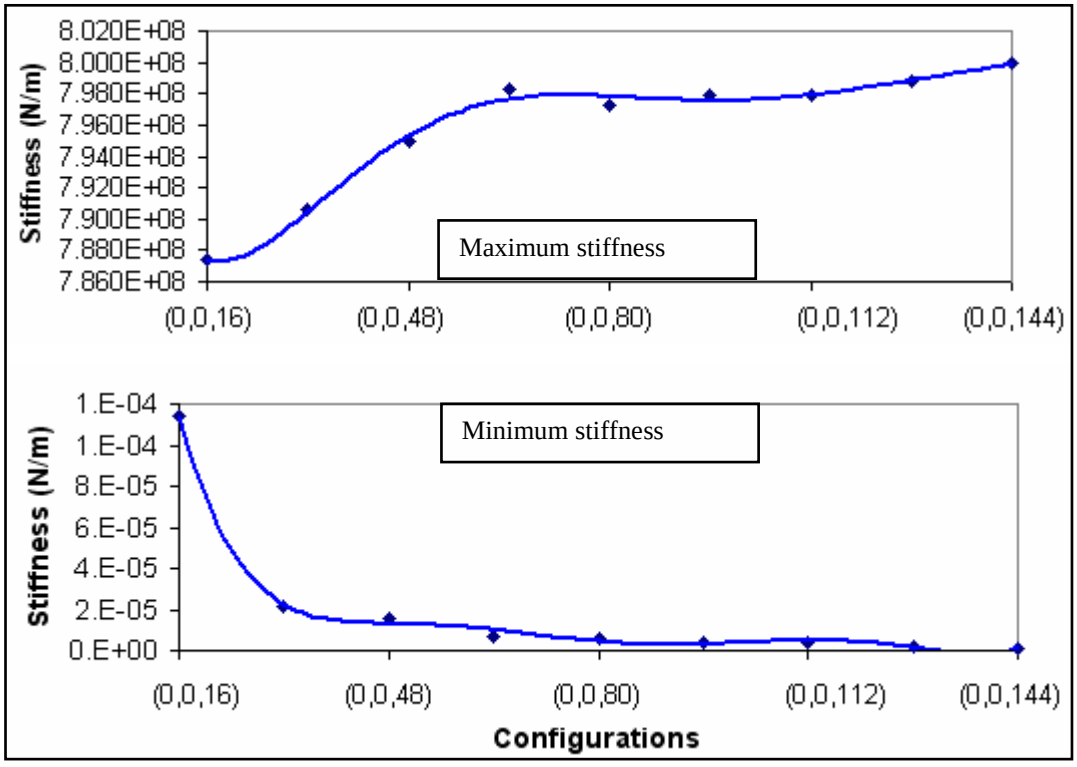

Figure 4.17 The stiffness of the PZT 3 actuation.

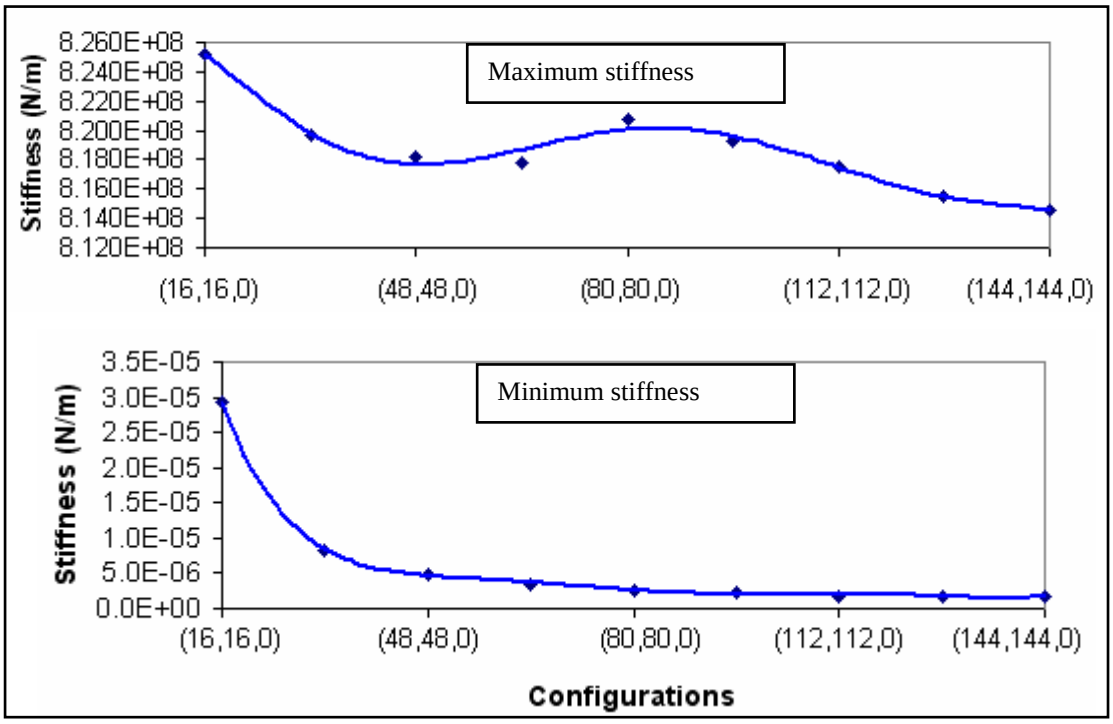

Figure 4.18 The stiffness of the PZT 1 and 2 actuation.

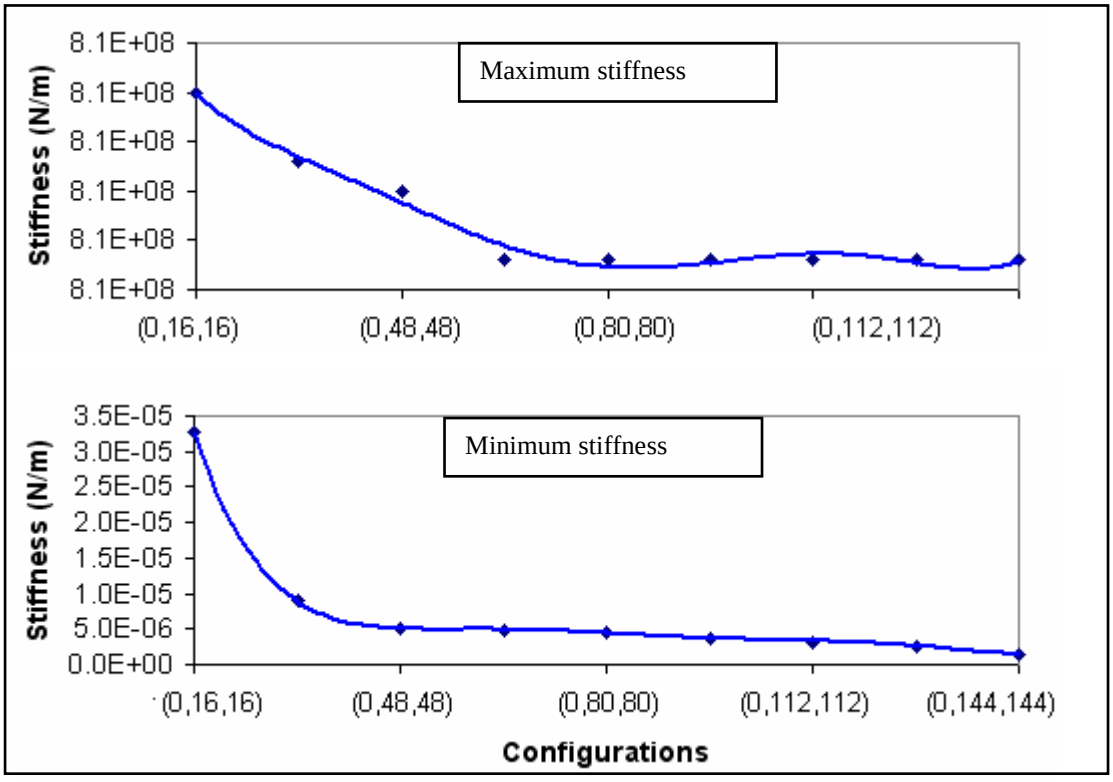

Figure 4.19 The stiffness of the PZT 2 and 3 actuation.

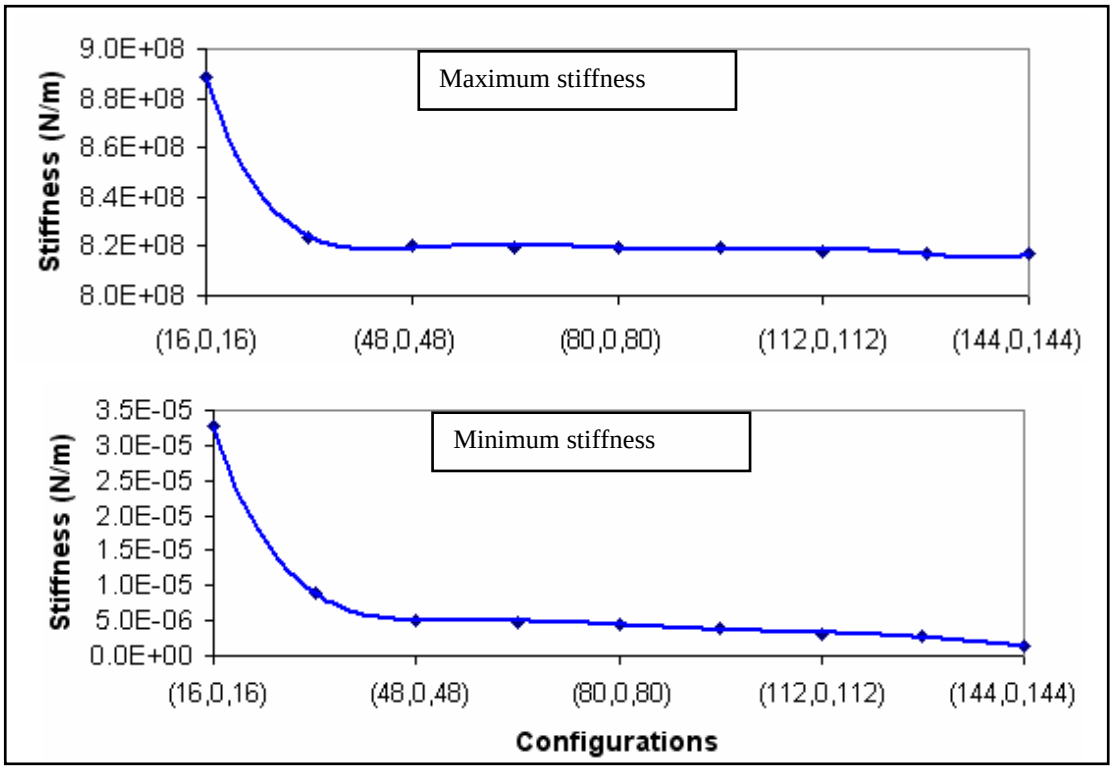

Figure 4.20 The stiffness of the PZT 1 and 3 actuation.

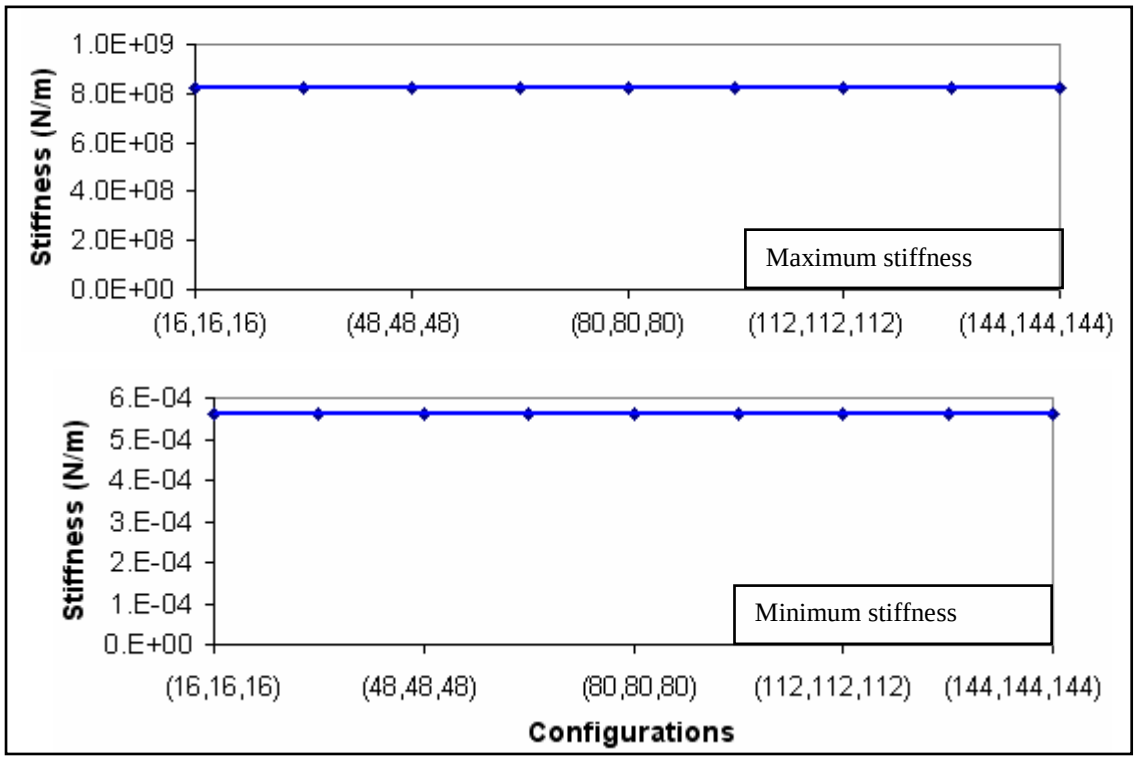

Figure 4.21 The stiffness of the PZT 1, 2, and 3 actuation.

4.4 Conclusion

New methods for predicting the natural frequency and the global stiffness of a compliant mechanism have been developed, respectively. They are easily implemented on a general purpose finite element program, such as ANSYS. These two methods have been validated by comparing the simulation results produced by them with the known reference results. It should be noted that the popular paradigm for analysis of compliant mechanism, called pseudo rigid body model, is generally not suitable to the calculation of the natural frequency and global stiffness for compliant mechanisms.

CHAPTER 5

EXPERIMENTAL VALIDATION

5.1 Introduction

In this chapter, measurement results based on a prototype PZT RRR mechanism is presented. This is essential in order to validate the theoretical developments described in the previous chapters. Measurements were performed at both the actuator level and the end-effector level. Section 5.2 presents the test bed which includes the instrument and related fixture devices. Section 5.3 presents the measurement results together with the simulation results based on the models (both the other previous model and the model developed with this thesis study. A discussion about these results is also included in Section 5.3. Section 5.4 is a conclusion.

5.2 Measurement Test-bed Set-up

5.2.1 Measurement at the end-effector

Fig. 5.1 illustrates the measurement instrumentation system to measure the end-effector motion. The manufacturer of this system is KAMAN and its model name is

SMU 9000-15N-001. The system is based on the magnetic-induction principle, specifically eddy current phenomenon. An eddy (swirl) current is a local electric current induced in a conductive material by the magnetic field produced by the active coil (see Fig. 5.2). When an AC current flows in a coil in certain proximity to a conductive material, the developed magnetic field in the coil will induce circulating (eddy) currents in the conductive material. The electromagnetic sensors sense impedance variation as the gap changes and then the calibration box translates the impedance variation into a usable displacement signal. The measurement resolution of the system is 0.1 microns. The system is hereafter also called the induction sensor.

There are some requirements that need to be met regarding the mounting of the induction senor with respect to an object to be measured (target for short). They are (1) distance requirement, (2) sensor mounting requirement, (3) parallelism requirement, (4) target requirements, and (5) sensor to sensor proximity requirement. These requirements are briefly discussed below.

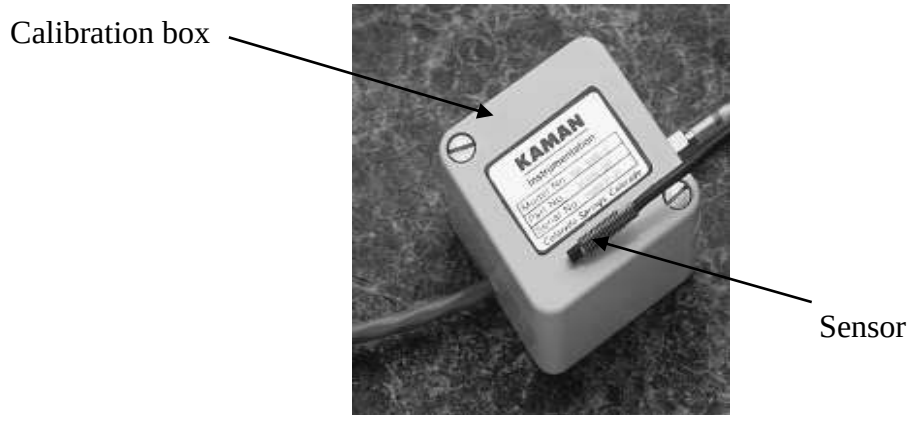

Figure 5.1 SMU 9000-15N-001 [Kaman, 2000].

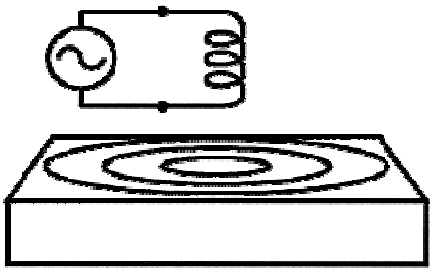

Figure 5.2 Eddy current behavior [Kaman, 2000].

The distance requirement refers to the minimum and maximum distances within which the target and the sensor must stay (see Fig. 5.3). The sensor mounting requirement is about the minimum empty area around the tip of the sensor (see Fig. 5.4). The parallelism requirement is about the maximum allowable tilt angle of the target (i.e., 3 degrees, see Fig. 5.5). The target requirements are restrictions on (a) the material of the target, (b) the minimum diameter of the target, and (c) the thickness of the target. The material requirement for the target is Aluminum T6. Fig. 5.6 illustrates the diameter of the target and the thickness of target. Fig. 5.7 shows the sensor to sensor proximity requirement.

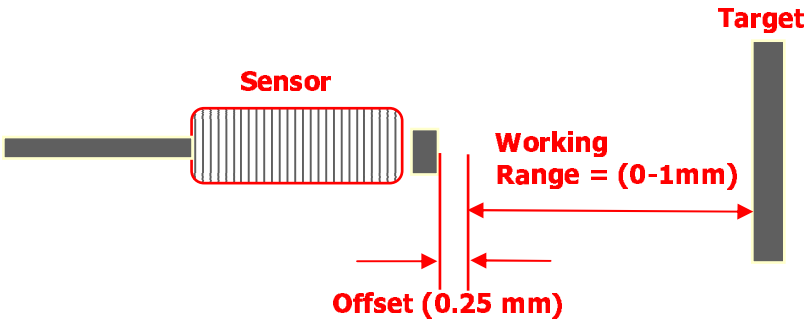

Figure 5.3 Required distance between sensor and target [Kaman, 2000].

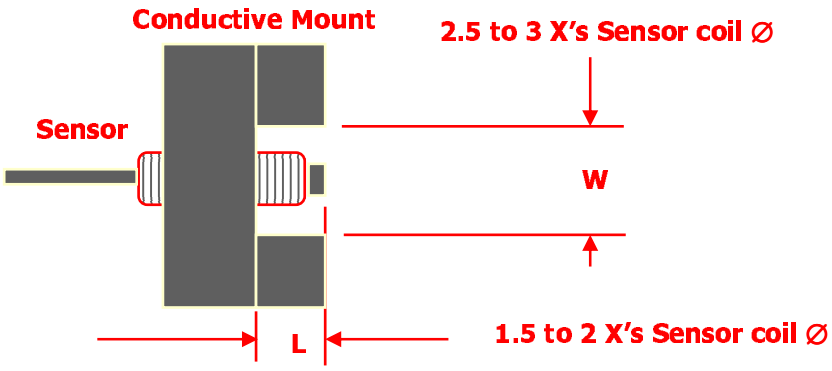

Figure 5.4 Sensor mounting requirement [Kaman, 2000].

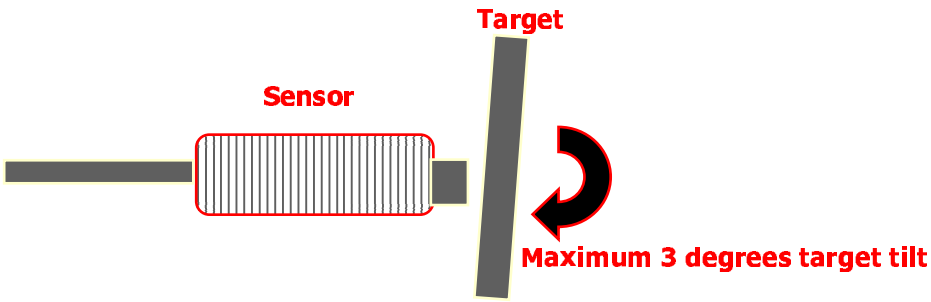

Figure 5.5 Parallelism requirement [Kaman, 2000].

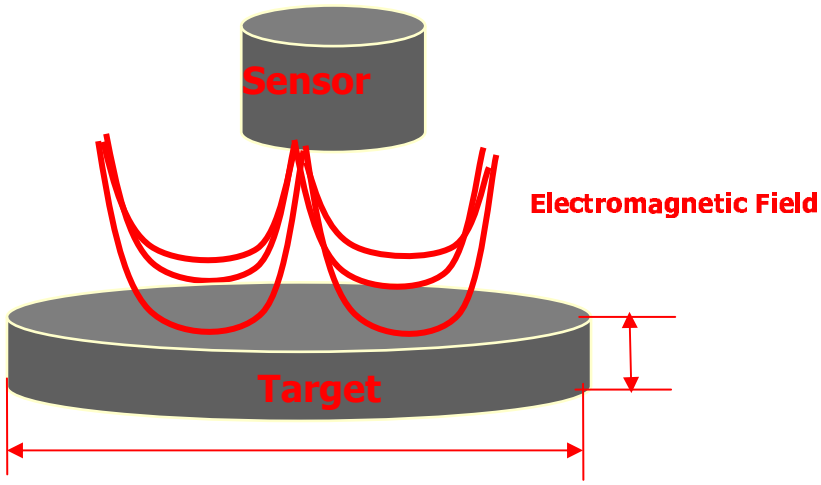

Figure 5.6 Target requirements [Kaman, 2000].

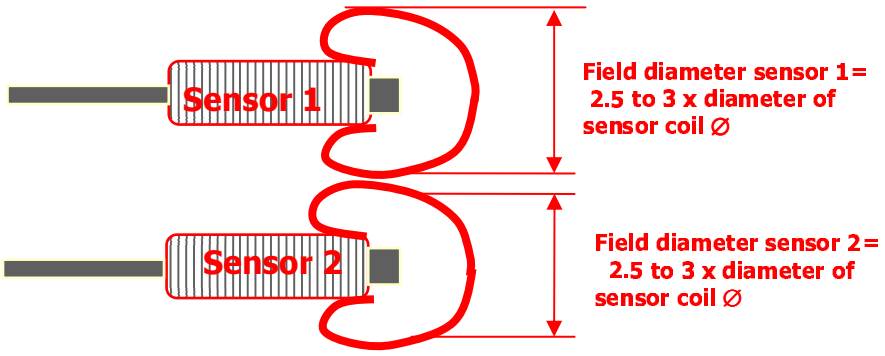

Figure 5.7 Requirement for sensor to sensor proximity [Kaman, 2000].

KAMAN [2000] defines calibration as a means to verify that system output (in the form of an output voltage) relates to a known physical displacement with a known degree of accuracy. KAMAN provides the calibration equation as follows:

$$Y = 2.191e\text{-}5\ X^5 - 4.259e\text{-}4\ X^4 + 3.497e\text{-}3\ X^3 - 1.297e\text{-}X^2 + 8.674e\text{-}2\ X - 4.92\ e\text{-}4 \quad (5.1)$$

where X : the resulted sensors'reading in forms of the voltages,

and Y : the computed distance

Note that Eqn. (5.1) cannot be directly applied to the RRR mechanism because its environment and that of the manufacturer are different. This type of difference is sensitive to the accuracy of measurement. There were two options for coping with this problem. One was to make the application measurement environment similar to the manufacturer environment, which is costly. The other was to recalibrate the measuring instrument. The latter option was chosen in this study because an X-Y-Z stage with 0.2 μm displacement resolution (manufacturer: Newport company; model: M-461) is available to this study, which can be used to act as a reference measurement. The recalibration was conducted by following the steps shown in Fig. 5.8.

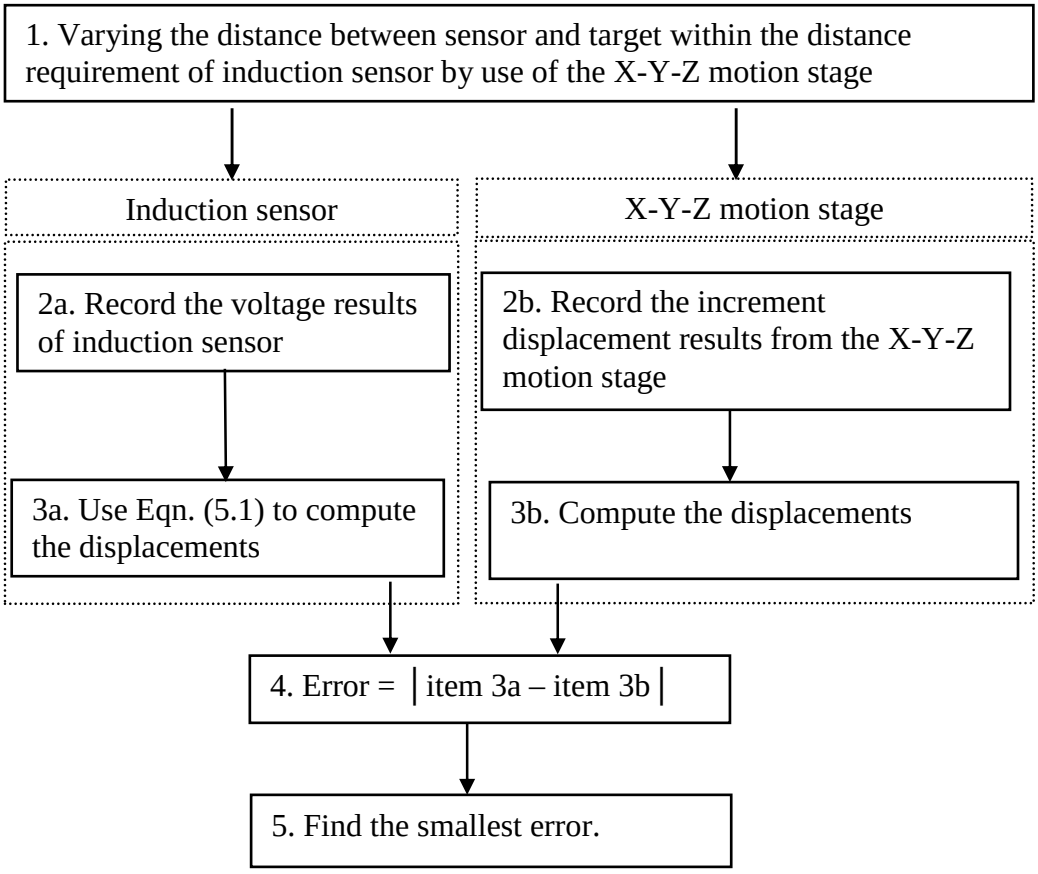

Figure 5.8 The procedure to calibrate SMU 9000-15N-001 for the RRR mechanism application.

Table 5.1 presents the calibration result. The detailed physical setting for the recalibration can be found in Appendix D.

Table 5.1 The configurations of the RRR mechanism when all the PZT actuators are activated.

Configuration	PZT 1 (volts)	PZT 2 (volts)	PZT 3 (volts)
1	0	0	0
2	16	16	16
3	32	32	32
4	48	48	48
5	64	64	64
6	80	80	80
7	96	96	96
8	112	112	112
9	128	128	128

In order to measure three motions (X, Y, θ) simultaneously, three induction sensors are required, see Fig. 5.9. From Fig. 5.9 one can get the end-effector motion as follows:

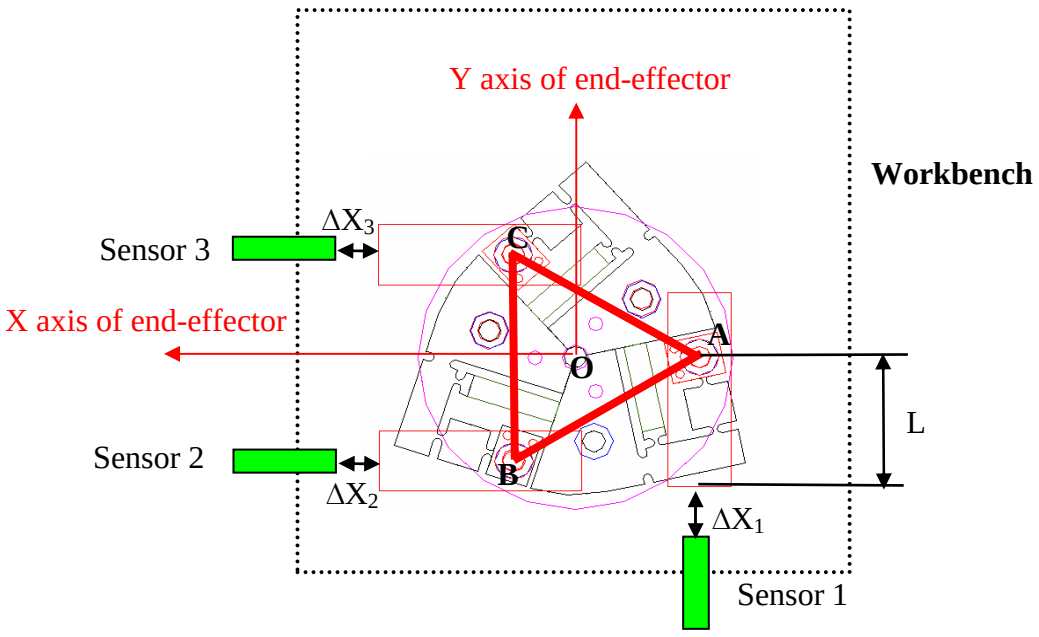

Figure 5.9 The RRR mechanism set-up in experiment.

$$\Delta X = \frac{\Delta X_2 + \Delta X_3}{2} \tag{5.5}$$

$$\Delta Y = \sqrt{(AO^2 + L^2)}\Delta\gamma + \Delta X_1 \tag{5.6}$$

$$\Delta\gamma = -\tan^{-1}\left(\frac{\Delta X_2 - \Delta X_3}{BC}\right) \tag{5.7}$$

where ΔX and ΔY are displacements along the X-axis and the Y-axis, respectively, while $\Delta\gamma$ is the angular displacements of the end-effector. All these displacements are with respect to the X-Y coordinate system in the measurements situation.

To physically realize the above scheme for obtaining the end-effector motion, a workbench was designed; see Fig. 5.10.

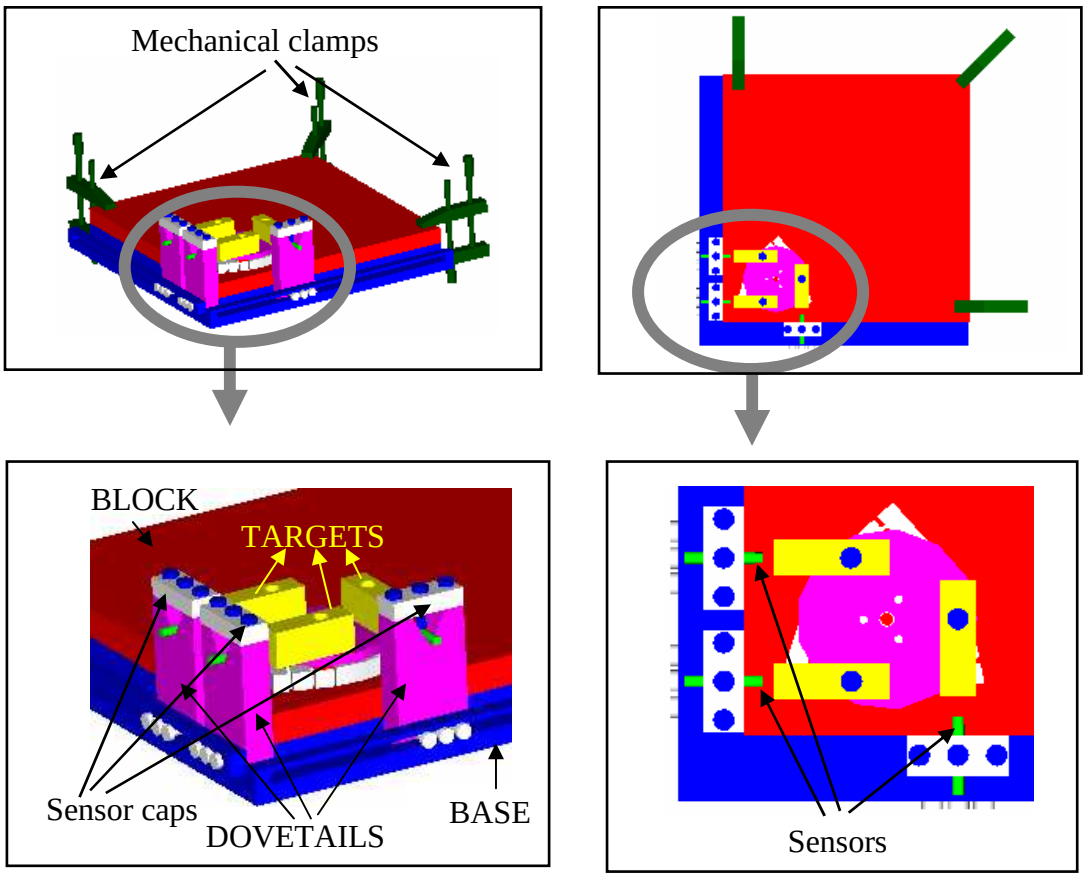

Figure 5.10 Adjustable Workbench.

The workbench has a certain degree of adaptability in the sense that it can accommodate different physical configurations of a target. The detailed design of the workbench can be found in Appendix C.

The reference coordinate system for the measurement was different from that for the simulation based on the model developed in Chapter 3. Such a difference is shown in Fig. 5.11. Conversion of the simulation result from the reference for the simulation to the reference for the measurement was conducted. It is noted that the X axis in the experiment perpendicularly cuts the half of the line BC. The conversion equation is given as below:

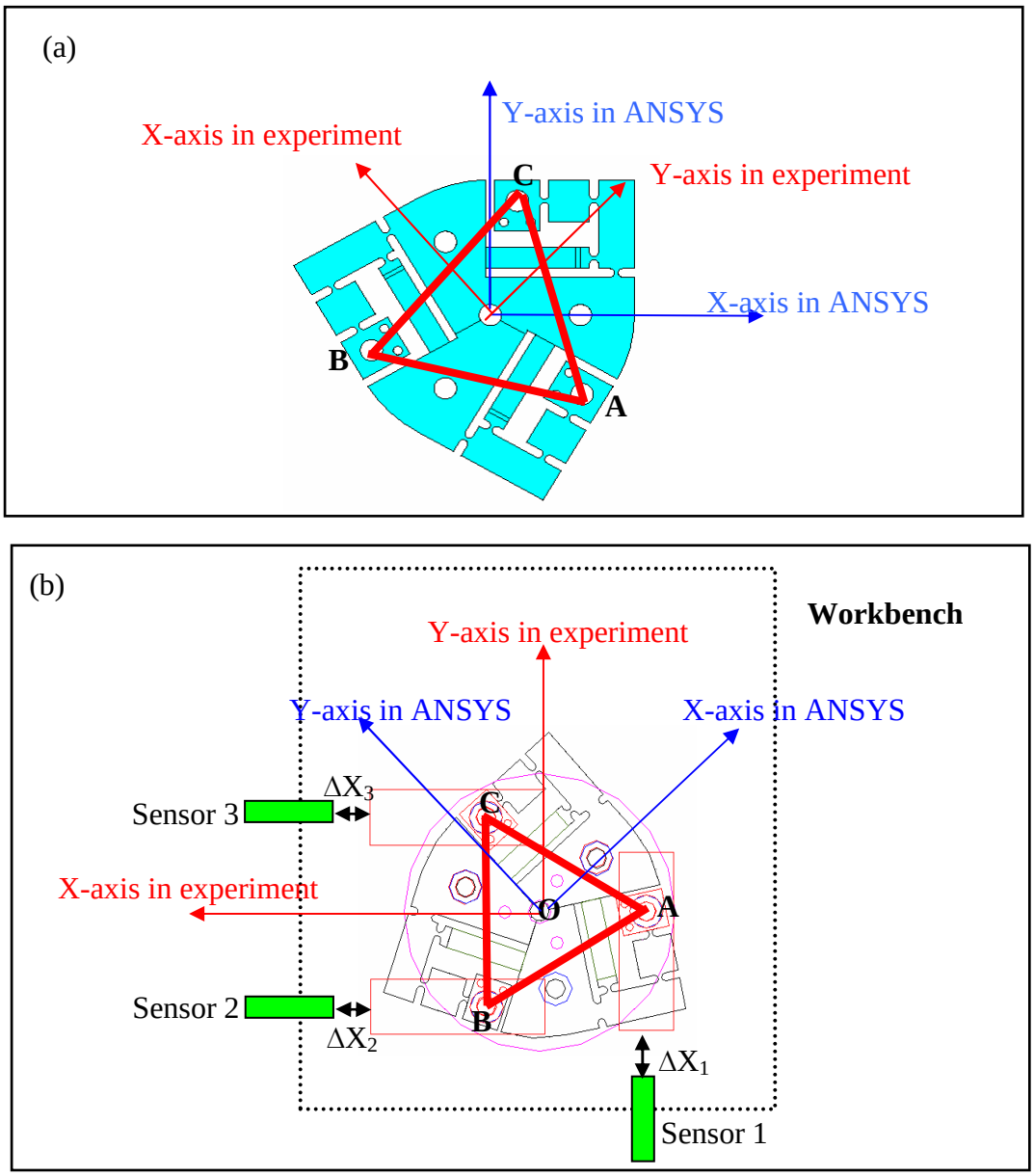

Figure 5.11 The reference in simulation versus the reference in measurement (a: the reference in the measurement; b: the reference in the simulation).

5.2.2 Measurement at the actuator level

The measurement at the actuator level concerns the displacement of the PZT actuator and was directly obtained from the strain gauge on the PZT actuator. Fig. 5.12 shows a schematic diagram of the measurement at the actuator level. The manufacturer of the strain gauge is Vishay Measurements Group, Inc, the model name is EA-06-125TG-350, and its accuracy is ± 0.05 %.

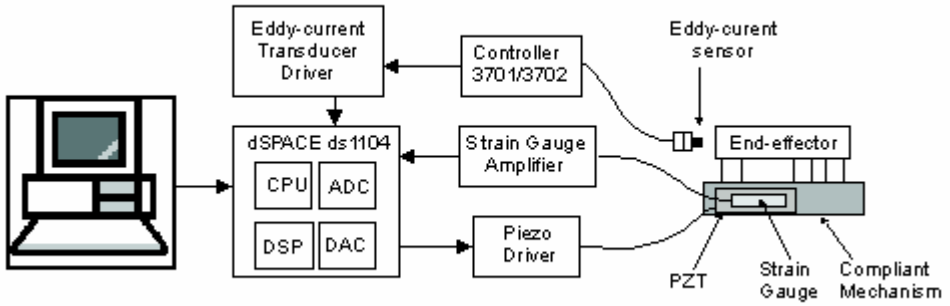

Figure 5.12 A schematic diagram of the measurement system [Handley et al. 2002].

5.3 Results and Discussions

The measurement on a prototype PZT RRR mechanism was currently limited to the configurations where all the three PZT actuators are activated in the same amount (see Table 5.1 for a list of these configurations). This is because a poor repeatability has been found in other configurations, which is further attributed to the fatigue problem with any compliant mechanism. Specifically, the measurement at the end-effector level was made prior to over thousand times of operations for the measurement at the actuator level.

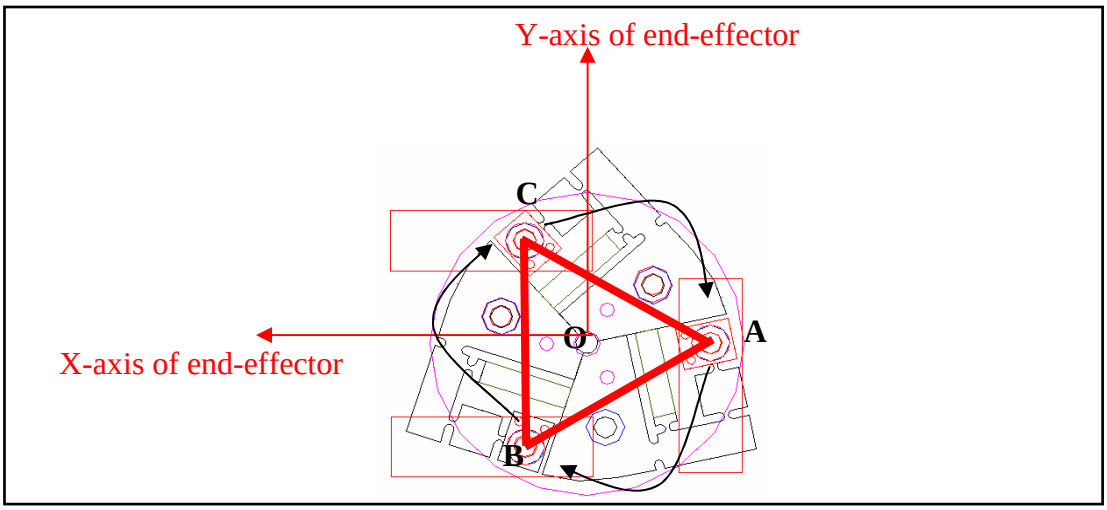

Figure 5.13 Rotating the positions of A, B and C.

The reliability test on these configurations was ensured by rotating the placement of the RRR mechanism. The first measurement was made at the original placement, while the second measurement was made by rotating the mechanism, say A to B, B to C, and C to A (see Fig. 5.13). The results from these two replacements were shown in Fig. 5.14. The average errors for the two replacements are about 1 micron for X-direction, 0.2 micron for Y-direction and 0.1 mrad for rotational direction. The errors are very small, which confirms the high repeatability of the measurements at these configurations.Fig. 5.15 presents the comparison of the results at the end-effector, at which both the simulations (Zou [2000], Zettl [2003], and the model developed in this thesis) and the measurement are shown. From the figure it can be seen that the results of this thesis are the closest to the measurement data, but still some significant deviations (the maximum deviation: 1.49 microns) exist. Such deviations are explained as follows. In the experiment, the RRR mechanism has some non-identical pre-load forces acted on the PZT actuators and the unmeasured initial deformation of the RRR mechanism due to the limitations of the manufacturing tool to produce the identical thickness of the thin plates. This is because that the piezoelectric actuators were assembled / pressed into the RRR mechanism by hand (to create a tight fit), in order to ensure the PZT actuators stay in its individual slots within the main body.

However, the information regarding the accurate values of the thickness of the thin plates and the initial deformation of the RRR mechanism are necessary in finite element modeling, which is in fact either not very accurate (due to the limitations of the measurement instrument to measure the thickness of the thin plates) or unavailable (due to the unavailability of a measurement instrument to measure the initial deformation experienced by the RRR mechanism due to prestress). This also explains the deviation of the results among Zou [2000], Zettl [2003], the measurement and the present model. The results presented in the present model are closer to the measurement results because the model has, to a certain extent, captured the non-identical thickness of the thin plates; whereas Zou [2000] and Zettl [2003] did not capture the information regarding the assembly of the RRR mechanism. This means that their results for the deformations of the RRR mechanism in X and Y directions (as all the PZT actuators are activated on the same input loadings as shown in Fig. 5.15) are insignificant compared to the measurement and the present model. Fig. 5.16 presents the comparison of measurement and simulation at the actuator level. In particular, the axial deformations of the piezoelectric actuators within the PZT-RRR mechanism as only a single piezoelectric actuator was activated (PZT 3) are presented. Similar to the results presented at the end-effector level, the results presented in the present model lie closer to the measurement results. To conclude, the simulation results validate the ‘uncoupling’ nature of the inactivated piezoelectric actuators that were observed during the experiment [Handley et al., 2002]. This result should enhance the reliability of the model developed in this thesis.

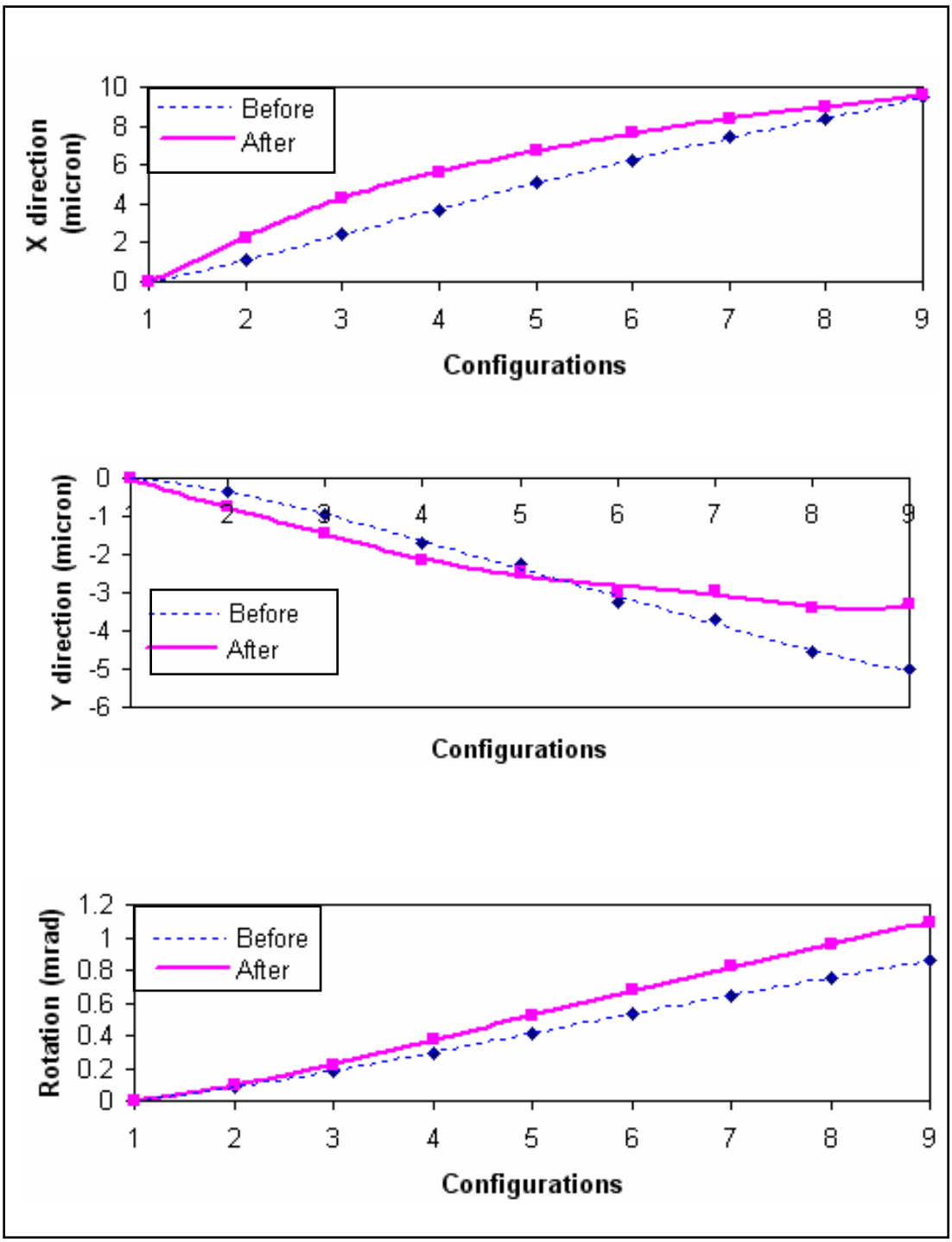

Figure 5.14 Check the data repeatability of the end-effector deformations in experiment.

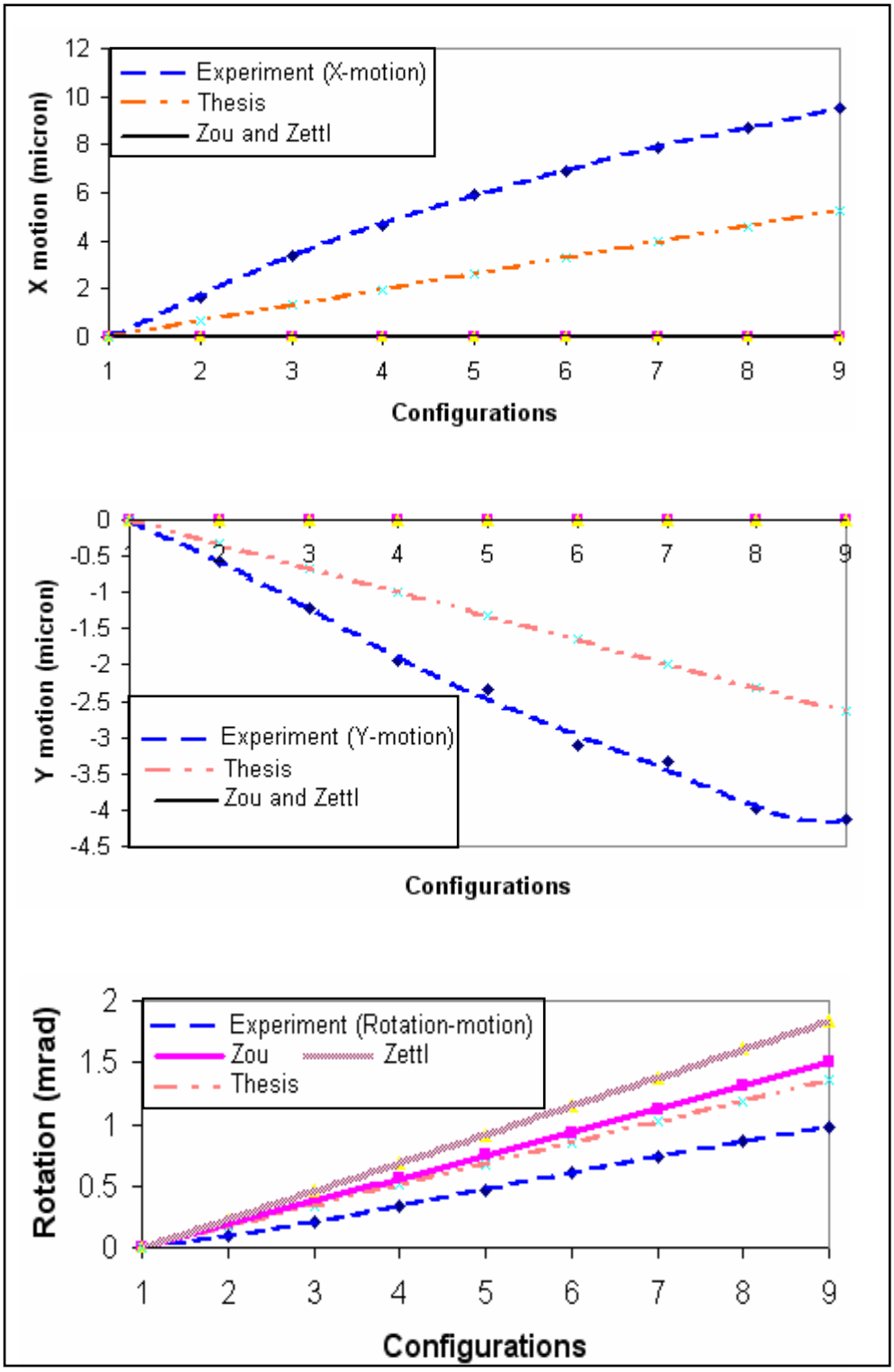

Figure 5.15 Comparison of the end-effector deformation results.

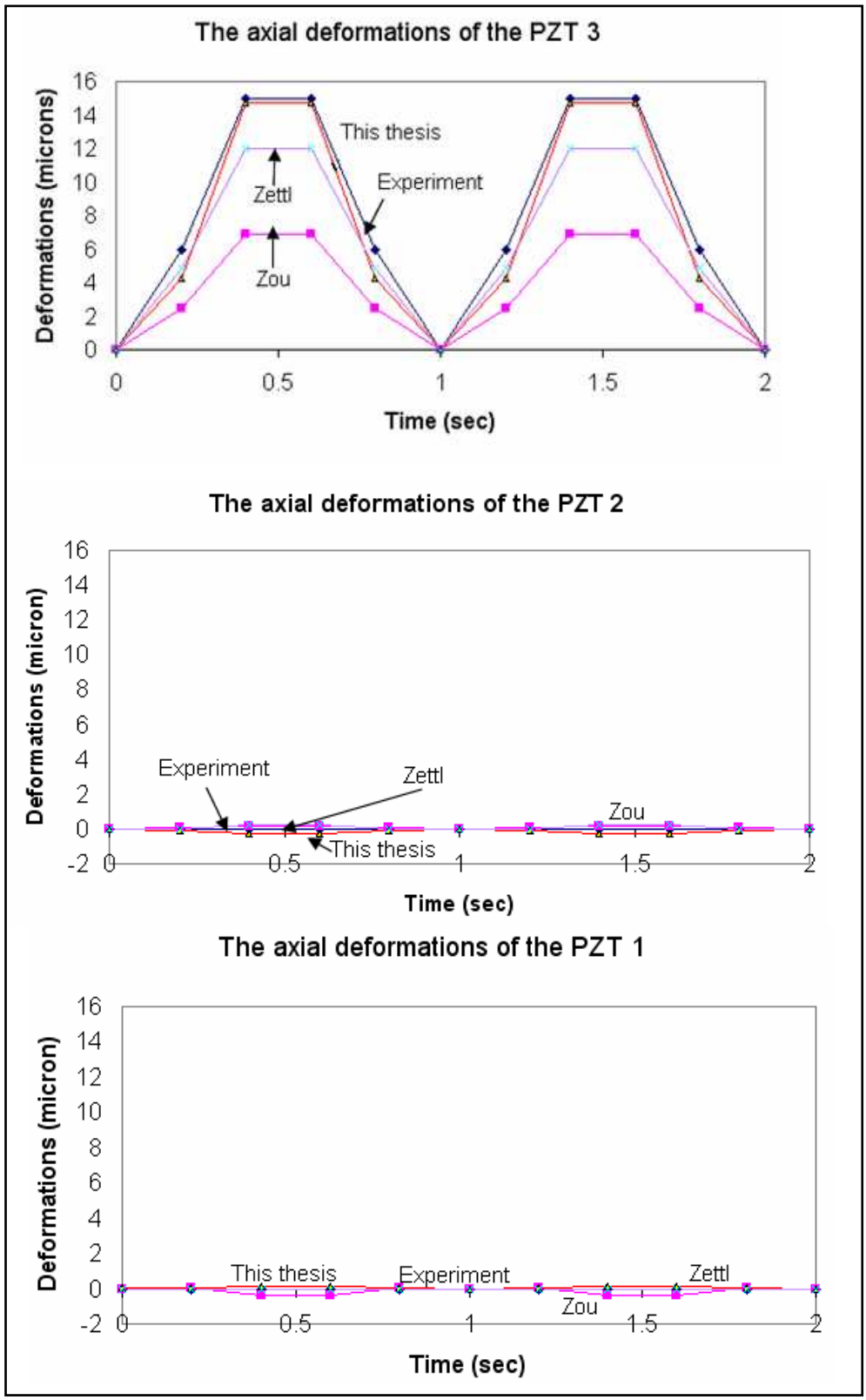

Figure 5.16 The comparison of measurement and simulation at the actuator level

5.4 Summary and Conclusion

The experiment test bed was established and described in this chapter, which included the measurement both at the actuator and the end-effector levels. The three simulation models, the model by Zou [2000], the model by Zettl [2003], and the one developed in this thesis study, were compared with the real measurements for two purposes. The first purpose is to explore the accuracy of the models, and the second purpose is to explore the design and assembly of the compliant mechanism. The comparison has shown that our model corresponds strongest with measurement. This is because our model has captured the physical property of the PZT actuator more fully, which includes (1) the pre-stress behaviour of the PZT actuator, and (2) the physical property of the piezoelectric material. Furthermore, the comparison also reveals the importance of design and assembly of the PZT actuator with the compliant mechanism. The current practice with the PZT RRR mechanism produces considerable uncertainty in achieving non-uniformity among three PZT actuators.

CHAPTER 6

CONCLUSIONS AND FUTURE WORK

6.1 Overview

This thesis presents a study toward a finite element approach to compliant mechanisms. In the current literature, the compliant mechanism is usually analyzed by use of the so-called pseudo rigid body (PRB) method. The basic idea of the PRB method is to lump continuous materials into a set of lumped materials that are connected by the rigid members. The problems with the PRB method are uncontrolled inaccuracy and high computation resource due to a complex dynamic model. Furthermore, the PRB method appears to be too complex to calculate the natural frequency and the global stiffness of the compliant mechanism.

A pioneer study using a general-purpose finite element program for analysis of compliant mechanisms was conducted at the Advanced Engineering Design Laboratory (AEDL) at the Department of Mechanical Engineering at the University of Saskatchewan [Zou et al., 2000]. A recent study at AEDL refers to Ref. [Zettl, 2003]. These studies have not considered the PZT actuator in a systematic way. Furthermore, there has been no published method, to the best of the author's knowledge, that computes the natural frequency and the global stiffness of a compliant mechanism using a finite element approach. Based on a detailed analysis

of literature presented in Chapter 2, the following objectives were proposed for the research presented in this thesis.

Objective 1: To develop a more accurate finite element model of the compliant mechanism for motion analysis with special attention to capturing the physical behaviour of the piezoelectric actuator, which is embedded in and drives the compliant mechanism.

Objective 2: To develop a more reliable test bed for the compliant mechanism with the objective to provide a test environment for the validation of the model for motion analysis.

Objective 3: To develop methods based on finite element analysis for predicting the global stiffness and natural frequency properties of the compliant mechanism.

These objectives have been achieved. The following are the details.

A literature review (Chapter 2) was conducted to confirm the statement of the objectives. Specifically, it was found that the finite element model of the compliant mechanism, incorporating the PZT actuator, was not previously reported in literature. The method for the calculation of the natural frequency and the global stiffness of the compliant mechanism using any general purpose finite element method was not reported elsewhere.

In Chapter 3, a finite element model for the compliant mechanism with consideration of the PZT actuator was presented. The model was implemented in the ANSYS environment; in particular, a type of element which deals with interdisciplinary domains (mechanical, electrical, etc), available in ANSYS, was employed. The pre-stress in the PZT actuator was also considered.

In Chapter 4, a finite element approach for calculating the natural frequency of the compliant mechanism was presented. The key to this problem is to view a mechanism as a series of “frozen” configurations, at each of which the mechanism becomes a structure. There are several solvers in ANSYS for calculating the natural frequency problem for a structure. They were reviewed and analyzed, resulting in the employment of the Block Lanczos Method. Another piece of the study presented in Chapter 4 is the calculation of the global stiffness of the compliant mechanism. A novel procedure based on the finite element method was formulated. The matrix size to calculate the global stiffness of the compliant mechanism is at most six by six.

In Chapter 5, a test bed was established for validating the displacement analysis of the compliant mechanism with the developed finite element approach described in Chapter 3. The comparison also included the studies conducted by Zou [2000] and Zettl [2003], respectively. The result of comparison shows that the method developed in this thesis has improved the other existing methods in terms of agreement between the measured result and the simulation result.

The finite element approach developed in this thesis was implemented by the general-purpose finite element program system ANSYS. The study presented in this thesis concludes:

(1) The finite element model for the PZT driven compliant mechanism should consider the piezoelectric material property more fully. The use of a block element or a spring element to simulate the PZT actuator stiffness does not work very well.
(2) The pre-stress in the piezoelectric element has significant influences over the accuracy of the finite element model.
(3) The piezoelectric element driven RRR mechanism has a kinematical uncoupling property among three actuators.
(4) The design of the assembly of the piezoelectric element and the compliant mechanism needs to be revisited carefully. The current design can lead to

considerable uncertainty in maintaining the symmetry of the whole mechanism (with respect to the center of the material).

6.2 Contributions

The main contributions of this thesis are described below:

(1) A more accurate model of the piezoelectric element driven compliant mechanism based on a special type of element available in ANSYS that represents the properties that are related to two different disciplines was developed.
(2) A finite element approach to compute the global stiffness of the compliant mechanism, which captures the stiffness of both the actuator and the compliant material was developed.
(3) A test bed upon which comparison of the models and the real measurements can be made was developed.

6.3 Future Work

The optimal design of the RRR mechanism warrants investigation. One of the design objectives is to have a large range of micro-motion without compromising the accuracy of motion. However, the large range may very likely involve reduced system stiffness. Therefore, a design trade-off is highly needed. The optimal design is to get the best trade-off. Furthermore, the optimal design may also be integrated with the optimal planning of motion to meet the requirement on the end-effector regarding motion and force.

The uncoupling property among actuators needs to be investigated together with the topology and geometry of the mechanism. A further verification of whether this property is exclusively related to the symmetry of the compliant mechanism system.

The current design has not considered the inertia term in the context of a general dynamic model of a mechanism system $[m]\ddot{x}+[c]\dot{x}+[k]x=f(t)$. The finite element model needs to be extended to consider the inertia term for motion analysis of the compliant mechanism.

References

Abdalla, M. M., Frecker, M., Gurdal, Z., Johnson, T., and Lindner, D. K., 2003. “Maximum Energy-Efficiency Compliant Mechanism Design for Piezoelectric Stack Actuators”, *American Society of Mechanical Engineers, Aerospace Division (Publication) AD*, 68, pp. 53-61.

Alik, H. and Hughes, T.J.R., 1970. "Finite Element Method for Piezoelectric Vibration", *International Journal for Numerical Methods in Engineering,* 2, pp. 151-157.

Angelino, M. R. and Washington, G.N., 2002. “Design and Construction of a Piezoelectric Point Actuated Active Aperture Antenna”, *Journal of Intelligent Material Systems and Structures*, 13, pp. 125-136.

ANSYS, 2004. *ANSYS Release 8.1 Documentation Preview*, Swanson Analysis System, Inc., Houston.

Bathe, K. J., 1982. *Finite Element Procedures in Engineering Analysis*, Prentice-Hall, Englewood Cliffs.

Bharti, S. and Frecker, M., I., 2004. “Optimal Design and Experimental Characterization of a Compliant Mechanism Piezoelectric Actuator for Inertially Stabilized Rifle’, *Journal of Intelligent Material Systems and Structures*, 15, pp. 93-106.

Braun, S. G., Erwins, D.J., and Rao, S.S, 2001. *Encyclopedia of Vibration*, 1-3, Academic Press-A Division of Hartcourt, Inc.London, UK.

Cattafesta,L., Mathew,J., and Kurdila,A, 2000. “Modeling and Design of Piezoelectric Actuators for Fluid Flow Control (online posting)’, SAE International and AIAA, Inc. <http://www.img.ufl.edu/publications/Modeling%20and%20Design%20of%20Piezoelectric%20Actuators%20for%20Fluid%20Control_Conference_October2000.pdf>

Chen, W. and Lin, W., 2003. “A miniature gripper system for optical fiber handling”, *Proceedings of SPIE - The International Society for Optical Engineering*, 4902, pp. 436-443.

Committee on Piezoelectric and Ferroelectric Crystals, 1958. “IRE Standards on Piezoelectric Crystals: Determination of the Elastic, Piezoelectric, and Dielectric Constants - The Electromechanical Coupling Factor”.

De Camp, L.S., 1974. *Ancient Engineers*, Ballantine, NewYork.

El-Khasawneh and Ferreira [1999]. El-Khasawneh,B.S., Ferreira, P.M., 1996.”Computation of stiffness and stiffness bounds for parallel link manipulators”, *International Journal of Machine Tools and Manufacture*, pp. 321-342.

Gosselin, C., 1990. “ Stiffness Mapping for Parallel Manipulators,” *IEEE Transactions on Robotics and Automation*, 6 (3), pp.377-382, June 1990.

Gosselin, C., 1990. “Determination of the Workspace of 6-DOF Parallel Manipulators,” *Journal of Mechanical Design*, 112, pp.331-336, September 1990.

Zhang, D., 1999. "Stiffness Analysis of Parallel Mechanism Using A Lumped Model," Doctoral Dissertation, Universite Laval, 1999.

Grimes, R.G., Lewis, J.G., and Simon, H.D, 1994. “A Shifted Block Lanczos Algorithm for Solving Sparse Symmetric Generalized Eigen-problems“, *SIAM Journal Matrix Analysis Applications*, 15 (1), pp. 228-272.

Guyan, R. J., 1965. "Reduction of Stiffness and Mass Matrices", *AIAA Journal*, 3 (2).

Han, C.S., Tesar, D., and Traver, A.E., 1989. “Optimum design of a 6 DOF fully-parallel micromanipulator for enhanced robot accuracy”, *American Society of Mechanical Engineers, Design Engineering Division (Publication) DE*, 19 (3), n pt 3, *Mechanical Systems Analysis, Design and Simulation*, pp. 357-363.

Handley, D.C., Zhao, W., Zhang, W. J., Li, Q., and Lu, Tien-Fu., 2002. “An Experimental Observation of Uncoupling of Multi-DOF PZT Actuators in a Compliant Mechanism”, *Proceedings of the 7th International Conference on Control, Automation, Robotics and Vision*, ICARCV 2002, 1, pp. 1354-1358.

Hara, A. and Sugimoto, K., 1989. "Synthesis of Parallel Micromanipulators", *ASME Trans Journal of Mechanisms, Transmissions, and Automation in Design*, 111, pp. 34-39.

Her, I. and Chang, J. C., 1994. "A linear Scheme for the Displacement Analysis of Micropositioning Stages With Flexure Hinges", *ASME Trans Journal of Mechanical Design*, 116, pp. 770-776.

Howell, L. L., 2001. *Compliant Mechanisms*, John Wiley & Sons, Inc Publishing Company.

The Institute of Electrical and Electronics Engineers, Inc. (IEEE), 1978.”IEEE Standard on Piezoelectricity,” *the Institute of Electrical and Electronics Engineers, Inc. (IEEE)*, Std. 176-1978.

Iwatsuki, N., Hayashi, I., and Morishige, K., 1996. “Vibration analysis of elastic manipulators with the adjacent link joint method”, *JSME International Journal, Series C: Dynamics, Control, Robotics, Design and Manufacturing*, 39(1), pp. 94-101.

Jen, C.W. and Johnson, D. A., 1991. “Modal Sensitivity Analysis of Planar Robots, Based on a Simplified CMS Approach”, Journal *of Robotics System*, 8, pp. 443-463.

KAMAN, 2000. *Application Handbook and Manual for SMU 9000 System*, KAMAN Corporation.

Kardestuncer, H. and Norrie, D.H., 1987. *Finite Element Handbook*, McGraw Hill.

Kim, J., Ko, B., Lee, J-K., and Cheong, C-C., 1999. ”Finite element modeling of a piezoelectric smart structure for the cabin noise problem”, *Smart Material Structure*, 8, pp. 380-389.

Kitis, L. and Lindenberg, R.K., 1989. “Natural Frequencies and Mode Shapes of Flexible Mechanisms By a Transfer Matrix Method”, *Finite Elements in Analysis and Design*, 6, pp. 267-285.

Lee, K. M and Arjunan, S., 1989. "A Three-Degrees-of-Freedom Micromotion In-Parallel Actuated Manipulator", *IEEE Trans on Robotics and Automation*, 7(5), pp. 634-641.

Lerch, R., 1990.”Simulation of Piezoelectric Devices by Two-and Three-Dimensional Finite Elements”, *IEEE Transactions on Ultrasonics. Ferroelectrics. and Frequency Control,* 37(02), pp. 233-247.

Li, C-J. and Sankar, T.S., 1992. “Systematic Method of Dynamics for Flexible Robot Manipulators,” *Journal of Robotics System*, 9(5-8), pp 861-891.

Lyon, S.M., Erickson, P.A., and Howell,L.L., 1999. “Prediction of the first modal frequency of compliant mechanisms using the pseudo-rigid-body model”, *Journal of Mechanical Design Transactions of the ASME*, 121(2), pp. 309-313.

Lorenz, R. D., Meyer, K. M., and Van De Riet, D. M., 1990. “Novel, Compliant, Four-degree-of-freedom, Robotic Tip Sensor“, *IEEE Transactions on Industry Applications*, 26 (4), pp. 613-619.

Maple, 1997. Maple V Release 5 reference, Waterloo Maple Inc.

Mason,W.P. and Jaffe, H, 1954. “Methods for measuring Piezoelectric, Elastic, and Dielectric Coefficients of Crystals and Ceramics”, *Proceedings of the Institute of Radio Engineers*, 42, pp. 921–943.

McEwen, E., Miller, R.L., and Bergman, C.A., 1991. “Early Bow Design and Construction,” *Scientific American*, 264, pp. 76-82.

Peelamedu, S.M., Dukkipati, R.V., and Naganathan, N.G., 2001. “Finite element approach to model and analyze piezoelectric actuators,” *JSME International Journal, Series C: Mechanical Systems, Machine Elements and Manufacturing*, 44(2), pp. 476-485.

Piefort,V. and Preumont, A., 2001. “Finite Element Modeling of Piezoelectric Structures (on-line posting)”, Active Structure Laboratory, Belgium. <http://www.ulb.ac.be/scmero/documents/piezo/js2001_ulb_vp.pdf>

Portman, V.T., Sandler,B-Z., and Zahavi, E., 2000. “Rigid 6 X 6 Parallel Platform for Precision 3-D Micromanipulation: Theory and Design Application,” *IEEE Transactions on Robotics and Automation*, 16 (6), pp. 629-643.

von Preissig,F.J. and Kim,E.S., 2000.”Topics in Finite Element Modeling of Piezoelectric MEMS (on-line posting)”, University of Hawaii and University of South Carolina, USA, 2000.
<http://www.comppub.com/publications/MSM/2000/pdf/T45.09.pdf>

Rajakumar, C. and Ali, A., 1992. "A Solution Method for Acoustic Boundary Element Eigenproblem With Sound Absorption Using Lanczos Algorithm", *Proceedings of 2nd International Congress on Recent Developments in Air- and Structure-Borne Sound and Vibration*, Auburn University, AL, pp. 1001-1010.

Ryu, J. W., Gweon, D. G., and Moon, K. S., 1997. "Optimal Design of a Flexure Hinge Based XYθ Wafer Stage", *Precision Engineering*, 21, pp.18-28.

Sanger, D. J., Chen, J. Q., Zhang, S. J., and Howard, D., 2000. “A General Method for the Stiffness Analysis of Manipulator Mechanisms”, *Proceedings of the Institution of Mechanical Engineers, Part C: Journal of Mechanical Engineering Science*, 214 (5), pp. 673-685.

Setter, N., 2002. “Piezoelectric Materials in Devices”, EPFL Swiss Federal Institute of Technology, Switzerland.

Standards Committee and Piezoelectric Crystals Committee, 1949. “Standards on Piezoelectric Crystals”, *Proceedings of the Institute of Radio Engineers*, 37, pp. 1378 –1395.

Tokin, 1996. *Multilayer Piezoelectic Actuators: User’s Manual*, Tokin Corporate Publisher.

Tomita, Y., Sato, F., Ito, K., and Koyanagawa, Y., 1992. “Decoupling Method of Ultraprecision Stage using Parallel Linkage Mechanism,” *Journal of the Japan Society of Precision Engineering,* 57 (6), pp. 1078-1084.

Turcic, D. A., 1982. *A General Approach to the Dynamic Analysis of Elastic Mechanism Systems*, Doctoral Dissertation, Pennsylvania State University.

Vishay Measurements Group, Inc., 1992. *Student Manual for Strain Gage Technology*.

Wilson, E. L. and Itoh, Tetsuji, 1983. "An Eigensolution Strategy for Large Systems”, *Computers and Structures*, 16 (1-4), pp. 259-265.

Zettl, B., 2003. *Effective Finite Element Modeling of Micro-Positioning Systems*. M.Sc., University of Saskatchewan, Saskatoon, Canada.

Zou, J. 2000. *Kinematics, Dynamics, and Control of a Particular Micro-Motion System*. M.Sc., University of Saskatchewan, Saskatoon, Canada.

Appendix A: Physical Design of the RRR Mechanism

The RRR mechanism studied in this thesis consists of the following components:

(1) Main body;
(2) Three PZT actuators;
(3) One end effector platform;
(4) Three bolts; and
(5) Three thin metal plates.

They are assembled into a mechanism, as shown in Fig. A.1

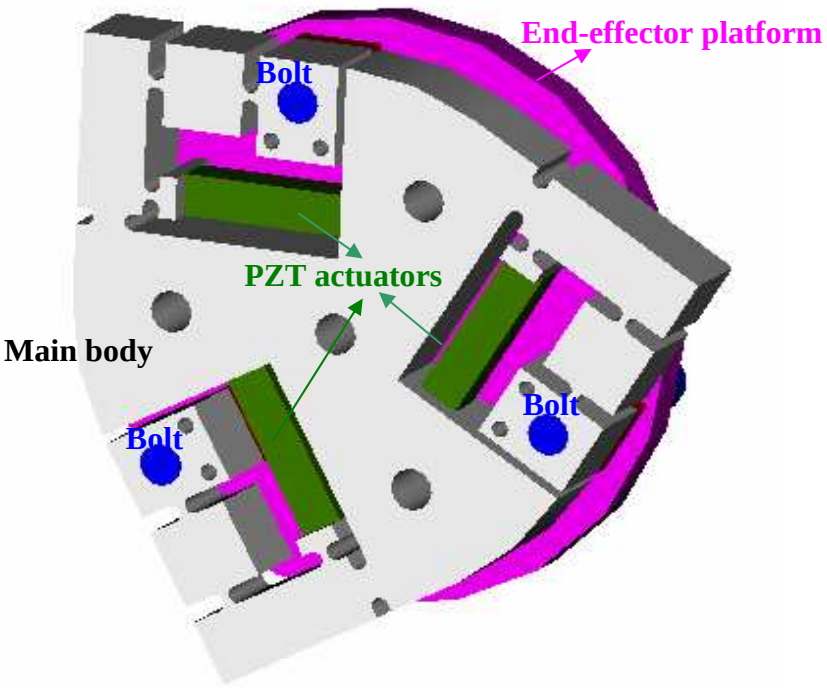

Figure A.1 The assembly of the RRR mechanism.

A.1 The main body

Fig. A.2 illustrates the topology and geometry of the main body, where holes A, B and C are used to fix the main body onto a ground, while holes 1, 2 and 3 are used to fix the main body to the end-effector platform. As such, when the main body deforms under the action of the PZT actuator, the end-effector will exercise motion with respect to the ground. This main body was made up of bronze material and named C 61000 based on the UNS (Unified Numbering Standard). The main body has the following properties.

- 8% Aluminum Bronze,
- Modulus Elasticity: 117×10^9 Pa, and
- Density: 7.78×10^3 Kg/m^3.

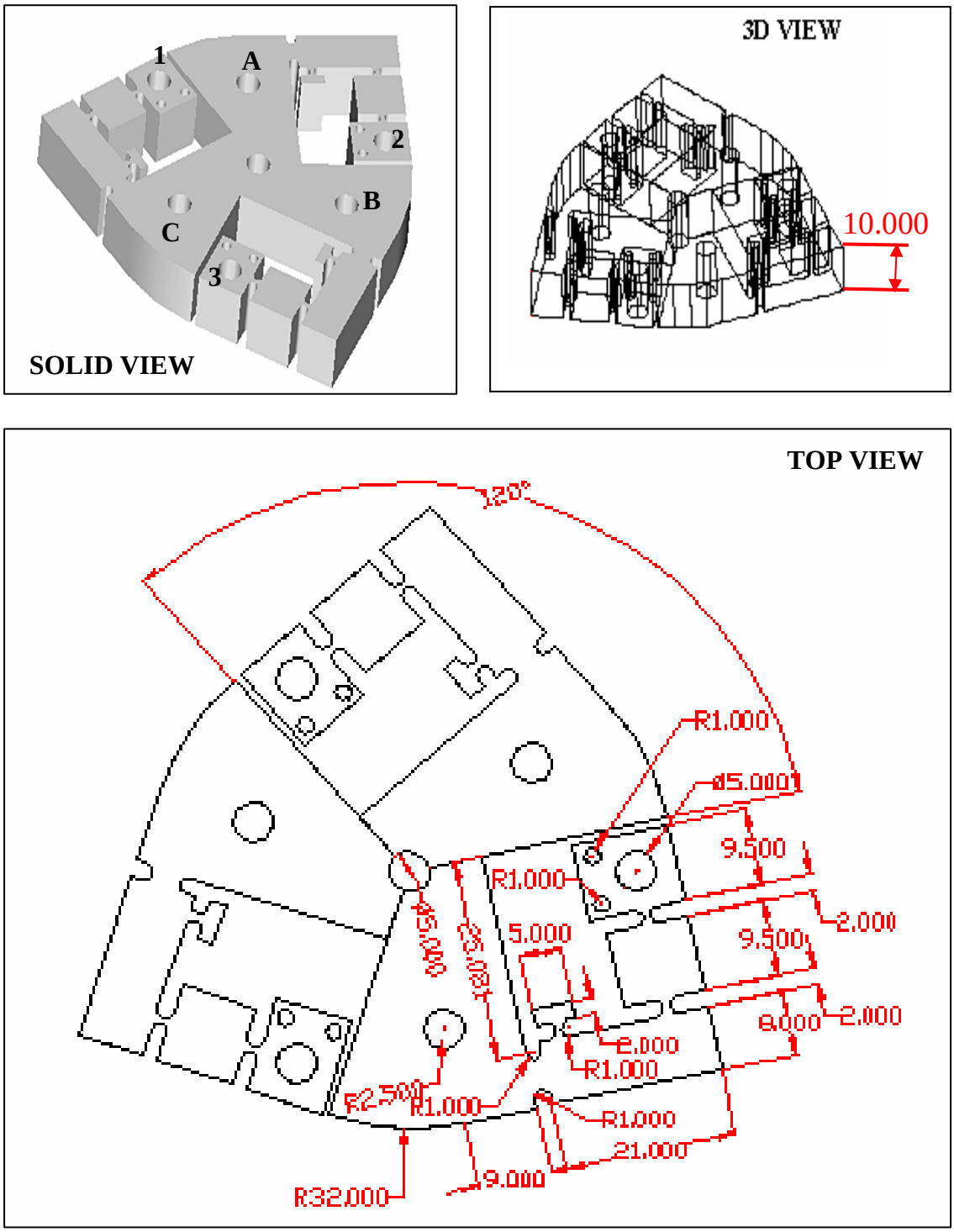

Figure A.2 The main body (all the units are mm)

A.2 The PZT actuator

The PZT actuator used in this thesis study is the product of Tokin manufacturer [Tokin, 2000], specifically the model AE0505D16. Both the geometry and material properties of this actuator were given in Chapter 2. The displacement of the PZT actuator is measured by a strain gage. In this study the strain gage is a product of Vishay Measurements Group, Inc.; specifically the model EA-06-125TG-350. Prior to measurement of the PZT actuator by use of the strain gage, one should pay close attention to the process of attaching the strain gage onto the PZT actuator due to the fact that the strain gage has capability of measuring the smallest effects of an imperfect bond. The imperfect bond will result in the inaccurate reading results. The procedure of gluing the strain gage onto the PZT actuator can be classified into surface preparation, strain gage bonding, and soldering. In surface preparation, the objectives are to develop chemically clean surface (by use of special chemical agent, M-Bond 200, to remove the oil and the grease), to create the appropriate surface roughness (by use of a special abrading paper, silicon-carbide paper, to remove rust and paint), to build the correct PH of the surface (by use of the special agent, M-Prep Neutralizer 5A, to neutralize the PH of the surface) of the object that will be measured (i.e., the PZT actuator) and to create the clear and visible gage layout lines for positioning the strain gage onto the PZT actuator. In strain gage bonding, it is important to ensure that the bonded strain gage stays still on the surface (visible gage layout lines in particular) that is going to be measured due to the fact that its performance is absolutely dependent on the bond between itself and the test part. Thus, the procedure that was discussed in [Vishay Measurements Group, 1992] should be followed. The purpose of soldering is to install the wires into the glued strain gage such that the specified resistance requirement from the manufacturer is met. There is a measurement instrument recommended by manufacturer (Model 1300 Gage Installation Tester) to ensure if the specified resistance requirement from the manufacturer is met (10,000 to 20,000 ohms).

Fig. A.3 shows the installed strain gage on the PZT actuator. The strain gages are glued to two sides of the PZT actuator and act as a pair. Each pair is wired to their own strain gage conditioner. The strain gage conditioner is to compute the response of the PZT actuators by use of the calibration equations. These calibration equations are then used to determine the displacement of each PZT. Based on the experiment, the strain gage has the position resolution of 10 nm.

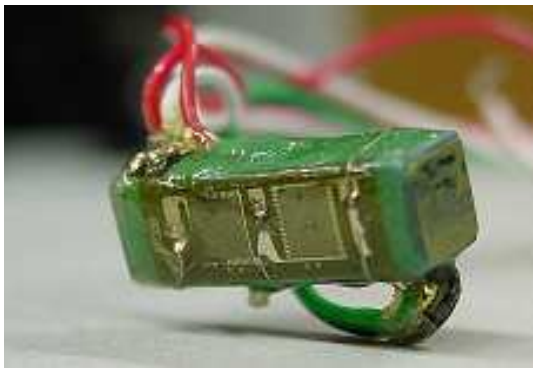

Figure A.3 The attached strain gage on the PZT actuator.

A.3 The end effector platform

The topology and geometry of the end-effector is given in Fig. A.4. It is noted that the holes 1, 2, 3 on the end-effector platform are assembled with the corresponding holes on the base. The material properties of the end-effector platform are given as follows:

- Standard name based on ASM (American Society for Metals Specialty Handbook): Aluminum 6061-T6,
- Modulus Elasticity: 69 x 10^9 Pa,
- Proportional limit: (σ_p)$\leq$ 275 x 10^6 Pa, and
- Density : 2.768 x 10^4 Kg/m^3 .

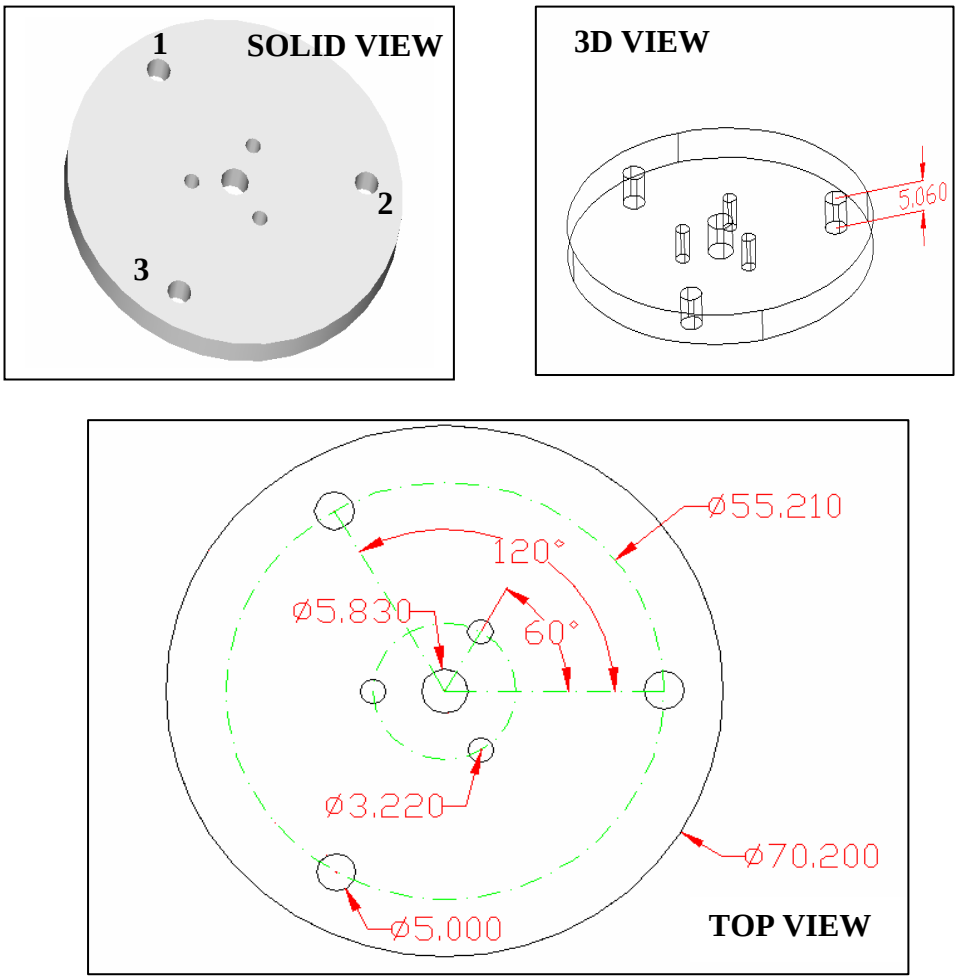

Figure A.4 The end-effector platform.

A.4 The bolt

Fig. A.5 illustrates the geometric information of a bolt. The three identical bolts are to attach the end-effector platform and the main body at holes 1, 2 and 3, respectively. The material properties presented as follows:

- *Standard name based on ASTM (American Society for Testing and Materials*: 10/32 Fine Thread Screw,
- *Modulus elasticity*: 358.28 x 10^6 Pa, and
- *Density:* 8.780 x 10^3 kg/m^3 .

Figure A.5 Geometric boundaries of a bolt.

A.5 The adjusting (thin metal) plate and the pre-stress

The thin metal plate is a plate inserted between the PZT actuator and the main body to create fitting tolerance as illustrated in Fig. A.6. The rationales of employing such components are available in Section 3.4.1. The material properties of the thin metal plate are illustrated as follows:

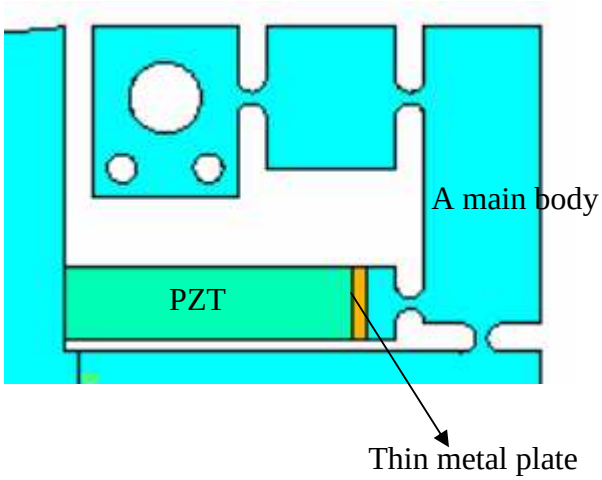

Figure A.6 Location of the thin metal plate within the RRR.

- *Standard name based on ASTM (American Society for Testing and Materials*: C1018, and
- *Modulus elasticity*: 344.5 x 10^6 Pa.

Torsional loads are not an issue because the driving elements (piezoelectric actuators) for the RRR compliant mechanism only exhibit the axial loading. Eliminating shear loading was done in the assembly process of the RRR compliant mechanism. During the assembly process, the compliant mechanism was attached using a special manufactured plate (a simple structural plate that has uniform thickness along its length inserted between PZT and the part of compliant piece) that was manufactured such that the axis polarization of piezoelectric actuator aligns with the center axis of flexure hinge. After that, the prestress state was applied on compliant mechanism. Fig. A.7 illustrates the compliant piece under prestress state.

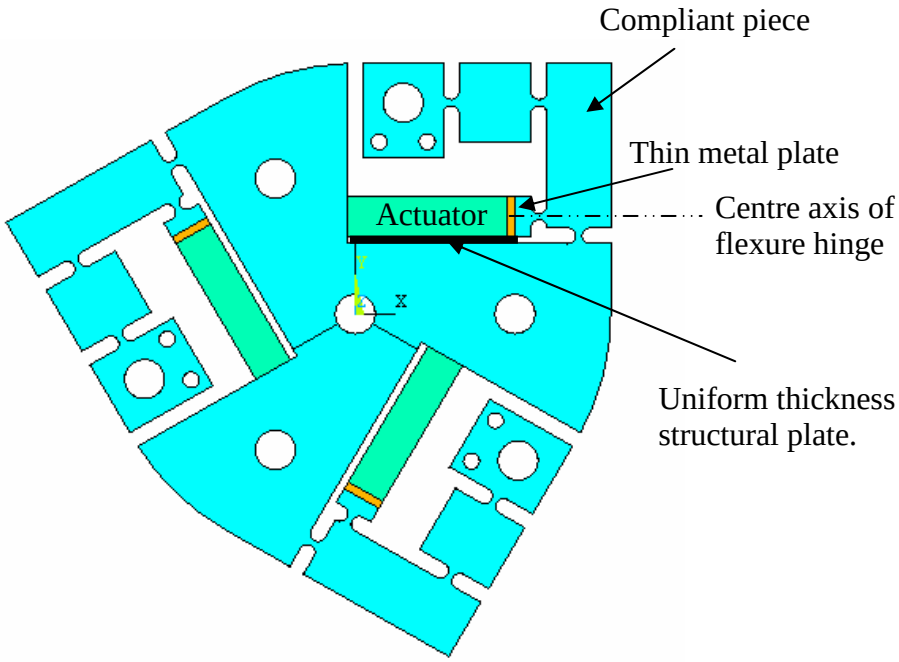

Figure A.7 Compliant piece under prestress state.

The prestress state was realized by inserting a thin metal plate into the gaps between actuators and actuators' slots within compliant piece, to create tight fit (causing actuators to be compressed). When the compliant piece is in motion, the prestress is to ensure the position and orientation of the actuators (that have been aligned with the bracket) do not change with respect to the center axis of flexure hinge (in order to

prevent shear loads from occurring on flexure hinges' surfaces), to prevent separation between actuators and compliant piece, and to prevent tension condition in actuators from occurring that can damage actuators. The measurement of the pre-deformation due to the plate is given in Appendix B.

Appendix B: The measurement of the pre-deformation

Step1. Obtained the original length of the PZT slot (see Fig. B.1)

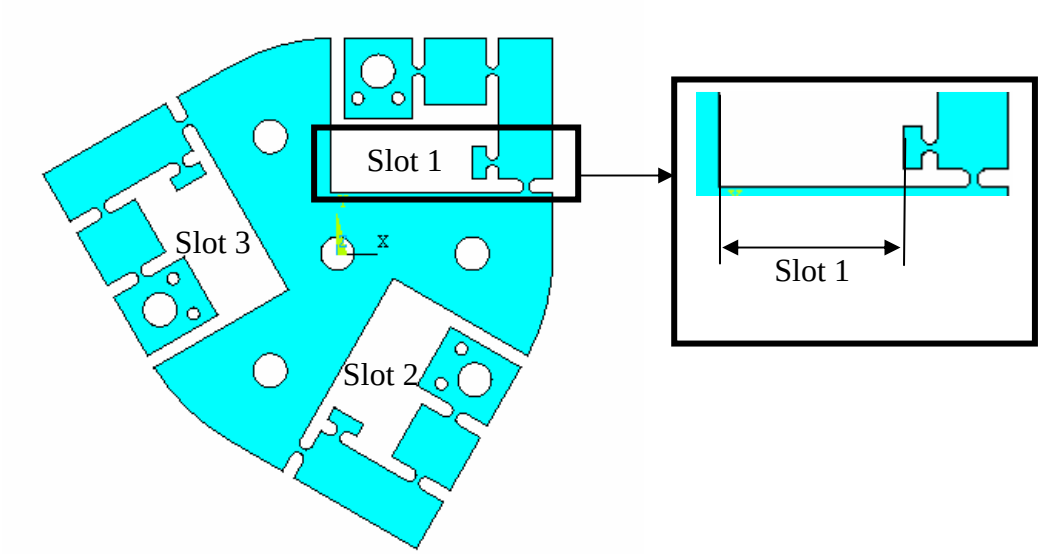

Figure B.1 The slots of the PZT actuators.

The length of the slots of the PZT actuator prior to pre-deformation was obtained through the original design drawing of the RRR mechanism. The length of each PZT slot prior to pre-deformation is 21 mm.

Step 2. Measured each slot of the pre-deformed RRR mechanism

By use of a measurement instrumentation (a digital caliper), the length of each slot of the pre-deformed RRR mechanism was obtained. The lengths of the pre- deformed slots of PZT 1, PZT 2, and PZT 3 are 20.24 mm, 20.51 mm, and 19.97 mm respectively.

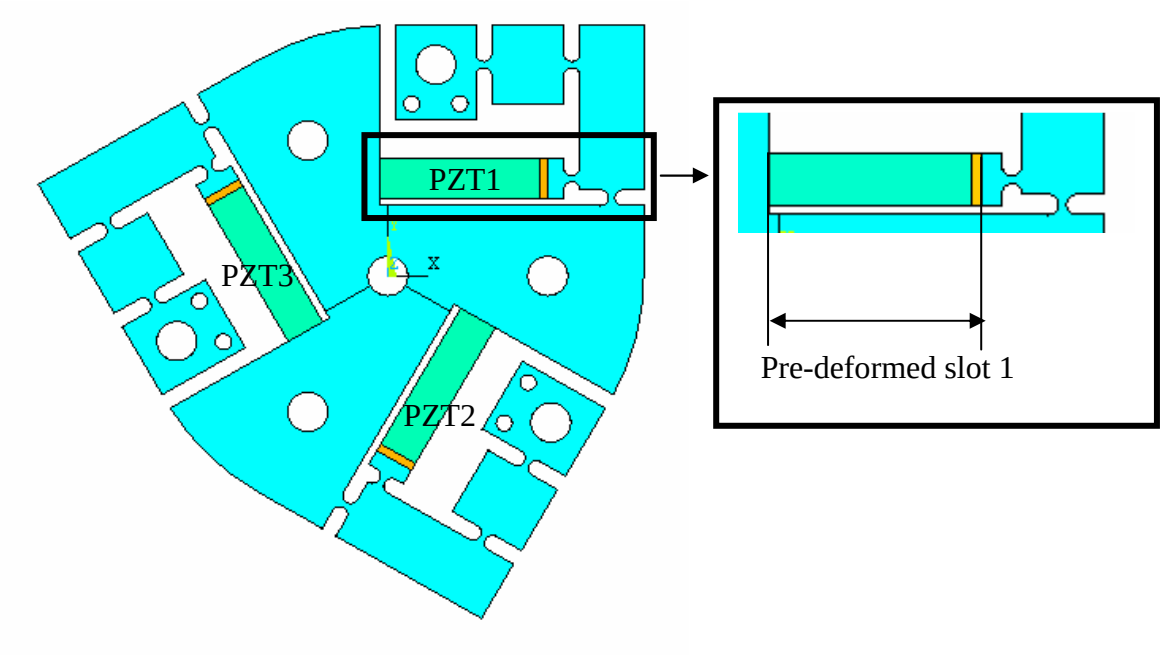

Figure B.2 The pre-deformed slot of the PZT actuators.

Step 3. Calculated the pre-deformed forces

Based on the following equation

$$F = E \times A \times \frac{\Delta l}{l} \qquad \text{From Eqn. (3.20)}$$

where F : the prestress force or load (N),

E : the Young modulus of the PZT material (4.4e10 N/m^2),

A : the cross sectional area of the PZT actuator (25e-6 m^2),

l : the length of the PZT slot (21e-3 m),

and Δl : the displaced length of the PZT slot due to the prestress (m).

The values of Δl were obtained by subtracting the original length of the PZT slot (as discussed in step 1) with the pre-deformed length of the PZT slot (as discussed in step 2. The values of Δl_1, Δl_2, and Δl_3 are 0.76e-3 m, 0.49e-3 m, and 1.03e-3 m,

respectively. Finally, the values of the pre-deformed forces of PZT 1, PZT 2, and PZT 3 can be calculated. The pre-deformed forces of PZT 1, PZT 2, and PZT 3 are 3.981e4 N, 2.56667e4 N, and 5.395 e4 N, respectively.

Appendix C: Design of a Workbench

There are the following requirements for assembly of the sensor and the target, i.e.,

(1) Distance requirement
(2) Sensor mounting requirement
(3) Parallelism requirement
(4) Target requirements
(5) Sensor to sensor proximity requirement

The detailed design of an adjustable workbench upon which the sensor and the target can be assembled in meeting the above requirements is described below.

C1. Distance requirement

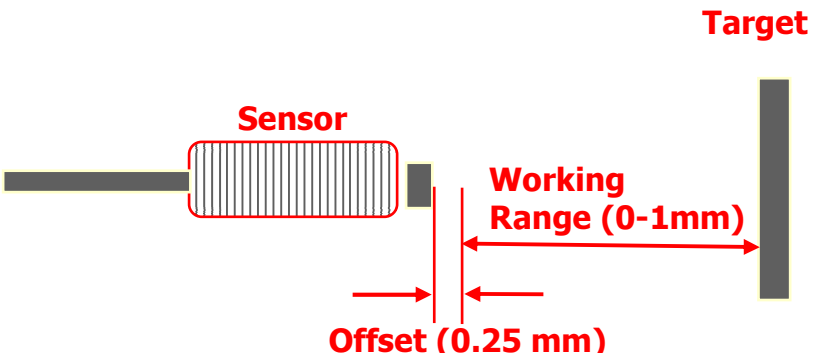

Figure C.1 Required distance between sensor and target [Kaman, 2000].

Fig. C.1 shows the required distance between the sensor and the target. There are two types of required distance; the offset distance and the working range distance. The offset distance is a minimum distance that needs to be maintained between the sensor and the target without degrading the reading accuracy, while the working range distance refers to the range limits (the minimum and maximum limits) that have to be maintained between the sensor and the target during the measurement. So, the distance between the sensor and target need to be situated from 0.25 mm to 1.25 mm.

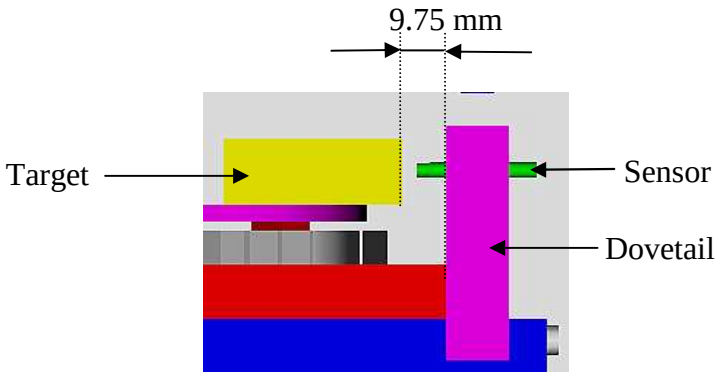

Figure C.2 Distance between sensor and target in the workbench

As illustrated in Fig C.2, the distance between the dovetail and the target is 9.75 mm. This value is not only to overcome the distance requirement, but also to provide some sufficient space for the adjustment of the sensor's position on the dovetail for the calibration purpose.

C2. Sensor mounting requirement

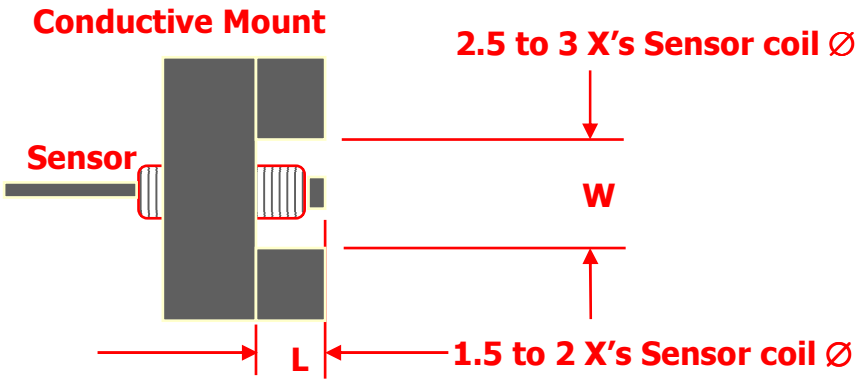

Figure C.3 Sensor mounting requirement [Kaman, 2000].

Fig. C.3 shows the minimum empty area, which is represented by variables W and L, around the tip of the sensor. This area needs to be maintained. The dovetail was designed to maintain L and W.

(a)

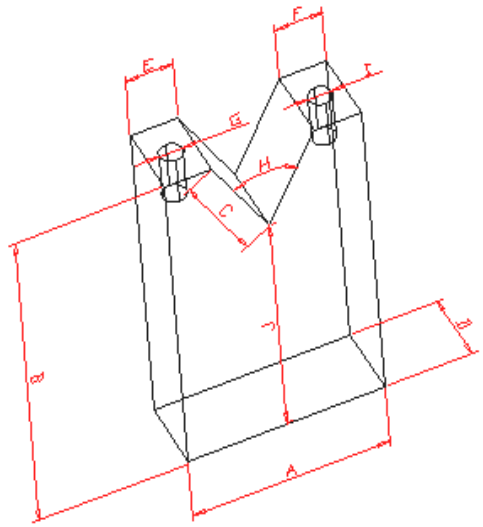

Variables	Values (mm)
A	41.579
B	67.539
C	10
D	12.840
E	10
F	10
G	$\phi 5$
H	60^0
I	$\phi 5$
J	58.879

(b)

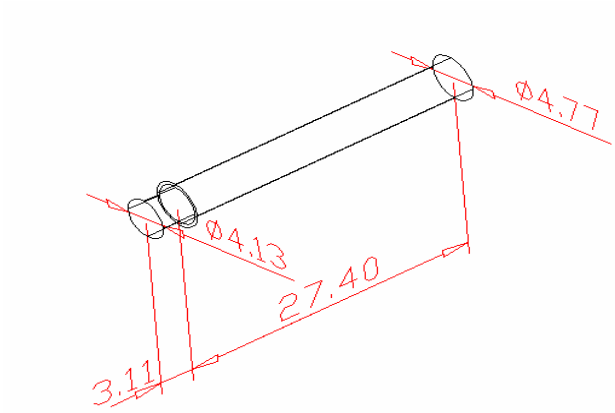

Figure C.4 Geometric boundaries of dovetail and sensor.

Figs. C.4a and C.4b present the geometric boundaries of the dovetail and those of the sensor. Variable D (see Fig. C.4a) is an important variable of the dovetail's variables in maintaining variable L (see Fig. C.3). In this thesis work, the variable D is manufactured to be 12.840 mm. The dovetail supports the part of sensor body in the value of 12.840 mm; consequently, a part of the sensor body that is not supported by the dovetail is about 17.67 mm. This value is sufficient not only to compensate L

(calculated to be 8.26 mm due to the fact the sensor's coil diameter is 4.13 mm), but also to provide some adequate adjustment for the purpose of sensor calibration.

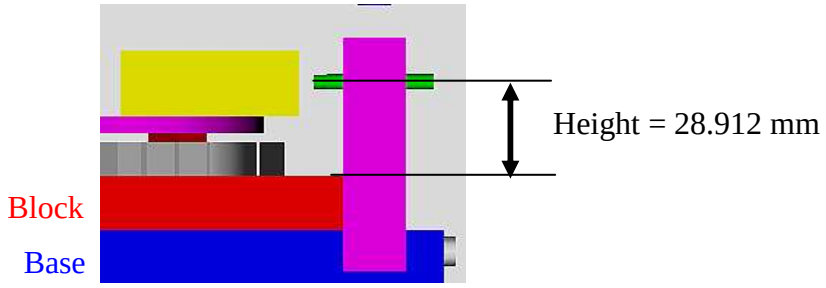

Figure C.5 The height of the sensor.

Fig. C.5 is to determine the height of the sensor that is measured from the block. This height is manufactured to be 28.912 mm in order to compensate half of W (calculated to be 12.39 mm divided by two, which is equal to 6.195 mm). Note that W is divided by two because W applies to the both areas of interest, in particular the area below the sensor's position and the area above the sensor's position. The height of the sensor that is measured from the block (28.912 mm) should compensate half of the W (6.195 mm).

C3. Parallelism requirement

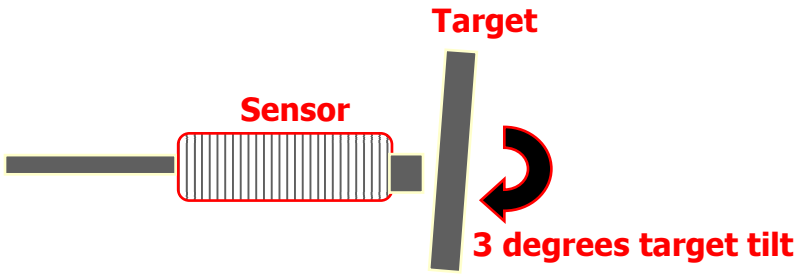

Figure C.6 Parallelism requirement [Kaman, 2000].

To maintain the parallelism requirement, a guiding plate is inserted between the sensor and the block prior to fixing the sensor onto the dovetail. During the measurement, this plate is removed.

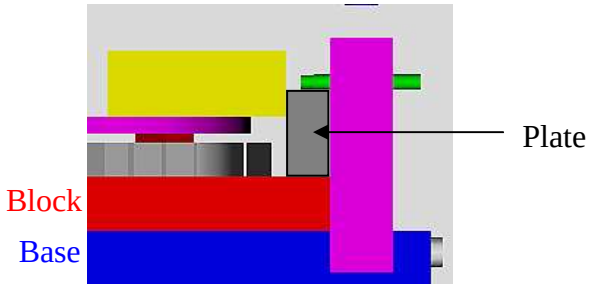

Figure C.7 Solution to compensate the parallelism requirement.

C4. Target requirement

The target requirements comprises of the material of the target, the minimum diameter of the target, and the thickness. As previously mentioned, Kaman determines that the material requirement for the target is Aluminum T6, while the minimum diameter of the target and the thickness requirement is re-illustrated in Fig. C.8.

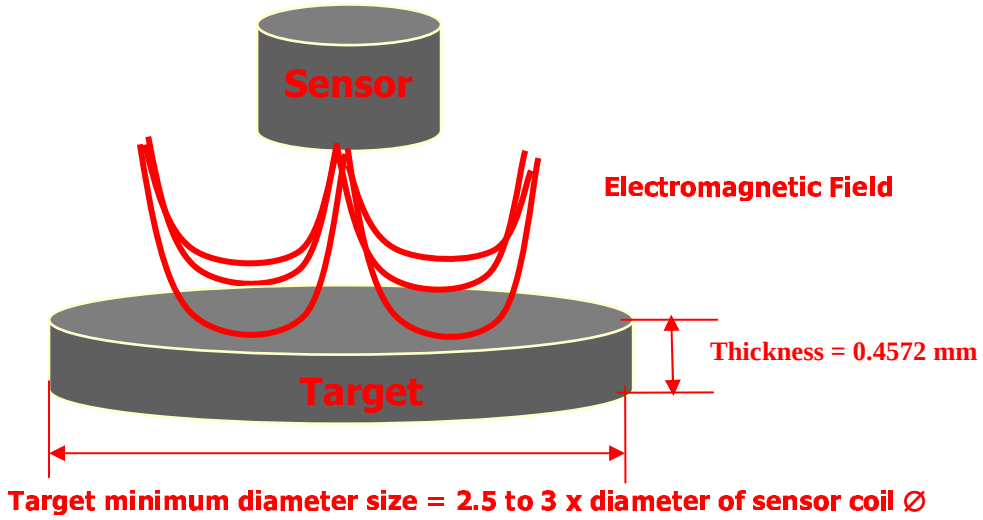

Figure C.8 Target requirements [Kaman, 2000].

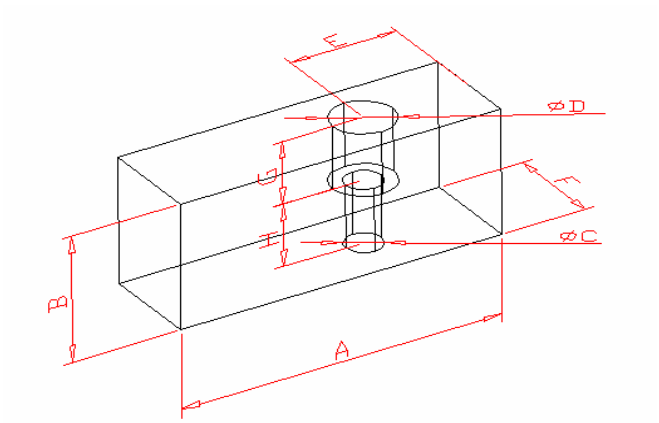

Variables	A	B	ϕC	ϕD	E	F	G	H
Values (mm)	45	19.05	5	8.5	15	17	9.525	9.525

Figure C.9 Geometric boundaries of a target.

Fig. C.9 presents the geometric boundaries of a target. The minimum thickness of a target is 0.4572 mm (see Fig. C.8). To compensate the geometric boundaries of a target, this value is in particular variable B is 19.05 mm. As for the minimum diameter size of the target (12.39 mm based on the computation), such a requirement has been overcome in the target by providing the variables B and F with the values of 19.05 mm and 17 mm respectively.

C5. Sensor to sensor proximity requirement

It is important to maintain the distance between the sensors in order to prevent the electromagnetic interference between sensors that leads to the reading accuracy degradation. Fig. C.10 shows the sensor to sensor proximity requirements. Based

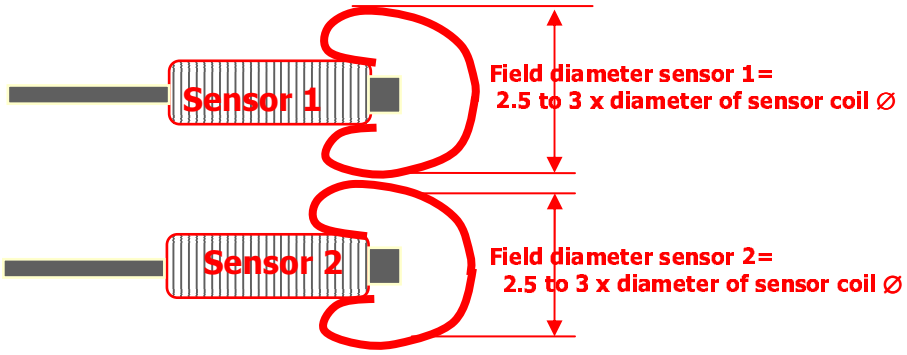

Figure C.10 Requirement for sensor to sensor proximity [Kaman, 2000].

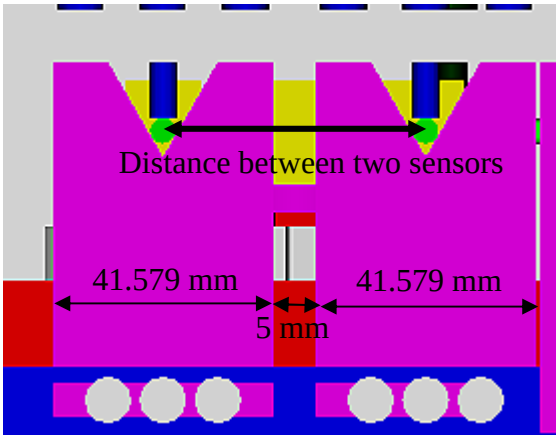

Figure C.11 The distance between two sensors.

on the calculation from Fig. C.10, the minimum distance between two sensors is 12.39 mm. From Fig. C.11, the length of each dovetail is 41.579 mm, while the space that separates the dovetails is 5 mm. Thus, the distance between the sensors in the workbench is equal to 46.579 mm, which is sufficient to compensate the requirement for sensor to sensor proximity, which is 12.39 mm.

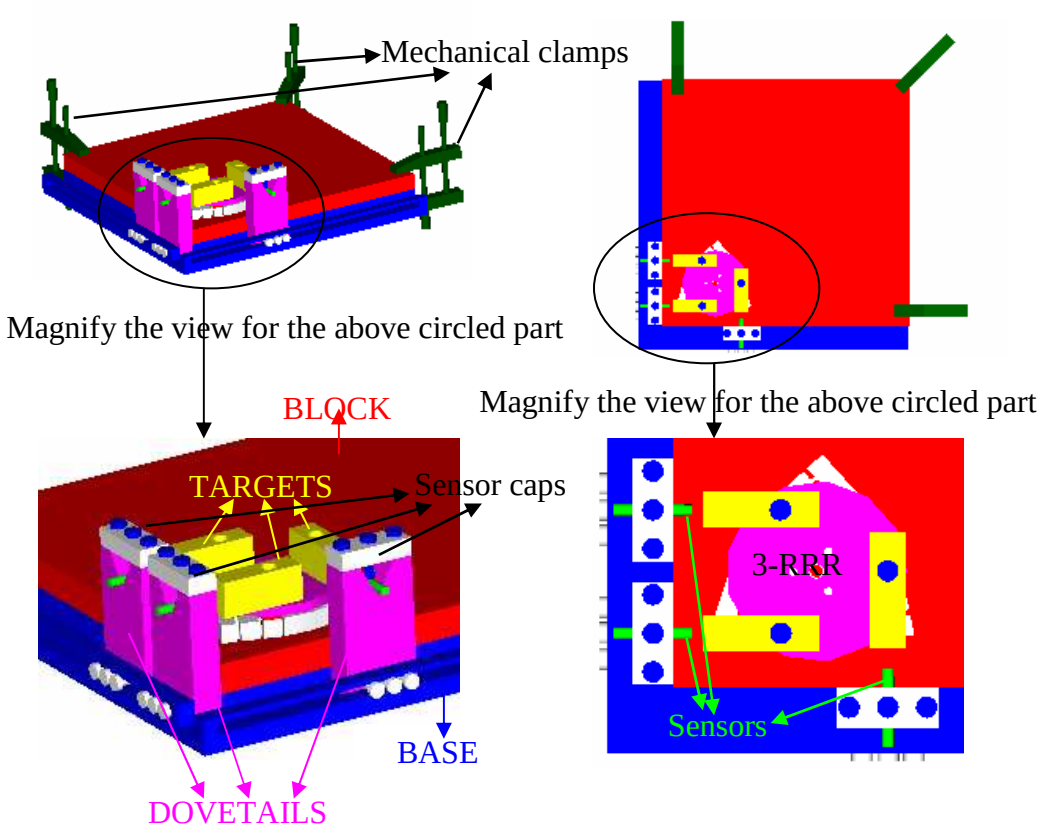

Figure C.12 An assembled workbench.

The assembly diagram of the workbench is shown in Fig. C 12. Components are, shown in Fig. C.13, while details can be found in the following files ("workbench1.doc" and "workbench2.doc") in the attached CD disk.

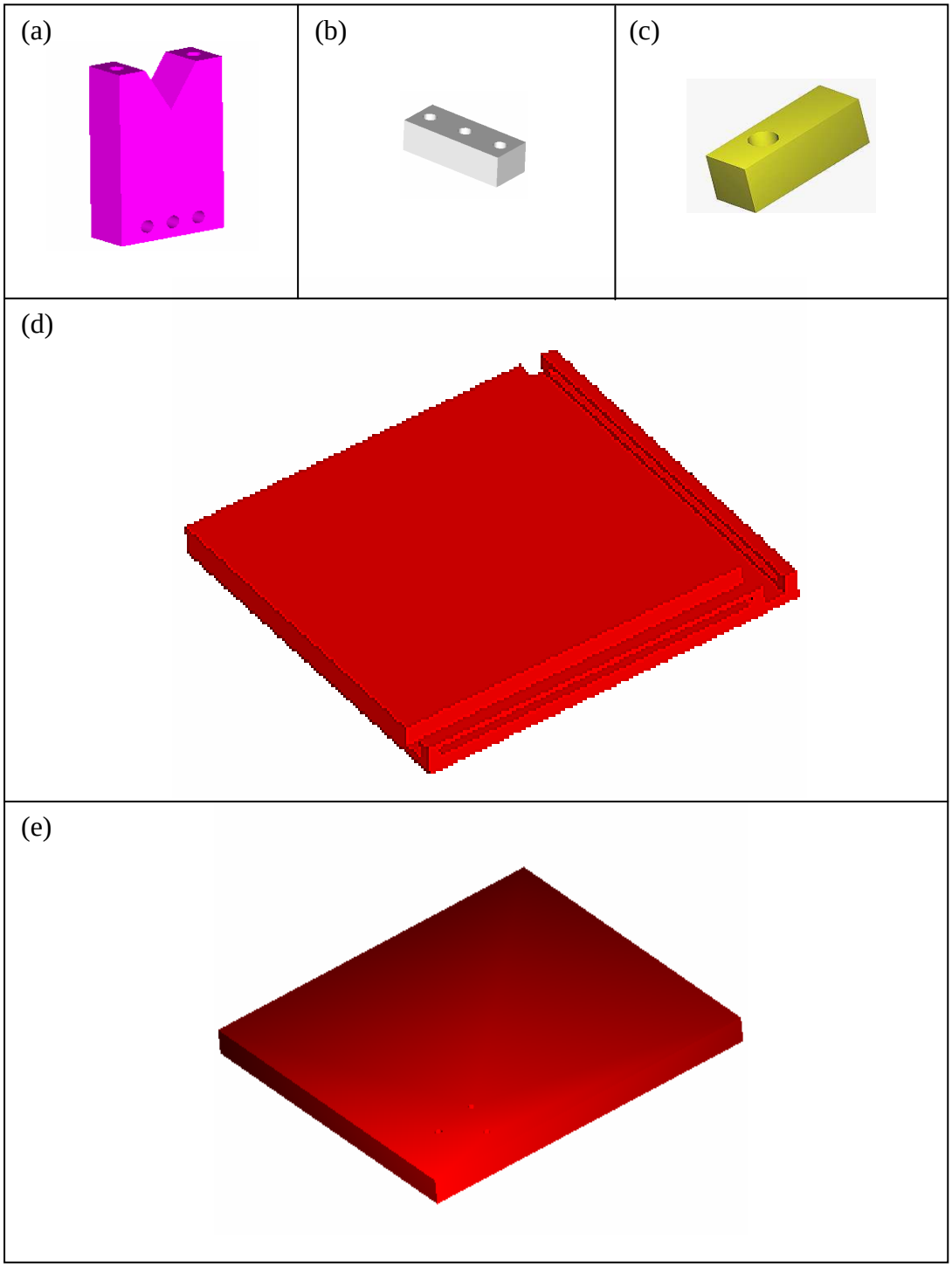

Figure C.13 Components of a workbench.

The dovetail (see Fig. C.13a) functions to hold sensor in its place. The dovetail has three taps and two holes on the top. The taps are to accommodate the screws' entrance, in particular to fix the dovetail into the base. Two taps were used to fix the sensor cap on the top. The sensor cap (see Fig. C.13b) has three taps. Two taps in the corners are to accommodate the screws' entrance, while the tap in the middle is to facilitate the screw's entrance in order to facilitate fixing the sensor so that the sensor remains on its place. Note that the screws are made of rubber material in order the fixing process do not harm the sensor's body. The target (see Fig. C.13c) is placed on the end-effector platform of the RRR mechanism (see Fig. C.12). The base (see Fig. C.13d) is a foundation of all components. The base has two slots. By use of the screws, these slots are to facilitate the dovetails adjustment prior to fixing the dovetail onto the base. Block (see Fig. C.13e) is a platform as a place for attaching the 3-RRR. The block is the last component to be manufactured, due to the fact that the block must not only provide the proper fixing of the RRR mechanism (with three special designed taps) but also to ensure that the height of the sensors is aligned with the height of the targets (measured from the base).

Appendix D: Calibration of the sensor

This calibration has the following procedure:

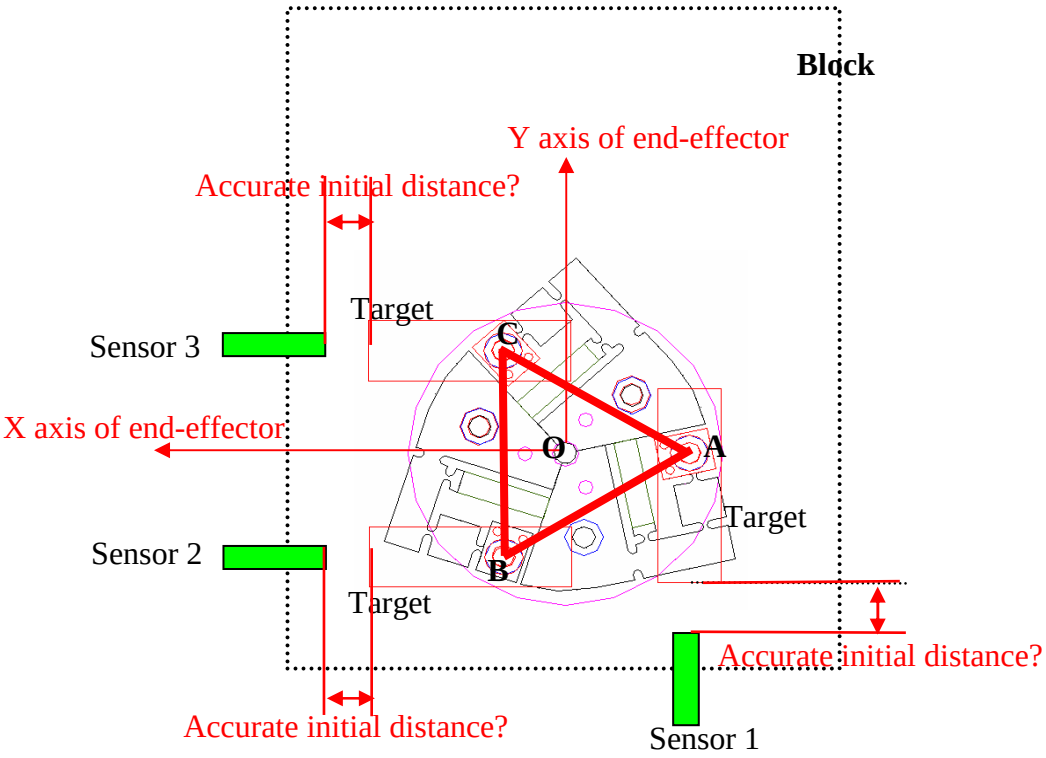

Figure D.1 Find the accurate distances between sensors and targets.

(1) Varying the distance between the sensor and the target within the distance *requirement* of the sensor (*SMU 9000-15N-001) by use of the X-Y-Z stage (M-461, Newport Company)*

It is noted that the main reason that this X-Y-Z stage was used is that this stage has 0.2 microns, compared to the RRR mechanism (1 micrometer accuracy).

In this step, a target is placed onto the platform of the X-Y-Z stage, while a sensor is placed onto the platform of the microscope (see Fig. D.2). Next, the distance between the target and the sensor is adjusted by actuating the left-manipulator.

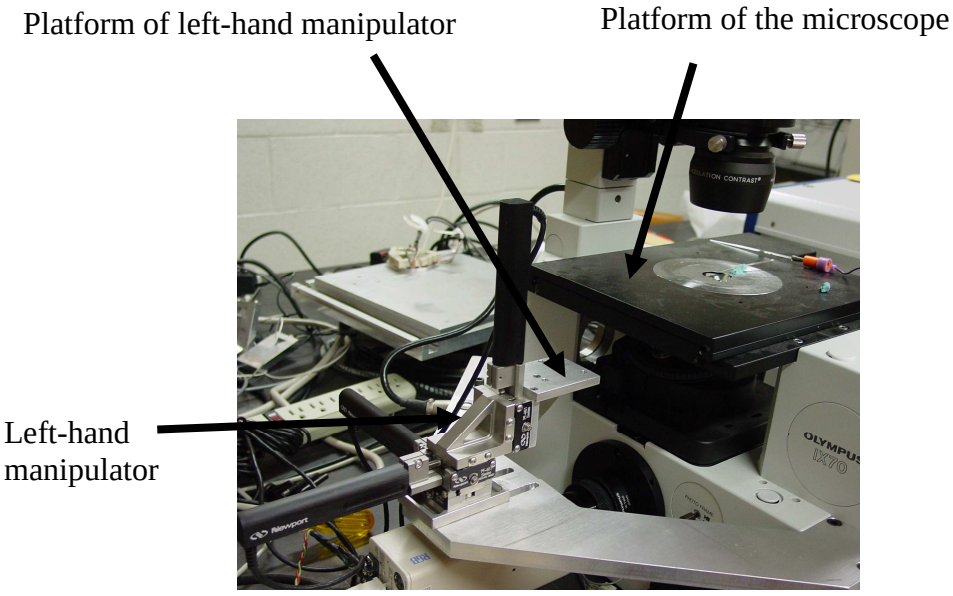

Figure D.2 The X-Y-Z stage (M-461, Newport Company).

(2) Record the reading results

Both the reading results from the sensor and the X-Y-Z stage were recorded simultaneously. Note that the sensors displayed the values in the form of voltages, while the X-Y-Z stage presented the values in the form of microns.

(3) Calculate errors (results deviation)

For the purpose of calculating errors, the obtained results from the sensor are then converted by use of Eqn. (5.1), prior to subtracting them from the reading results of the X-Y-Z stage.

(4) Locate the smallest errors

From the experiment, it was obtained that the smallest errors for sensors 1, 2 and 3 are presented in the below table.

Table D.1 The smallest errors of the three sensors.

Sensors	Sensor output readings	Smallest errors
Sensor 1	4.791 volts	0.0787 microns
Sensor 2	5.181 volts	0.0494 microns
Sensor 3	5.47 volts	0.0154 microns

One should pursue the sensor output readings relating to the smallest errors prior to perform the measurement by tapping carefully the position of the sensor on the dovetail.

Fig. D.2 presents the flow chart of the process of measuring the end-effector displacements to facilitate general understanding of the process. Every performed measurement consists of two processes, which are calibration process and measurement process.

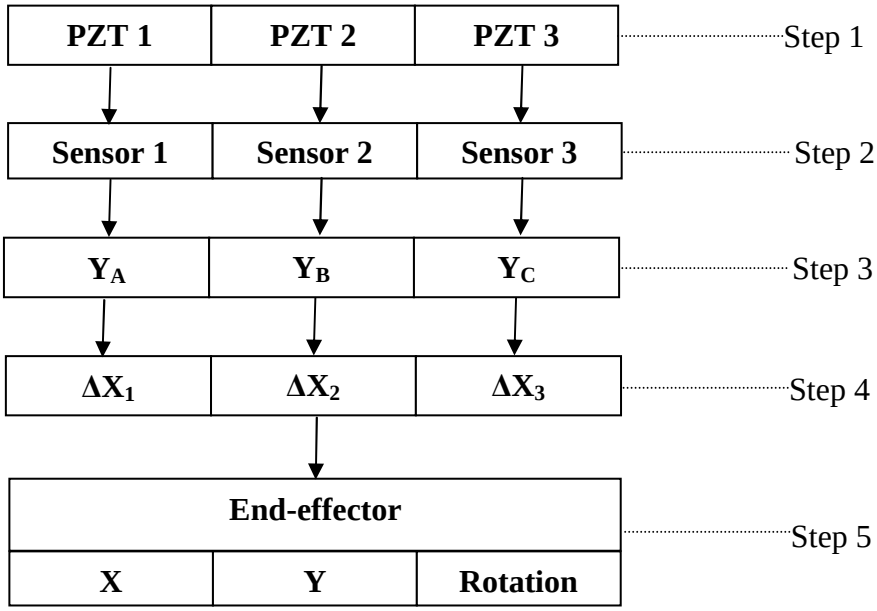

Figure D.3 The measuring process of the end-effector displacements

During the calibration process, the distance between the sensor and its corresponding target should be conditioned such that the sensor output readings in Table D.1 are achieved. Note that the PZT actuators should not have any loading during the calibration process. After the sensor output readings in Table D.1 are achieved, Eqn (5.1) is to convert those readings into the computed distances (represented as Y_A, Y_B, and Y_c in Fig. D3). Y_A, Y_B, and Y_c are 332.851, 362.009, and 384.249 microns, respectively. These values are the initial positions of the targets. Consequently, ΔX_1, ΔX_2 and ΔX_3 that represent the deformations of the three targets are zero. The end-effector deformations, which can be computed by use of Eqns. (5.5), (5.6), and (5.7), are zero as well.

During the measurement process, the PZT 1, PZT 2 and PZT 3 would have different type of loadings. This will affect the sensor output voltage readings (Sensor 1, Sensor 2, and Sensor 3, as shown in Fig. D.3). This will result in the new values of Y_A, Y_B, and Y_c. The differences between the new values of Y_A, Y_B, and Y_c and the initial positions of the targets (332.851, 362.009, and 384.249 microns) result in the non-zero values of the deformations of the targets (ΔX_1, ΔX_2 and ΔX_3). Accordingly, the end-effector deformations can also be computed.

Appendix E: ANSYS codes

E.1. Introduction

This Appendix contains the ANSYS codes that will generate the finite element models in Chapter 3 and Chapter 4. This Appendix comprises of:

1. PIEZMAT macro; the codes supplied by the ANSYS technical support.
2. Three dimensional model of the PZT actuator.
3. Two dimensional model of the PZT actuator.
4. The PZT-RRR mechanism model.
5. The modified MATLAB codes based on the original [Zou, 2000] to be used along with the PZT-RRR mechanism model; for computing the system stiffness
6. The case study of the four-bar mechanism model; for validating the procedure to compute the natural frequency in Chapter 4.
7. The case study of the two-bar mechanism model; for validating the procedure to compute the system stiffness in Chapter 4.

E.1. PIEZMAT macro

```
!MACRO TO CREATE PIEZOELECTRIC INPUT FROM !MANUFACTURER'S DATA PROCESSING WILL REQUIRED THE !INVERSION OF THE MANUFACTURER'S  COMPLIANCE MATRIX INTO !ANSYS STIFFNESS FORM
!
!  5/25/99 - Initial Release
!  2/14/00 - Revision to remove 5.5 inversion technique
!          Add arg4, arg5 and arg6  to convert units after processing
!          User must supply conversion factors
!          arg4 to convert stiffness matrix
!          arg5 to convert piezoelectric matrix
!          arg6 to convert permittivity matrix
!          Add Fatal if negative permittivity
!  THE FOLLOWING MATRICES WILL BE NEEDED
!  MPIEZC - MANUFACTURER'S COMPLIANCE MATRIX - 6 X 6
!  MPIEZD - MANUFACTURER'S PIEZOELECTRIC MATRIX - 6 X 3
```

```
!  MPIEZDT - TRANSPOSE OF MPIEZD - 3 X 6
!  MPIEZP - MANUFACTURER'S DIELECTRIC MATRIX - 3 X 3
!  PIEZCINV - ANSYS STIFFNESS MATRIX - 6 X 6
!  PIEZEANS - ANSYS PIEZOELECTRIC MATRIX - 6 X 3
!  PIEZEPP - ANSYS DIELECTRIC MATRIX - 3 X 3
!
!  DIFFERENT PROCESSING FOR BATCH AND INTERACTIVE
!
!!!!/nopr
*GET,IBATCH,ACTIVE,,INT
!
!  START BY SAVING CURRENT PARAMETERS TO A FILE
!
PARSAV,ALL,PIEZTEMP,PAR
!
*IF,IBATCH,LE,.5,THEN
  PARRES,CHANGE,ARG2,ARG3
  PIEZMAT=ARG1
*ELSE
!
!  ASK IF DATA IS ON FILE OR TO BE ENTERED
!
!!!!   CREATION OF INTERACT MACRO LET AS AN EXERCISE
!!!!   *ASK,IFILE,ENTER FILE NAME, 0 FOR KEYBOARD ENRTY,'0'
!!!!   *IF,IFILE,EQ,'0',THEN
!!!!     *ASK,PIEZMAT,ENTER THE MAT NUM FOR PIEZO DATA,1
!    READ DATA FROM KEYBOARD
!!!!   *ELSE
!    PARRES,CHANGE,IFILE,PAR
     PARRES,CHANGE,ARG2,ARG3
     PIEZMAT=ARG1
!!!!   *ENDIF
*ENDIF
!  AT THIS POINT THE MATRICES HAVE BEEN DEFINED
!  INVERT THE C MATRIX
!
*GET,REVN,ACTIVE,,REV
*IF,REVN,GE,5.6,THEN
!
  *MOPER,PIEZCINV(1,1),MPIEZC(1,1),INVERT
!
!  FOR 5.5, INVERT BY APDL
!
*ELSE
  *MSG,ERROR
```

```
  CONTACT ANSYS TECHNICAL SUPPORT FOR A 5.5 VERSION OF THIS
MACRO
*ENDIF
!  FORM THE ANSYS PIEZOELECTRIC MATRIX
!  PIEZEANS = PIEZCINV * MPIEZD
!
*MOPER,PIEZEANS(1,1),PIEZCINV(1,1),MULT,MPIEZD(1,1)
!
!  FORM THE DIELECTRIC MATRIX
!  FIRST TRANSPOSE MPIEZD,
!  THEN POST MULTIPLY TO PIEZEANS
!  FINALLY SUBTRACT FROM MPIEZP
!
*MFUN,MPIEZDT(1,1),TRAN,MPIEZD(1,1)
*MOPER,PIEZEPP(1,1),MPIEZDT(1,1),MULT,PIEZEANS(1,1)
*DO,II,1,3
  *VOPER,PIEZEPP(1,II),MPIEZP(1,II),SUB,PIEZEPP(1,II)
*ENDDO

!
!   STOP IF PERMITTIVITY IS NEGATIVE
  *VWRITE
  ( PERMITTIVITY MATRIX)
  *VWRITE,PIEZEPP(1,1), PIEZEPP(1,2), PIEZEPP(1,3)
  (3E14.7)
JMTPIEZ=0
JMTPIEZ=MIN(JMTPIEZ,PIEZEPP(1,1))
JMTPIEZ=MIN(JMTPIEZ,PIEZEPP(2,2))
JMTPIEZ=MIN(JMTPIEZ,PIEZEPP(3,3))
*IF,JMTPIEZ,LT,0,THEN
  *MSG,ERROR,JMTPIEZ
  PERMITTIVITY VALUE = %E IS LESS THAN ZERO
*ENDIF
!   CONVERT UNITS IF APPROPRIATE
!   PIEZCINV FROM N/SQ M TO LBF/SQ IN
!   PIEZEANS FROM COULOMBS/SQ M TO COULOMBS/SQ IN
!   PIEZEPP  FROM FARADS/M TO FARADS/IN
*IF,ARG4,GT,0,THEN
  *DO,II,1,6
    *VOPER,PIEZCINV(1,II),PIEZCINV(1,II),MULT,arg4
  *ENDDO
  *DO,II,1,3
    *VOPER,PIEZEANS(1,II),PIEZEANS(1,II),MULT,arg5
    *VOPER,PIEZEPP(1,II),PIEZEPP(1,II),MULT,arg6
  *ENDDO
*ENDIF
```

```
!
!   CREATE THE TBDATA COMMANDS
!
TB,PIEZ,PIEZMAT
!
TBDATA,1,PIEZEANS(1,1),PIEZEANS(1,2),PIEZEANS(1,3)
TBDATA,4,PIEZEANS(2,1),PIEZEANS(2,2),PIEZEANS(2,3)
TBDATA,7,PIEZEANS(3,1),PIEZEANS(3,2),PIEZEANS(3,3)
TBDATA,10,PIEZEANS(4,1),PIEZEANS(4,2),PIEZEANS(4,3)
TBDATA,13,PIEZEANS(5,1),PIEZEANS(5,2),PIEZEANS(5,3)
TBDATA,16,PIEZEANS(6,1),PIEZEANS(6,2),PIEZEANS(6,3)
!
MP,PERX,PIEZMAT,PIEZEPP(1,1)
MP,PERY,PIEZMAT,PIEZEPP(2,2)
MP,PERZ,PIEZMAT,PIEZEPP(3,3)
!
TB,ANEL,PIEZMAT
TBDATA,1,PIEZCINV(1,1),PIEZCINV(2,1),PIEZCINV(3,1),PIEZCINV(4,1),PIEZ
CINV(5,1),PIEZCINV(6,1)
TBDATA,7,PIEZCINV(2,2),PIEZCINV(3,2),PIEZCINV(4,2),PIEZCINV(5,2),PIEZ
CINV(6,2)
TBDATA,12,PIEZCINV(3,3),PIEZCINV(3,4),PIEZCINV(3,5),PIEZCINV(3,6)
TBDATA,16,PIEZCINV(4,4),PIEZCINV(4,5),PIEZCINV(4,6)
TBDATA,19,PIEZCINV(5,5),PIEZCINV(5,6)
TBDATA,21,PIEZCINV(6,6)
!
!  CLEAN UP AFTER PIEZOELECTRIC MATERIAL DEFINITION
!  SAVE AND RESUME TO RESTORE PREVIOUS PARAMETERS
!
PARSAV,ALL,PIEZANS,PAR
PIEZMAT=
MPIEZC(1,1)=
MPIEZD(1,1)=
MPIEZP(1,1)=
MPIEZDT(1,1)=
PIEZCINV(1,1)=
PIEZEANS(1,1)=
PIEZEPP(1,1)=
PARRES,CHANGE,PIEZTEMP,PAR
/GOPR
!
```

E.2. Three dimensional model of the PZT actuator

```
! For ANSYS educational version 8.1, only electrical properties (dielectric !constant)
require conversion (by use of PIEZMAT macro)
!130=number of layers of the PZT TOKIN AE0505D16
!1.4 = the manufacturer's constant

/PREP7
PZT=0   !Adjust voltage here

!!PZT MATERIAL PROPERTIES!!!
TB,PIEZ,1,,,1
TBMODIF,1,1,
TBMODIF,1,2,
TBMODIF,1,3,(-287e-12)
TBMODIF,2,1,
TBMODIF,2,2,
TBMODIF,2,3,
TBMODIF,3,1,
TBMODIF,3,2,
TBMODIF,3,3,130*(635e-12)*1.4
TBMODIF,4,1,
TBMODIF,4,2,
TBMODIF,4,3,
TBMODIF,5,1,(930e-12)
TBMODIF,5,2,
TBMODIF,5,3,
TBMODIF,6,1,
TBMODIF,6,2,
TBMODIF,6,3,

! !MECHANICAL PROPERTIES
TB,ANEL,1,1,21,1
TBTEMP,0
TBDATA,,(14.8e-12) ,,,,,
TBDATA,,,,,,,(18.1e-12)*130*1.4
TBDATA,,,,,,,
TBDATA,,,,,,,
MPTEMP,,,,,,,,
MPTEMP,1,0

! !ELECTRICAL  PROPERTIES
MPDATA,PERX,1,,2536.045198  ! This has been converted by use of PZT macro
MPDATA,PERY,1,,2536.045198  !
MPDATA,PERZ,1,,130*1.4*2815.141243 !
```

```
ET,1,SOLID5                ! 3-D COUPLED-FIELD SOLID, PIEZO OPTION
KEYOPT,1,1,3

!!!!Modeling PZT ! Actual measurement is 5 x 5 x 20 mm
k,1,0,0,0
k,2,5e-3,0,0
k,3,5e-3,5e-3,0
k,4,0,5e-3,0
k,5,0,0,20e-3
k,6,5e-3,0,20e-3
k,7,5e-3,5e-3,20e-3
k,8,0,5e-3,20e-3
type,1
mat,1
real,1
NKPT,NODE,ALL          ! CREATE NODES ON KEYPOINTS
E,1,2,3,4,5,6,7,8 ! CREATE ELEMENT

!Apply voltages
FINISH
/SOL
FLST,2,4,1,ORDE,2
FITEM,2,5
FITEM,2,-8
/GO
D,P51X,VOLT,0
FLST,2,4,1,ORDE,2
FITEM,2,1
FITEM,2,-4
/GO
D,P51X,VOLT,PZT
```

E.3. Two dimensional model of the PZT actuator

```
/PREP7

VOLTAGES=40
length=1
width=1

ET,1,PLANE13
KEYOPT,1,1,7  ! UX, UY, XOLT
KEYOPT,1,3,0  ! PLANE STRAIN
!KEYOPT,1,3,2  ! PLANE STRESS
```

```
/PREP7
TB,PIEZ,1,,,1
TBMODIF,1,1,130*1.35*(635e-12)
TBMODIF,1,2,
TBMODIF,1,3,
TBMODIF,2,1,-287e-12
TBMODIF,2,2,
TBMODIF,2,3,
TBMODIF,3,1,
TBMODIF,3,2,
TBMODIF,3,3,
TBMODIF,4,1,
TBMODIF,4,2,930e-12
TBMODIF,4,3,
TBMODIF,5,1,
TBMODIF,5,2,
TBMODIF,5,3,
TBMODIF,6,1,
TBMODIF,6,2,
TBMODIF,6,3,


TB,ANEL,1,1,21,1
TBTEMP,0
TBDATA,,130*1.4*18.1e-12
TBDATA,,14.8e-12 ,,,,,
TBDATA,,,,,,,
TBDATA,,,,,,,
MPTEMP,,,,,,,,
MPTEMP,1,0
MPDATA,PERX,1,,130*1.4*2815.045198
MPDATA,PERY,1,,2536.045198
MPDATA,PERZ,1,,

type,1
mat,1
real,1



!CREATE KEYPOINTS!
K,1,0,0
K,2,20e-3,0
K,3,20e-3,5e-3
```

```
K,4,0,5e-3

!CREATE LINES!
LSTR, 1, 2
LSTR, 2, 3
LSTR, 3, 4
LSTR, 4, 1

!!!! dividing length line !!!!!!
FLST,5,2,4,ORDE,2
FITEM,5,1
FITEM,5,3
CM,_Y,LINE
LSEL, , , ,P51X
CM,_Y1,LINE
CMSEL,,_Y
LESIZE,_Y1, , ,length, , , , ,1

!!!! dividing width line !!!!!!
FLST,5,2,4,ORDE,2
FITEM,5,2
FITEM,5,4
CM,_Y,LINE
LSEL, , , ,P51X
CM,_Y1,LINE
CMSEL,,_Y
LESIZE,_Y1, , ,width, , , , ,1

!!!create area!!!
FLST,2,4,4
FITEM,2,1
FITEM,2,3
FITEM,2,4
FITEM,2,2
AL,P51X

!!!MESHING AREA!!
MSHKEY,0
CM,_Y,AREA
ASEL, , , ,      1
CM,_Y1,AREA
CHKMSH,'AREA'
CMSEL,S,_Y
AMESH,_Y1
CMDELE,_Y
CMDELE,_Y1
```

```
CMDELE,_Y2
FINISH

!!!!!apply PZT volts

/SOLU
FLST,2,2,1,ORDE,2
FITEM,2,1
FITEM,2,4
/GO
D,P51X,VOLT,VOLTAGES
FLST,2,2,1,ORDE,2
FITEM,2,2
FITEM,2,-3
/GO
D,P51X,VOLT,
```

E.4. The PZT-RRR mechanism model

```
PZT1=0
PZT2=100
PZT3=100
long=1
short=1


!***Creating geometric boundaries of compliant mechanism*****************
/PREP7
/UNITS,SI            ! SPECIFY MKS UNITS
*SET,R,32e-3          !
*SET,pi,3.14159       !constant for converting deg. to rad
*set,l,9e-3           !
*SET,rr,1e-3          !
*SET,h,10e-3          !
*SET,t,0.8e-3         !
*SET,g,(h-t-2*rr)/2   !
*Set,w,8e-3           !
*SET,g2,(w-t-2*rr)/2  !
*SET,lab,17e-3        !
*SET,lbc,11e-3        !
*SET,h1,l+rr+h/2+lab  ! Declaration of parameters
*SET,h2,R-w-lbc       !
*SET,flg,3*rr+t/2     !
*SET,r0,4.5e-3        !
*SET,clr,0
```

```
k,1,0,0                                 !
k,2,l*cos(-30/180*pi),l*sin(-30*pi/180)     !
k,3,l*cos(-30/180*pi)+1e-3*cos(60/180*pi),l*sin(-30*pi/180)+1e-3*sin(60*pi/180) !
k,4,r*cos(-30/180*pi)+1e-3*cos(60/180*pi),r*sin(-30*pi/180)+1e-3*sin(60*pi/180) !
k,5,R,0                                 ! Key
k,6,R,l                                 ! point
k,7,r-g2,l                                  ! assign
k,8,r-g2-rr,l+rr                                    ! ment
k,9,r-g2,l+2*rr                                     !
k,10,R,l+2*rr                                       !
k,11,R,l+rr+lab+h/2                                 !
k,12,R-w,h1                                         !
k,13,R-w,h1-g                                       !
k,14,R-w-rr,h1-g-rr                                 !
k,15,R-w-2*rr,h1-g                                          !
k,16,R-w-2*rr,h1                                    !
k,17,h2,h1                                          !
k,18,h2,h1-g                                        !
k,19,h2-rr,h1-g-rr                          !
k,20,h2-2*rr,h1-g                                   !
k,21,h2-2*rr,h1                                     !
k,22,h2-h-2*rr,h1                                   !
k,23,h2-h-2*rr,h1-h-2*1e-3                                  !
k,24,h2-2*rr,h1-h-2*1e-3                            !
k,25,h2-2*rr,h1-h+g                                 !
k,26,h2-rr,h1-h+g+rr                                !
k,27,h2,h1-h+g                                      !
k,28,h2,h1-h                                        !
k,29,R-w-2*rr,h1-h                                  !
k,30,r-w-2*rr,h1-h+g                                !
k,31,r-w-rr,h1-h+g+rr                               !
k,32,r-w,h1-h+g                                     !
k,33,r-w,l+r0+t/2+rr+clr                            !
k,34,r-w-rr,l+r0+t/2+clr                            !
k,35,r-w-2*rr,l+r0+t/2+rr+clr                               !
k,36,r-w-2*rr,l+r0+2.5e-3+clr                               !
k,37,r-w-2*rr-2e-3,l+r0+2.5e-3+clr                          !
k,38,r-w-2*rr-2e-3,l+r0-2.5e-3+clr                          !
k,39,r-w-2*rr,l+r0-2.5e-3+clr                               !
k,40,r-w-2*rr,l+r0-t/2-rr+clr                       !
k,41,r-w-rr,l+r0-t/2+clr                            !
k,42,r-w,l+r0-t/2-rr+clr                            !
k,43,r-w,l+2*rr                                     !
k,44,r-w+g2,l+2*rr                                  !
k,45,r-w+g2+rr,l+rr                                 !
```

```
k,46,r-w+g2,l                                  !
k,47,0,l                                       !
k,48,r-12e-3,0                                      !
k,49,r-w-2*rr-lbc-h/2,l+rr+lab                           !
k,50,r-w-2*rr-lbc-h/2+3e-3,l+rr+lab-5e-3         !
k,51,r-w-2*rr-lbc-h/2-3e-3,l+rr+lab-5e-3         !
k,52,-1e-3,11e-3,,                             !
k,53,-1e-3,16e-3,,                             !


l,1,2        !
l,2,3        !
l,3,4        !
larc,4,5,1,32e-3 !
l,5,6        !
l,6,7        !
larc,7,8,6,rr ! Creating lines between key points
larc,8,9,6,rr !
l,9,10       !
l,10,11      !
l,11,12      !
l,12,13      !
larc,13,14,16,rr !
larc,14,15,12,rr !
l,15,16     !
l,16,17     !
l,17,18     !
larc,18,19,21,rr !
larc,19,20,17,rr !
l,20,21     !
l,21,22     !
l,22,23     !
l,23,24     !
l,24,25     !
larc,25,26,28,rr !
larc,26,27,24,rr !
l,27,28     !
l,28,29     !
l,29,30     !
larc,30,31,29,rr   !
larc,31,32,29,rr   !
l,32,33     !
larc,33,34,14,rr   !
larc,34,35,14,rr   !
l,35,36     !
l,36,37     !
```

```
l,37,38     !
l,38,39     !
l,39,40     !
larc,40,41,48,rr   !
larc,41,42,48,rr   !
l,42,43     !
l,43,44     !
larc,44,45,47,rr   !
larc,45,46,47,rr   !
l,46,47     !
l,47,1      !

lsel,all !Create area of 1/3 of compliant
al,all    !mechanism without holes
aplot


circle,48,2.5e-3   !
circle,49,2.5e-3          !
circle,50,1e-3  !
circle,51,1e-3  !
circle,1,2.5e-3

lplot               !Generate areas representing holes
al,48,49,50,51  !
al,52,53,54,55  !
al,56,57,58,59 !
al,60,61,62,63  !
al,64,65,66,67  !

CSYS,1                        ! Copying one area
FLST,3,7,5,ORDE,2           ! to create one
FITEM,3,1                  ! whole area
FITEM,3,-7                 !
AGEN,3,P51X, , , ,120, , ,0 !

FLST,2,3,5,ORDE,3  !         Subtracting holes in
FITEM,2,1                !         compliant piece
FITEM,2,7                !
FITEM,2,13               !
FLST,3,9,5,ORDE,9              !
FITEM,3,2                !
FITEM,3,4                !
FITEM,3,-5               !
FITEM,3,8                !
FITEM,3,10               !
```

```
FITEM,3,-11             !
FITEM,3,14              !
FITEM,3,16              !
FITEM,3,-17             !
ASBA,P51X,P51X     !

FLST,2,3,5,ORDE,2
FITEM,2,19
FITEM,2,-21
ASBA,P51X,       6
/REPLOT
FLST,2,3,5,ORDE,3
FITEM,2,1
FITEM,2,-2
FITEM,2,4
ASBA,P51X,      12
/REPLOT
FLST,2,3,5,ORDE,2
FITEM,2,5
FITEM,2,-7
ASBA,P51X,      18
/REPLOT

FLST,2,3,5,ORDE,3 !  Selecting 3 areas
FITEM,2,1       !
FITEM,2,-2      !
FITEM,2,4       !
AGLUE,P51X              !  Gluing compliant mechanism

CSYS,1                      ! Change coordinate system
FLST,3,1,3,ORDE,1                   !
FITEM,3,49                  !
KGEN,3,P51X, , , ,120, , ,0  ! Copy kps

GPLOT
FLST,2,3,5,ORDE,3
FITEM,2,1
FITEM,2,5
FITEM,2,-6
FLST,3,3,5,ORDE,3
FITEM,3,3
FITEM,3,9
FITEM,3,15
ASBA,P51X,P51X
GPLOT
```

```
!****************Creating KP for thin plate**********************
CSWPLA,11,0,1,1,
K,210,19e-3,16e-3,,
K,211,19e-3,11e-3,,
CSWPLA,11,1,1,1,
FLST,3,2,3,ORDE,2
FITEM,3,210
FITEM,3,-211
KGEN,3,P51X, , , ,120, , ,1

!!!*******************************create area for PZT + thin plate
CSWPLA,11,0,1,1,
FLST,2,4,3
FITEM,2,53
FITEM,2,210
FITEM,2,211
FITEM,2,52
A,P51X
FLST,2,4,3
FITEM,2,210
FITEM,2,37
FITEM,2,38
FITEM,2,211
A,P51X
CSWPLA,11,1,1,1,
FLST,3,2,5,ORDE,2
FITEM,3,1
FITEM,3,3
AGEN,3,P51X, , , ,120, , ,0

!*************glue PZT-Thinplate-compliant
FLST,2,9,5,ORDE,2
FITEM,2,1
FITEM,2,-9
AGLUE,P51X




!************create elements for PZT
ET,1,PLANE13
KEYOPT,1,1,7  ! UX, UY, VOLT DOF
KEYOPT,1,3,0  ! PLANE STRAIN ASSUMPTION


/PREP7
```

```
TB,PIEZ,1,,,1
TBMODIF,1,1,130*1.4*(635e-12)
TBMODIF,1,2,
TBMODIF,1,3,
TBMODIF,2,1,-287e-12
TBMODIF,2,2,
TBMODIF,2,3,
TBMODIF,3,1,
TBMODIF,3,2,
TBMODIF,3,3,
TBMODIF,4,1,
TBMODIF,4,2,930e-12
TBMODIF,4,3,
TBMODIF,5,1,
TBMODIF,5,2,
TBMODIF,5,3,
TBMODIF,6,1,
TBMODIF,6,2,
TBMODIF,6,3,


TB,ANEL,1,1,21,1
TBTEMP,0
TBDATA,,0.0013*130*1.4*18.1e-12
TBDATA,,14.8e-12 ,,,,,
TBDATA,,,,,,,
TBDATA,,,,,,,
MPTEMP,,,,,,,,
MPTEMP,1,0

MPDATA,PERX,1,,130*1.4*2815.045198 !
MPDATA,PERY,1,,2536.045198
MPDATA,PERZ,1,,

!************************************mesh area PZT 1
FLST,5,2,4,ORDE,2
FITEM,5,69
FITEM,5,134
CM,_Y,LINE
LSEL, , , ,P51X
CM,_Y1,LINE
CMSEL,,_Y
LESIZE,_Y1, , ,long, , , , ,1 !!!!!long=5 divisions along longer body of PZT
FLST,5,2,4,ORDE,2
FITEM,5,114
FITEM,5,136
```

```
CM,_Y,LINE
LSEL, , , ,P51X
CM,_Y1,LINE
CMSEL,,_Y
LESIZE,_Y1, , ,short, , , , ,1 !!!!!short=3 divisions along longer body of PZT
MSHKEY,0
CM,_Y,AREA
ASEL, , , ,      1
CM,_Y1,AREA
CHKMSH,'AREA'
CMSEL,S,_Y
AMESH,_Y1
CMDELE,_Y
CMDELE,_Y1
CMDELE,_Y2



!!!!!!!mesh area PZT 2
FLST,5,2,4,ORDE,2
FITEM,5,212
FITEM,5,214
CM,_Y,LINE
LSEL, , , ,P51X
CM,_Y1,LINE
CMSEL,,_Y
LESIZE,_Y1, , ,long, , , , ,1
FLST,5,2,4,ORDE,2
FITEM,5,213
FITEM,5,215
CM,_Y,LINE
LSEL, , , ,P51X
CM,_Y1,LINE
CMSEL,,_Y
LESIZE,_Y1, , ,short, , , , ,1
MSHKEY,0
CM,_Y,AREA
ASEL, , , ,      8
CM,_Y1,AREA
CHKMSH,'AREA'
CMSEL,S,_Y
AMESH,_Y1
CMDELE,_Y
CMDELE,_Y1
CMDELE,_Y2
```

```
!!!!!!!mesh area PZT 3
FLST,5,2,4,ORDE,2
FITEM,5,200
FITEM,5,205
CM,_Y,LINE
LSEL, , , ,P51X
CM,_Y1,LINE
CMSEL,,_Y
LESIZE,_Y1, , ,long, , , , ,1
FLST,5,2,4,ORDE,2
FITEM,5,201
FITEM,5,208
CM,_Y,LINE
LSEL, , , ,P51X
CM,_Y1,LINE
CMSEL,,_Y
LESIZE,_Y1, , ,short, , , , ,1
MSHKEY,0
CM,_Y,AREA
ASEL, , , ,      5
CM,_Y1,AREA
CHKMSH,'AREA'
CMSEL,S,_Y
AMESH,_Y1
CMDELE,_Y
CMDELE,_Y1
CMDELE,_Y2

!**********Create element for thin plate
et,2,combin14
keyopt,2,3,2  ! UX, UY DOF
r,2,1.7225e6 ! Spring constant k = EA/L; E= 344.5e6 Pa (A and L average measurements)


!!!!mesh thin plate on PZT 1
TYPE,   2
REAL,      2
FLST,5,2,4,ORDE,2
FITEM,5,37
FITEM,5,114
CM,_Y,LINE
LSEL, , , ,P51X
CM,_Y1,LINE
CMSEL,,_Y
```

```
LESIZE,_Y1, , ,1, , , , ,1
FLST,5,2,4,ORDE,2
FITEM,5,180
FITEM,5,199
CM,_Y,LINE
LSEL, , , ,P51X
CM,_Y1,LINE
CMSEL,,_Y
LESIZE,_Y1, , ,1, , , , ,1

!!!mesh thin on PZT 1
MSHKEY,0
CM,_Y,AREA
ASEL, , , ,      3
CM,_Y1,AREA
CHKMSH,'AREA'
CMSEL,S,_Y
AMESH,_Y1
CMDELE,_Y
CMDELE,_Y1
CMDELE,_Y2

!!!!mesh thin plate on PZT 2
FLST,5,2,4,ORDE,2
FITEM,5,171
FITEM,5,213
CM,_Y,LINE
LSEL, , , ,P51X
CM,_Y1,LINE
CMSEL,,_Y
LESIZE,_Y1, , ,1, , , , ,1
FLST,5,2,4,ORDE,2
FITEM,5,221
FITEM,5,-222
CM,_Y,LINE
LSEL, , , ,P51X
CM,_Y1,LINE
CMSEL,,_Y
LESIZE,_Y1, , ,1, , , , ,1
MSHKEY,0
CM,_Y,AREA
ASEL, , , ,     11
CM,_Y1,AREA
CHKMSH,'AREA'
CMSEL,S,_Y
AMESH,_Y1
```

```
CMDELE,_Y
CMDELE,_Y1
CMDELE,_Y2


!!!!mesh thin plate on PZT 3
FLST,5,2,4,ORDE,2
FITEM,5,104
FITEM,5,201
CM,_Y,LINE
LSEL, , , ,P51X
CM,_Y1,LINE
CMSEL,,_Y
LESIZE,_Y1, , ,1, , , , ,1
FLST,5,2,4,ORDE,2
FITEM,5,219
FITEM,5,-220
CM,_Y,LINE
LSEL, , , ,P51X
CM,_Y1,LINE
CMSEL,,_Y
LESIZE,_Y1, , ,1, , , , ,1
MSHKEY,0
CM,_Y,AREA
ASEL, , , ,      10
CM,_Y1,AREA
CHKMSH,'AREA'
CMSEL,S,_Y
AMESH,_Y1
CMDELE,_Y
CMDELE,_Y1
CMDELE,_Y2


!***********create element for MESHING COMPLIANT PIECE
et,3,plane82          ! choose element type for compliant mechanism and end effector
keyopt,3,3,2          ! PLANE STRAIN assumption
mp,ex,3,117e9  ! modulus young (Pa)    !compliant !
mp,nuxy,3,0.3         ! poisson ratio         !properties!


!***********MESHING COMPLIANT PIECE
TYPE,3
MAT,3

MSHAPE,1,2D
```

```
FLST,5,3,5,ORDE,2
FITEM,5,12
FITEM,5,-14
CM,_Y,AREA
ASEL, , , ,P51X
CM,_Y1,AREA
CHKMSH,'AREA'
CMSEL,S,_Y
AMESH,_Y1
CMDELE,_Y
CMDELE,_Y1
CMDELE,_Y2

!****************Creating bolts' element**********************
et,4,plane2          ! choose element type for bolts
keyopt,4,3,2         ! PLANE STRAIN ASSUMPTION
mp,ex,4,358.28e6   ! modulus young (Pa)
mp,nuxy,4,0.3        ! poisson ratio

TYPE,4
MAT,4

!!!!!create nodes on KP bolts
FLST,3,3,3,ORDE,3
FITEM,3,1
FITEM,3,49
FITEM,3,74
NKPT,0,P51X

e,8290,448,450
e,8290,450,452
e,8290,452,441
e,8290,441,444
e,8290,444,446
e,8290,446,442
e,8290,442,461
e,8290,461,463
e,8290,463,454
e,8290,454,456
e,8290,456,458
e,8290,458,448


e,8291,5931,5933
e,8291,5933,5922
e,8291,5922,5925
```

```
e,8291,5925,5927
e,8291,5927,5923
e,8291,5923,5942
e,8291,5942,5944
e,8291,5944,5935
e,8291,5935,5937
e,8291,5937,5939
e,8291,5939,5929
e,8291,5929,5931

e,8289,3192,3211
e,8289,3211,3213
e,8289,3213,3204
e,8289,3204,3206
e,8289,3206,3208
e,8289,3208,3198
e,8289,3198,3200
e,8289,3200,3202
e,8289,3202,3191
e,8289,3191,3194
e,8289,3194,3196
e,8289,3196,3192

!!!***create elements for end-effector plate
et,5,plane2
keyopt,5,3,2
mp,ex,5,69000000000   ! modulus young (Pa) !end effector !
mp,dens,5,7860        ! Density (kg/m^3)   !properties   !
mp,nuxy,5,0.3         ! poisson ratio


type,5
mat,5



!******* create big end-effector circle
CYL4, , ,35.1e-3

!******* create one small circle
CYL4,6e-3,27e-3,2.5e-3

!! copy small circle
CSYS,1
FLST,3,1,5,ORDE,1
FITEM,3,4
```

```
AGEN,3,P51X, , , ,120, , ,0

!!! subtract all small circles
FLST,3,3,5,ORDE,3
FITEM,3,4
FITEM,3,6
FITEM,3,-7
ASBA, 2,P51X
/REPLOT
CSYS,0 !!BACK TO CARTESIAN

!!!create small circle for end-effector
CYL4, , ,2.5e-3

!!!!substract small circle from end-effector plate
ASBA,9, 2

!!mesh end-effector platform
MSHKEY,0
CM,_Y,AREA
ASEL, , , ,4
CM,_Y1,AREA
CHKMSH,'AREA'
CMSEL,S,_Y
AMESH,_Y1
CMDELE,_Y
CMDELE,_Y1
CMDELE,_Y2
MSHKEY,0


!******* create node for end-effector and circle
N,9310,0,0

e,9310,8388,8399
e,9310,8399,8397
e,9310,8397,8395
e,9310,8395,8405
e,9310,8405,8403
e,9310,8405,8403
e,9310,8403,8401
e,9310,8401,8410
e,9310,8410,8408
e,9310,8408,8389
e,9310,8389,8393
e,9310,8393,8391
```

```
e,9310,8391,8388


!!!!couple nodes of end-effector-bolts

!!Bolt 1
cp,1,all,441,8316
cp,4,all,452,8327
cp,7,all,450,8325
cp,10,all,448,8323
cp,13,all,458,8333
cp,16,all,456,8331
cp,19,all,454,8329
cp,22,all,463,8338
cp,25,all,461,8336
cp,28,all,442,8317
cp,31,all,446,8321
cp,34,all,444,8319

!!Bolt 2
cp,37,all,5942,8384
cp,40,all,5923,8365
cp,43,all,5927,8369
cp,46,all,5925,8367
cp,49,all,5922,8364
cp,52,all,5933,8375
cp,55,all,5931,8373
cp,58,all,5929,8371
cp,62,all,5939,8381
cp,65,all,5937,8379
cp,68,all,5935,8377
cp,71,all,5944,8386


!!Bolt 3
cp,74,all,3208,8357
cp,77,all,3206,8355
cp,80,all,3204,8353
cp,83,all,3213,8362
cp,86,all,3211,8360
cp,89,all,3192,8341
cp,92,all,3194,8343
cp,95,all,3196,8345
cp,98,all,3191,8340
cp,102,all,3202,8351
cp,105,all,3200,8349
```

```
cp,108,all,3198,8347

!!!FIXING BOLTS
FINISH
/SOL
FLST,2,12,4,ORDE,6
FITEM,2,48
FITEM,2,-51
FITEM,2,115
FITEM,2,-118
FITEM,2,182
FITEM,2,-185
DL,P51X, ,ALL,
sbctran

!!! Shifting Element Coordinate System for PZTs 2 and 3
LOCAL,11,0,0,0,0,240, , ,1,1, !creation
LOCAL,12,0,0,0,0,120, , ,1,1, !of new cs


asel,s,,,8 !select area to be modified
allsel,below,area !activate selection for area
FINISH
/PREP7
EMODIF,all,ESYS,11, !modify elements

asel,s,,,5
allsel,below,area
EMODIF,all,ESYS,12,

allsel  !select all instead of the previously chosen ones

!!!!apply voltages on PZT1
/SOL
FLST,2,1,4,ORDE,1
FITEM,2,136
DL,P51X, ,VOLT,PZT1
FLST,2,1,4,ORDE,1
FITEM,2,114
DL,P51X, ,VOLT,
sbctran

!!!apply voltages on pzt2
FLST,2,1,4,ORDE,1
FITEM,2,215
DL,P51X, ,VOLT, PZT2
```

```
FLST,2,1,4,ORDE,1
FITEM,2,213
DL,P51X, ,VOLT,
sbctran

!!!apply voltages on PZT3
FLST,2,1,4,ORDE,1
FITEM,2,208
DL,P51X, ,VOLT,PZT3
FLST,2,1,4,ORDE,1
FITEM,2,201
DL,P51X, ,VOLT,
sbctran


P=4
!!!apply preloadforce on PZT1
FLST,2,2,3,ORDE,2
FITEM,2,210
FITEM,2,-211
FK,P51X,FX,-3.981eP
sbctran

!!!!apply preload on PZT2
FLST,2,2,3,ORDE,2
FITEM,2,217
FITEM,2,-218
FK,P51X,FX,0.5*2.56667eP
FLST,2,2,3,ORDE,2
FITEM,2,217
FITEM,2,-218
FK,P51X,FY,0.866*2.566667eP
sbctran

!!!apply preload on PZT3
FLST,2,2,3,ORDE,2
FITEM,2,205
FITEM,2,212
FK,P51X,FX,0.5*5.3950eP
FLST,2,2,3,ORDE,2
FITEM,2,205
FITEM,2,212
FK,P51X,FY,-0.866*5.3950eP
sbctran
finish
```

```
/prep7
!!!!To obtain rotation
!delete element in the center
edele,4331,4343,1

et,6,beam3
KEYOPT,6,6,1
KEYOPT,6,9,0
KEYOPT,6,10,0

mp,ex,6,69e9
mp,dens,6,7860
mp,nuxy,6,0.3
r,6,0.01,8.33e-8,0.01

type,6
mat,6
real,6


!******* create elements for end-effector in the centre


e,9310,8388
e,9310,8389
e,9310,8390
e,9310,8391
e,9310,8392
e,9310,8393
e,9310,8394
e,9310,8395
e,9310,8396
e,9310,8397
e,9310,8398
e,9310,8399
e,9310,8400
e,9310,8401
e,9310,8402
e,9310,8403
e,9310,8404
e,9310,8405
e,9310,8406
e,9310,8407
e,9310,8408
e,9310,8409
e,9310,8410
```

```
e,9310,8411


/solu
solve

!preparation of new coordinate systems imitating experiment axis (comparison purpose)
!/prep7
!csys,0   !
!dsys,0
!k,250,-10.2e-3,9.35e-3
!k,251,9.35e-3, 10.2e-3
!k,252,0,0,0


!KWPLAN,-1,252,250,251
!CSWPLA,1000,0,1,1,
!csys,1000
!dsys,1000

!FINISH
!/SOLU
!PSTRES,on
!SOLVE
!FINISH
!/POST1
!rsys,0
!NSEL,S,LOC,X,0,0,0
!prnsol,dof
!csys,0
!dsys,0
!rsys,0
!finish

!Modal analysis
!/SOLU
!ANTYPE,MODAL
!MODOPT,LANB,5,0,0  ! BLOCK LANCZOS, EXTRACT 5 MODES
!MXPAND,5
!PSTRES,on
!solve
```

E.5. The Modified MATLAB Codes

```
Rs = 29.546;    % Length of OCi
n=11;    % Length of Lbc
f1=1.1733;
f2=0.81569;
lab=17.720;
fa=f2+asin( n*sin(f2)/lab )
fai=f1+f2;
co = lab*sin(fa);

R0=3.5;


tt = [cos(fai+2*pi/3), sin(fai+2*pi/3), sin(fai)*Rs*1e3;
   cos(fai), sin(fai), sin(fai)*Rs*1e3;
   cos(fai+4*pi/3), sin(fai+4*pi/3), sin(fai)*Rs*1e3];  % unit is in
um



jme = -(co/R0) .* inv(tt)   %jacobian matrix JL

angle = 53.961*pi/180;
coordinate_transform = [ cos(angle), -sin(angle), 0;
                            sin(angle), cos(angle), 0;
                                 0,     0,          1 ] ;



jlca = [ 1.610797127, -1.298942876,-0.164324634;
   -0.6056938677, -1.42884239, 1.37702048;
   -3.269206385e-5, -2.830203574e-5 ,-2.019743117e-5 ] % matrix
obtained by experiment



JL = inv(coordinate_transform) * jme


V1= 0;     %  D = 635 e-12 m/V * 130 * 1.4 *V (The manufacturer eqn)
V2= 0 ;      %
V3= 32;      %

L1=(1.1557e-4)*V1;
L2=(1.1557e-4)*V2;
L3=(1.1557e-4)*V3;

in = [ L1; L2; L3];      % input displacement of PZT 1, 2, and 3
```

```
outme_transform = JL*in   % results in x, y and r direction, unit in
um, um, and rad

outjca=jlca*in   % experimental results



%************************  calibrated constant result

op_Rs=31.2969;
op_lab=16.3333;
op_n=10.7105;
op_f1=1.0951;
op_f2=0.3366;
op_fai=op_f1+op_f2;
op_fa=op_f2+asin( op_n*sin(op_f2)/op_lab );
op_co = op_lab*sin(op_fa);

R0=3.5;


op_tt = [cos(op_fai+2*pi/3), sin(op_fai+2*pi/3),
sin(op_fai)*op_Rs*1e3;
   cos(op_fai), sin(op_fai), sin(op_fai)*op_Rs*1e3;
   cos(op_fai+4*pi/3), sin(op_fai+4*pi/3), sin(op_fai)*op_Rs*1e3];



op_jme = -(op_co/R0) .* inv(op_tt)


angle = 53.961*pi/180;
coordinate_transform = [ cos(angle), -sin(angle), 0;
                             sin(angle), cos(angle), 0;
                         0,     0,          1 ] ;


jlca = [ 1.610797127, -1.298942876,-0.164324634;
   -0.6056938677, -1.42884239, 1.37702048;
   -3.269206385e-5, -2.830203574e-5 ,-2.019743117e-5 ] ;

op_JL = inv(coordinate_transform) * op_jme


in = [ L1; L2; L3];
```

```
opoutme_transform = op_JL * in  % calibrated results in x,y and r
direction,unit in um, um, and rad

Jacobian = op_JL   % jacobian matrix

Jacob_transpose = transpose(Jacobian)

ansys11= -15046404312.184;%input from ANSYS stiffness values
ansys12=  15274759135.731 ;
ansys13= -233931320.70317;
ansys21=  -14958247330.251;
ansys22= 15182139498.29   ;
ansys23=  -229361866.55399 ;
ansys31=   -13227266.1   ;
ansys32=  13155063.491757  ;
ansys33=   67399.571490299 ;

ansys_stiffness = [ansys11 ansys12 ansys13; ansys21 ansys22 ansys23;
ansys31 ansys32 ansys33]

total_stiffness = ansys_stiffness * Jacob_transpose* Jacobian ;


system_stiffness = eig(total_stiffness)
```

E.6. Four-Bar Mechanism Model

```
! The obtained frequency results in ANSYS are in Hertz.
! 1 Hertz = 6.2831853 radian/second

/prep7
/title, case study of the four-bar mechanism (model 2)

!!!Kinematics model of the four-bar mechanism
phi=0   ! Input angle
A2=-phi/57.29578
L1=10
L2=4.25
L3=11
L4=10.65
C2=COS(A2)
S2=SIN(A2)
XA=L2*C2
YA=L2*S2
L1XA=L1-Xa
LX2=L1Xa*L1Xa
YA2=YA*YA
D2=LX2+YA2
```

```
D=D2**0.5
CA=L1XA/D
SA=-YA/D
L32=L3**2
L42=L4**2
DL3=D*L3
DL32=DL3*2
D3=D2+L32
D34=D3-L42
CB=D34/DL32
CB2=CB*CB
CB21=-CB2+1
SB=CB21**0.5
L3CA=L3*CA
L3SA=L3*SA
L3CC=L3CA*CB
L3CS=L3CA*SB
L3SS=L3SA*SB
CCSS=L3CC-L3SS
L3SC=L3SA*CB
SCCS=L3SC+L3CS
XB=XA+CCSS
YB=YA+SCCS

!!!Develop elements for links and joints
ET,1,3   !mass element
ET,2,21,,,4 !mass element with activation
EX,1,10.3e6
DENS,1,.000254
R,1,.167,.0003881,.167  ! crank
R,2,.063,.00002084,.063 ! coupler
R,3,.000239

k,1,0,0
k,2,xa,ya
k,3,xb,yb
k,4,l1,0

KFILL,1,2,2,5,1,1,
KFILL,2,3,2,7,1,1
KFILL,3,4,2,9,1,1

nkpt,1,1
nkpt,2,5
nkpt,3,6
nkpt,4,2
```

```
nkpt,5,2
nkpt,6,7
nkpt,7,8
nkpt,8,3
nkpt,9,3
nkpt,10,9
nkpt,11,10
nkpt,12,4

e,1,2
e,2,3
e,3,4

real,2
e,5,6
e,6,7
e,7,8
e,9,10
e,10,11
e,11,12

type,2
real,3
e,5
e,9

cp,1,ux,4,5
cp,2,uy,4,5
cp,3,ux,8,9
cp,4,uy,8,9

d,1,ux,,,,,uy,rotz
d,12,ux,,,,,uy

!solving by static analysis
/solu
pstres,on
solve
finish

!solving by use of modal analysis
/solu
antype,modal
modopt, lanb, 3,
mxpand,3
pstres,on
```

```
solve
! Model 3
/prep7
/title, case study of the four-bar mechanism (model 3)
PHI=0  ! Adjust angle
A2=-phi/57.29578
L1=10
L2=4.25
L3=11
L4=10.65
C2=COS(A2)
S2=SIN(A2)
XA=L2*C2
YA=L2*S2
L1XA=L1-Xa
LX2=L1Xa*L1Xa
YA2=YA*YA
D2=LX2+YA2
D=D2**0.5
CA=L1XA/D
SA=-YA/D
L32=L3**2
L42=L4**2
DL3=D*L3
DL32=DL3*2
D3=D2+L32
D34=D3-L42
CB=D34/DL32
CB2=CB*CB
CB21=-CB2+1
SB=CB21**0.5
L3CA=L3*CA
L3SA=L3*SA
L3CC=L3CA*CB
L3CS=L3CA*SB
L3SS=L3SA*SB
CCSS=L3CC-L3SS
L3SC=L3SA*CB
SCCS=L3SC+L3CS
XB=XA+CCSS
YB=YA+SCCS


ET,1,3   !mass element
ET,2,21,,,4 !mass element with activation
EX,1,10.3e6
```

```
DENS,1,.000254
R,1,.167,.0003881,.167  ! crank
R,2,.063,.00002084,.063 ! coupler
R,3,.000239

k,1,0,0
k,2,xa,ya
k,3,xb,yb
k,4,l1,0

KFILL,1,2,3,5,1,1,
KFILL,2,3,3,8,1,1,
KFILL,3,4,3,11,1,1,


nkpt,1,1
nkpt,2,5
nkpt,3,6
nkpt,4,7
nkpt,5,2
nkpt,6,2 !will be for mass element
nkpt,7,8
nkpt,8,9
nkpt,9,10
nkpt,10,3!will be for mass element
nkpt,11,3
nkpt,12,11
nkpt,13,12
nkpt,14,13
nkpt,15,4

e,1,2
e,2,3
e,3,4
e,4,5

real,2
e,6,7
e,7,8
e,8,9
e,9,10
e,11,12
e,12,13
e,13,14
e,14,15
```

```
type,2
real,3
e,6
e,10


cp,1,ux,5,6
cp,2,uy,5,6
cp,3,ux,10,11
cp,4,uy,10,11

d,1,ux,,,,,uy,rotz
d,15,ux,,,,,uy

!solving by static analysis
/solu
pstres,on
solve
finish

!solving by use of modal analysis
/solu
antype,modal
modopt, lanb, 3,
mxpand,3
pstres,on
solve
```

E.7. Two-Bar Mechanism Model

```
!Define parameters
x=10e-2
y=10e-2

/prep7
k,1,0,0
k,2,X,Y
k,3,10e-2,0

nkpt,1,1
nkpt,2,2
nkpt,3,2
nkpt,4,3
```

```
et,1,combin14
KEYOPT,1,3,2
r,1,1000 !10 N/cm = 10*100

type,1
mat,1
real,1

e,1,2
e,3,4
cp,1,ux,2,3
cp,2,uy,2,3

!Constrain node 1
/SOL
d,1,ux,0
d,1,uy,0
!Constrain node 4
d,4,ux,0
d,4,uy,0


!Move CS to end-effector (P)
NWPAVE,2
CSWPLA,11,0,1,1,

csys,11
dsys,11

!Apply Fx=1 at node 2 or node 3
F,2,FX,1
solve
finish

/post1
rsys,11
*GET,DISPX_FX,NODE,2,u,x
*GET,DISPY_FX,NODE,2,u,y
finish

/solu
FDELE,2,FX

!Apply Fy=1 at node 2 or node 3
F,2,FY,1
```

```
solve
finish

/post1
rsys,11
*GET,DISPX_FY,NODE,2,u,x
*GET,DISPY_FY,NODE,2,u,y

/solu
FDELE,2,FY

*DIM, COMPLI, ARRAY,2,2
COMPLI(1,1)=DISPX_FX,DISPY_FX
COMPLI(1,2)=DISPX_FY,DISPY_FY

*DIM,STIFF,ARRAY,2,2
*MOPER,STIFF,COMPLI,INVERT !perform inversion

!Present the results in the output window

!Define  parameters
*DIM,LABEL,CHAR,1
LABEL(1) = " ! LABEL(1) is unchangeable


*DIM,VALUE,,2,2  !
*VFILL,VALUE(1,1),DATA,STIFF(1,1)
*VFILL,VALUE(1,2),DATA,STIFF(1,2)
*VFILL,VALUE(2,1),DATA,STIFF(2,1)
*VFILL,VALUE(2,2),DATA,STIFF(2,2)

/OUT,systiff,vrt     !save values in 'systiff' parameter

/COM,----------------------SYSTEM STIFFNESS MATRIX (2 x 2)----------------------
------

*VWRITE,LABEL(1),VALUE(1,1),VALUE(1,2)
(1X,A8,'  ', F15.4, '       ',  F15.4)
*VWRITE,LABEL(1),VALUE(2,1),VALUE(2,2)
(1X,A8,'  ', F15.4, '       ',  F15.4)

/COM,-------------------------------------------------------------------------------
/OUT
FINISH
*LIST,systiff,vrt   !produce values in 'systiff' parameter
```